Z' and W' gauge bosons in SU(2)xSU(2)xU(1) models : Collider phenomenology at LO and NLO QCD

Tomas Jezo

UNIVERSITÉ DE GRENOBLE

THÈSE

Pour obtenir le grade de

DOCTEUR DE L'UNIVERSITÉ DE GRENOBLE

Spécialité : **Physique Subatomique et Astroparticules**

Arrêté ministériel : 7 août 2006

Présentée par

Tomáš Ježo

Thèse dirigée par **Ingo Schienbein et Michael Klasen**

préparée au sein **Laboratoire de Physique Subatomique et Cosmologie**
et de **Ecole doctorale de Physique de Grenoble**

Z' and W' gauge bosons in SU(2)xSU(2)xU(1) models: Collider phenomenology at LO and NLO QCD

Thèse soutenue publiquement le **25 septembre 2013**,
devant le jury composé de :

Mr., Arnaud Lucotte
DR2 Laboratoire de Physique Subatomiques et de Cosmologie, Président
Mr., Aldo Deandrea
Prof. Université Claude Bernard Lyon 1, Rapporteur
Mr., Jean-Philippe Guillet
DR2 Laboratoire d'Annecy-le-Vieux de Physique Théorique, Rapporteur
Mr., Roberto Bonciani
Dr. Università degli Studi di Roma "La Sapienza", Examinateur
Mr., Benjamin Fuks
MCF Université de Strasbourg, Examinateur
Mr., Ingo Schienbein
MCF Université Joseph Fourier, Directeur de thèse
Mr., Michael Klasen
Prof. Universität Münster, Co-Directeur de thèse

Acknowledgments

I would like to express my most sincere gratitude to everyone that I have had the pleasure to collaborate with, or that has influenced my work during my doctoral studies, either on a professional or personal level. I have learned very much about myself and physics and I am very thankful for that.

I am particularly grateful to my supervisor, who besides sharing his wisdom, provided me with a great deal of support. Thank you Ingo for the opportunity to learn from you, for the broad choice of subjects for me to dig into and for teaching me to be patient and scrupulous – to verify my claims beyond a shadow of doubt. I sincerely hope that enough of this admirable skill, which I feel is being slowly abandoned by the community, has rubbed off on me. I am grateful to Michael for his warm welcome and for his advice during my Master's project that helped me smoothly transition into my doctoral studies. I would like to extend my endless appreciation to Roberto, who despite of not being in the list of my official supervisors, invested an extensive amount of time in, and played a crucial role in, my professional upbringing. Thank you Roberto for your guidance through the wonderland of precision calculations.

Listing all of my collaborators, colleagues and friends I am thankful to is too difficult a task, as the probability of me forgetting someone is too high, so let me just list a few. Florian, during my thesis and well beyond you were consistently the brightest source of motivation for me. I am so grateful for all our discussions and joint efforts on the many projects we share and hopefully will share in the future. Working with you brings me the satisfaction I was expecting to get from working in academia. Big thanks goes to all my colleagues at the LPSC for making my work experience so enjoyable. To the permanent and non-permanent staff members among which I would like to mention include Karol, Akin, Sabine, Mariane, Mauro and Suchita. To my fellow PhD. students Josselin, Quentin, Sylvain, Béranger and Jeremy from the Theory group and Poyua, Benjamin, Mathieu from various other groups.

To defend one's thesis is a major undertaking and I would like to thank everyone who helped me achieve it. Big thanks go to Florian and Josselin for carefully proofreading my thesis. Besides Ingo, Roberto and Michael I would like to thank the rest of the jury: the two referees Aldo and Jean-Philippe, the president of the jury Arnaud and last but not least Benjamin. Thank you all for a very useful critical discussion of my manuscript and many great suggestions on how to improve it.

Of course, my doctoral studies wouldn't have been feasible without the support of loved ones. My endless gratitude goes to my parents and my sister for their sacrifices and supporting me in each of my life decisions, even though most of them drive me so far away from home. Juliette, Lina and Jean-Luc, I thank you for being my substitute family and for giving me the opportunity to discover France and fall in love with it.

Résumé

Il n'est pas rare que les théories au-delà du Modèle Standard de physique des particules (MS) contiennent de nouveaux bosons vecteurs. Ils apparaissent dès que le groupe de jauge du MS est étendu. Dénotés Z' et W', il s'agit de particules massives de spin 1, respectivement neutres et charges. Ce sont les médiateurs des courants neutres et chargés des fermions du MS. Dans l'hypothése où leur couplage aux quarks et aux leptons est suffisamment important, et que leur masse respective n'est pas trop élevée, il est possible de les observer au sein de collisionneurs. Par exemple, des bosons Z' et W' avec des couplages de l'ordre de ceux du MS devraient être accessibles au LHC jusqu'à des masses de l'ordre de 5 TeV. Cependant, les données actuelles d'ATLAS et CMS excluent toute présence de telles résonances pour des masses inférieures à 3 TeV environ.

Dans ce manuscrit, nous étudions l'impact de l'existence hypothétique de bosons Z' et W' sur les observables habituellement mesurées au LHC. Nous présentons la phénoménologie d'une classe d'extensions du MS dans laquelle le groupe de jauge est élargi par l'addition d'un facteur de groupe SU(2). En scannant l'espace des paramètres, restreint par les limites d'exclusions obtenues à partir d'observables à basse énergie, nous obtenons des prédictions pour les sections efficaces de production des leptons et quarks de troisième génération au Leading Order (LO), au premier order en théorie des perturbations. En particulier, nous montrons comment les corrélations entre les sections efficaces peuvent être utilisées pour déterminer le modèle sous-jacent. Par la suite, le calcul de la section efficace de production électrofaible d'une paire de quarks top est présenté. Les corrections Next to Leading Order (NLO), à l'ordre $\mathcal{O}(\alpha_S \alpha_W^2)$ sont également incluses. Le résultat de ce calcul a été implémenté dans un générateur d'événements Monte Carlo qui permet de réaliser de maniére cohérente la fusion du calcul QCD NLO avec l'algorithme de parton shower.

Dans le chapitre 1, nous montrons comment les couplages des bosons Z' et W' peuvent être paramétrisés par un petit ensemble de paramètres communs. Les limites d'exclusion de ces paramètres, obtenues par une analyse globale récente des observables de basse énergie, ainsi que des donnes du LEP, sont discutées. Il est confirmé que les sections efficaces totales des bosons de jauge chargés et neutres se désintégrant en leptons et quarks de troisième génération sont accessibles au LHC jusqu'à des valeurs de masse de 5 TeV dans l'intervalle de paramètres autorisés. Une nouvelle méthode, très efficace pour distinguer les différents modèles basés sur le groupe de jauge $SU(2)\times SU(2)\times U(1)$ est également proposée. En effet, les sections efficaces totales ne permettent pas individuellement d'identifier le modèle sous-jacent de la classe G(221), alors que les corrélations de ces mêmes sections efficaces pourraient bien conduire à une identification unique.

Dans le chapitre 2, nous présentons le calcul des corrections NLO à la production électrofaible d'une paire de quarks top au sein de collisionneurs hadroniques dans les extensions du MS contenant un boson Z' supplémentaire. Au LHC, le quark top devrait être produit abondamment et toute déviation des prédictions du MS pourrait suggérer la présence de physique au-delà du MS. C'est pourquoi il est fondamental d'avoir des prédictions les plus précises possible pour les observables relatives au quark top. La contribution à l'arbre, ainsi que les corrections virtuelles et réelles à la production électrofaible d'une paire de quarks top sont calcules puis implémentées dans le générateur d'évènements Monte Carlo POWHEG BOX. Les divergences ultraviolettes, apparaissant dans le calcul des corrections NLO, sont traitées par la procédure de renormalisation, tandis que les divergences QCD infrarouges sont traitées automatiquement directement par POWHEG BOX dans le cadre du formalisme de soustraction de dipôle. Les divergences QED infrarouges sont pour

le moment régularisées en introduisant une masse non nulle pour le photon. La cohérence de notre calcul est minutieusement vérifiée. En effet, les prédictions au LO sont comparées aux prédictions de générateurs Monte Carlo à usage général. La cohérence des corrections NLO est vérifiée soit analytiquement, pour les corrections virtuelles, soit numériquement en utilisant les outils fournis par POWHEG BOX ou par comparaison avec les prédictions de générateurs Monte Carlo à usage général. Nous constatons que les corrections QCD NLO peuvent être très importantes, mais que les K-facteurs restent modestes dans la région de masse invariante centrée autour de la masse de la résonance. Il est également observé que les corrections réelles aux canaux quark-gluon à haute énergie contribuent de manière importante à la section efficace totale ce qui est dû à une forte luminosité quark-gluon.

Contents

Introduction

The Standard Model (SM) of particle physics [1, 2, 3, 4, 5, 6, 7, 8, 9] is very successful in describing a wealth of experimental data, but is widely believed to be incomplete. Be it by virtue of gauge group unification, extra dimensions or high scale strong dynamics, many theories beyond the SM predict the existence of new resonances with properties similar to that of the SM, namely the W and Z gauge bosons. The new resonances, often denoted as Z′- and W′-bosons, are massive, neutral and charged spin-1 particles respectively and mediate the neutral and charged current interactions of the SM fermions. If not too heavy, they could give clear signals at hadron colliders.

New heavy resonances with significant couplings to quarks and leptons are at hadron colliders most easily seen in the Drell-Yan (DY) process with dilepton and lepton plus missing transverse energy final states. The signals of the Drell-Yan channels are among the cleanest in the difficult environment of high-energy hadron colliders. Besides the DY channel, new heavy resonances are also searched for in processes in which a top quark is produced. The top quark is the only SM particle with a mass of the order of the electroweak symmetry breaking scale and a very short lifetime so that it decays before it can form any hadronic bound state. Owing to its extremely short lifetime and its large mass, careful measurements of top quark properties are likely to be sensitive to new physics.

While, in principle, it is possible to parametrize the interaction of new heavy resonances in a model independent manner, the Lagrangian describing such interactions has an abundance of free parameters. For practical reasons, therefore, it is desirable to restrict this freedom. In the Sequential Standard Model (SSM) [10], for example, the Z′ and W′ boson couplings are assumed to be SM-like and the only free parameter is their mass[1]. In other phenomenological studies such as [11, 12, 13, 14], the Z′- and W′-bosons are described by a *minimal* set of free parameters mimicking the behaviour of new resonances predicted in some popular models. If desirable, one can also study the phenomenology of a chosen model [15], or preferably study the collider signatures of a class of models, grouped by their theoretical origin, with a common parametrization in full generality [16, 17].

In this manuscript we present the collider phenomenology of a class of models motivated by the principle of gauge unification and characterized by an additional SU(2) group. The SM reposes on the ad hoc gauge group $\mathrm{SU}(3)_C \times \mathrm{SU}(2)_L \times \mathrm{U}(1)_Y$ with three unrelated factors. Their unification in a larger, simple group is theoretically very attractive. The possible unification groups have a rank equal or larger than the SM and thus also contain additional subgroups like a U(1) or a second SU(2). The SU(2) group has three generators and supplementing it to the gauge group of the SM implies the existence of three additional gauge bosons, out of which one turns out to be neutral, the Z′, and two charged, $\mathrm{W}'^{\pm}$.

After the discovery of a particle consistent with the SM Higgs boson [18, 19] at the Large

[1] Even though the width of Z′ and W′ bosons is fixed by their mass and couplings it is often taken to be a free parameter.

Hadron Collider (LHC), the search for new physics is one of the top priorities. The Z' and W' bosons are actively searched for but so far the LHC could only extend the bounds on the new physics scale. In experimental searches, in which the SSM is often taken as a benchmark scenario, the Z' and W' bosons should be accessible at LHC up to masses of 5 TeV [20], while with the present CMS (ATLAS) data masses below 2.96 (2.86) [21, 22] and 3.35 (2.55) TeV [23, 24] are excluded in the electron and muon channels. New neutral and charged resonances are also searched for in the top-pair and the single-top channels [25, 26, 27, 28] but the exclusion limits are typically less constraining than for new resonances decaying into leptons. Furthermore new resonances are searched for in τ lepton pairs [29, 30], dijets [31, 32], dibosons [33, 34, 35] or decaying into qW or qZ [36].

At the LHC, information about extended gauge symmetries can be obtained from cross section measurements, e.g. of pairs of leptons or top quarks [37, 38, 17, 16] or their associated production with W' bosons [39, 40], or measurements of the top quark polarization [41, 42, 43].

In Chapter 1 we study the LHC phenomenology of a class of models with an enlarged gauge sector in leading order accuracy. We start with a model independent Lagrangian describing charged and neutral currents beyond the SM. We then show how an extra gauge group implies the existence of new gauge bosons. Subsequently, we present the object of our study, namely the class of G(221) models. We derive a practical and intuitive common parametrization of Z' and W' masses and couplings and discuss their constraints derived from low-energy observables. Finally, we assume one of these bosons to have been observed and its mass to have been measured with a conservative error estimate and study how suitable correlations between cross sections at the LHC can be used to distinguish between the underlying G(221) models. We show that the total cross sections, while experimentally easily accessible, provide individually only partial information about the model realized in Nature. In contrast, correlations of these cross sections may well lead to a unique identification.

In Chapter 2 we shift towards next-to-leading order accuracy. We present a calculation of 1-loop corrections to the resonant production of a Z'-boson decaying into a pair of top quarks beyond the SM. Sections 2.2 and 2.3 present a detailed discussion on the analytic calculations followed by a description of the implementation of the NLO calculation in a Monte Carlo generator in Section 2.4. The calculation of next-to-leading corrections is a very time consuming task and we have tried to perform as much of it as possible in an automated fashion. Some aspects of the automation are described in Section 2.5 where we also give an overview of the tools we use and the way we interface them to minimize the user input. To conclude Chapter 2, in Section 2.6, we discuss the impact of 1-loop corrections to the top-pair production at the LHC.

A summary and an outlook is given in the last chapter and technical details of some of the calculations have been relegated to the appendices.

Chapter 1

Z′ and W′ bosons in theories with extended gauge symmetry

The SM of particle physics is very successful in describing a wealth of experimental data, but is widely believed to be incomplete. One of the reasons is that it reposes on the gauge group $\mathrm{SU}(3)_C \times \mathrm{SU}(2)_L \times \mathrm{U}(1)_Y$ with three unrelated factors, of which the second one violates parity, while the third one depends on the unphysical hypercharge. Their unification in a larger, simple group is theoretically very attractive. Beyond minimal SU(5), already ruled out from proton decay, the possible unification groups have a rank larger than the SM and thus also contain additional subgroups like U(1) or a second SU(2), which lead to additional neutral and charged gauge bosons, namely the Z′ and W′ bosons.

In this chapter we study the LHC phenomenology of SM extensions with an enlarged gauge group. We assume that the SM gauge group is supplemented by an additional SU(2) factor predicting the existence of both Z′- and W′-bosons. We begin by a looking at the Lagrangian describing the interaction of generic neutral and charged spin-1 gauge bosons with the SM fermions, referred to as the neutral and charged currents beyond the SM in Section 1.1. The appearance of Z′- and W′-bosons in theories with extended gauge sector is illustrated by a simple example in Section 1.2. In Section 1.3 we present the models from the G(221) class, explore the properties of Z′- and W′-bosons and show the exclusion limits on their masses and couplings derived from low-energy observables. Subsequently, we show the predictions for the new physics contribution to the total cross sections of lepton pair and third-generation quark pair production, their correlations and explore the reach and the distinguishability of G(221) models at the LHC. In the last section we draw our conclusions.

1.1 Neutral and charged currents beyond the Standard Model

The most general Lorentz and gauge invariant renormalizable Lagrangian describing the interaction of a neutral and a charged vector boson, here denoted as Z′- and W′-boson respectively, with the SM fermions can be written as [44]:

$$\mathcal{L}_{\mathrm{CC}}^{\mathrm{W}'} = \frac{g_W}{\sqrt{2}} \Big[\overline{\mathrm{u}}_i \gamma^\mu \left((C_{q,L}^{\mathrm{W}'})_{ij} P_L + (C_{q,R}^{\mathrm{W}'})_{ij} P_R \right) \mathrm{d}_j + \overline{\nu}_i \gamma^\mu \left((C_{\ell,L}^{\mathrm{W}'})_{ij} P_L + (C_{\ell,R}^{\mathrm{W}'})_{ij} P_R \right) \mathrm{e}_j \Big] \mathrm{W}'_\mu + h.c. \quad (1.1)$$

$$\mathcal{L}_{\rm NC}^{\rm Z'} = \frac{g_W}{\rm c_{\theta_W}} \left[\sum_q \overline{q}_i \gamma^\mu \left((C_{q,L}^{\rm Z'})_{ij} P_L + (C_{q,R}^{\rm Z'})_{ij} P_R \right) q_j \right.$$
$$\left. + \sum_\ell \overline{\ell}_i \gamma^\mu \left((C_{\ell,L}^{\rm Z'})_{ij} P_L + (C_{\ell,R}^{\rm Z'})_{ij} P_R \right) \ell_j \right] {\rm Z'}_\mu + h.c. \quad (1.2)$$

where $q \in \{\mathrm{u}_i, \mathrm{d}_j\}$, $\ell \in \{\nu_i, \mathrm{e}_j\}$ $(i,j = 1,2,3)$ are the SM fermions (including a right-handed neutrino) in the mass eigenstate basis. Furthermore, $P_{R,L} = (1 \pm \gamma_5)/2$, g_W is the $\mathrm{SU}(2)_L$ gauge coupling and θ_W is the Weinberg angle. The $C_{q,L(R)}$, $C_{\ell,L(R)}$ are arbitrary complex couplings that differ for quarks and leptons[1] and for trigonometric functions we use shorthand notation $\mathrm{s}_\phi = \sin\phi$, $\mathrm{c}_\phi = \cos\phi$, $\mathrm{t}_\phi = \tan\phi$. The form of the charged current (CC) and neutral current (NC) Lagrangians, $\mathcal{L}_{\rm NC}^{\rm Z'}$ and $\mathcal{L}_{\rm CC}^{\rm W'}$, is inspired by the Lagrangian describing the interactions of the SM Z- and W-boson. The CC and NC SM Lagrangian can be obtained from eqs. (1.1) and (1.2) by setting $C_{f,L}^{\rm Z'} = (T_3(f) - Q(f)\mathrm{s}^2_{\theta_W})\mathbb{1}$, $C_{f,R}^{\rm Z'} = -Q(f)\mathrm{s}^2_{\theta_W}\mathbb{1}$, $C_{q,L}^{\rm W'}$ to the CKM matrix, $C_{\ell,L}^{\rm W'}$ to the PMNS matrix and $C_{q(\ell),R}^{\rm W'} = 0$, where $T_3(f)$ and $Q(f)$ are the third component of the isospin and the charge of a given fermion f, respectively.

The Lagrangian in eqs. (1.1) and (1.2) contains many free parameters. For example, in the case of the W′-boson, there are 9 $q\overline{q}'$ vertices each of them having two couplings (independent combinations of vector, γ^μ, and axial-vector, $\gamma^\mu\gamma_5$, couplings) resulting in 18 free, complex couplings. Similarly, we have 18 free couplings to the leptons if right-handed neutrinos are included. Moreover, there are 6 $q\overline{q}$ and 6 $\ell\overline{\ell}$ neutral current vertices resulting in 24 free couplings[2]. If one would allow all of these parameters to be free a systematic and complete model independent collider phenomenology study would be unfeasible. On the other hand a detailed study of a particular realization of a chosen model may be too restrictive and thus not very interesting. The optimal approach may be to study a well motivated class of models predicting Z′- and W′-bosons with their couplings parametrized by a limited set of common free parameters. In this manuscript we present a collider phenomenology of such a class of models.

The Z′- and W′-bosons appear whenever the gauge group of the SM is extended, as the gauge bosons of the extra broken symmetries. An additional U(1) gauge group implies the existence of a Z′-boson, an additional SU(2) group the existence of both Z′- and W′-bosons. Note that, in the models with an extended gauge group, the discovery of a W′-boson naturally implies the existence of a Z′-boson, but not vice versa. In our work, we investigate the LHC phenomenology of a class of realistic theories beyond the SM with the electroweak gauge group extended to include an additional SU(2) group. Such models are often referred to as models belonging to the G(221) class. All our predictions are compared to the well known benchmark model often used in experimental analyses, the Sequential Standard Model (SSM), in which Z′- and W′-bosons have the same couplings to the SM fermions as the SM Z- and W-bosons and their masses are free parameters. We demonstrate that such a study is feasible and more importantly vital for the identification of the model realized in Nature, should a Z′- or W′-boson be observed at the LHC.

The best way to discover neutral and charged resonances that couple to SM quarks and leptons, such as the Z′- and W′-bosons, is in the spectrum of the invariant mass or transverse mass distribution. Resonant production of a vector boson and its subsequent decay into a pair of SM fermions

[1] If $(C_{\ell,R}^{\rm W'})_{ij} \neq 0$ then the ith generation includes a right-handed neutrino.

[2] Not counting the couplings to the right-handed neutrino.

will lead to a peak in the invariant (transverse) mass distribution of the fermion pair at the mass of the resonance. To be able to compute the invariant mass we have to know the momenta of both final states, which we do in the case that both final state particles are either charged (charged leptons), or their momentum can be fully reconstructed from their decay products (top quarks). If one final state particle is neutral its longitudinal component of the missing momentum cannot be reconstructed because of the collision fragments directed along the beam axis [45]. One, therefore, resorts to measuring the transverse mass instead. The invariant mass M_I and transverse mass M_T are defined as:

$$M_I^2 = (p_1 + p_2)^2 \ , \tag{1.3}$$

$$M_T^2 = (E_{T_1} + E_{T_2})^2 - (\vec{p}_{T_1} + \vec{p}_{T_2})^2 \ , \tag{1.4}$$

where p_i are the final state momenta, if known, or $\vec{p}_{T_i}$ the transverse momentum and $E_{T_i} = \sqrt{M_i^2 + p_{T_i}^2}$ the transverse energy, if the longitudinal component of the final state momenta cannot be reconstructed. Our work revolves around the searches of new gauge bosons in the invariant mass distribution of $\ell^+\ell^-$, $\mathrm{t\bar{t}}$, $\mathrm{t\bar{b}}$ and in the transverse mass distribution of $\ell^\pm\nu$ production at the LHC. Because the new physics contributions to the total cross section of the production of previously mentioned final states is rather low, we concentrate on observables measured right after the discovery like the total cross sections, the masses and eventually the widths of Z′-, W′-bosons. Most notably, we show that the total cross section for lepton and third-generation quark pairs, while experimentally accessible, provide individually only partial information about the model realized in Nature. In contrast, correlations of these cross sections in the neutral and charged current channels may well lead to a unique identification.

1.2 Extended electroweak gauge group

To illustrate the appearance of new neutral and charged gauge bosons when the electroweak gauge group of the SM is extended let us consider a simple quantum field theory with a local SU(2)×SU(2)×U(1) symmetry spontaneously broken down to a U(1) symmetry. Our aim is to show that, in general, a theory with a $\mathrm{SU}(2)_1\times\mathrm{SU}(2)_2\times\mathrm{U}(1)_X$ gauge group contains one additional neutral gauge boson, Z′, and two additional charged gauge bosons, $\mathrm{W}'^{\pm}$, as compared to a theory with a SU(2)×U(1) gauge group containing two neutral gauge bosons and two charged gauge bosons which are in the SM denoted as γ, Z and $\mathrm{W}^\pm$. We will also demonstrate how the particle content and its transformation properties, as well as the vacuum expectation values (VEVs) of the scalar sector enter the expressions for masses of the new gauge bosons and their couplings to the fermions summarized in eqs. (1.1) and (1.2).

For simplicity, let us assume that the particle content comprises of only two fermion fields F_1 and F_2, F_1 transforming as a doublet under $\mathrm{SU}(2)_1$ and as a singlet under $\mathrm{SU}(2)_2$, F_2 transforming as a doublet under $\mathrm{SU}(2)_2$ and as a singlet under $\mathrm{SU}(2)_1$. The $\mathrm{U}(1)_X$ charge of the fermions F_i, an analogue of the SM hypercharge, is equal to $-1/2$. After gauging the symmetry, the particle content will contain spin-1 fields W_1, W_2 and B corresponding to the factors of the underlying gauge group, $\mathrm{SU}(2)_1$, $\mathrm{SU}(2)_2$, and $\mathrm{U}(1)_X$, respectively. In order to break the symmetry $\mathrm{SU}(2)_1\times\mathrm{SU}(2)_2\times\mathrm{U}(1)_X$ down to U(1), we introduce two complex scalar fields H_1, H_2 transforming just like the fermions F_1, F_2, with the exception of the $\mathrm{U}(1)_X$ charge being equal to 1/2. The particle content can be summarized as

$$F_1 \sim (\mathbf{2},\mathbf{1},-1/2), \quad F_2 \sim (\mathbf{1},\mathbf{2},-1/2), \quad H_1 \sim (\mathbf{2},\mathbf{1},1/2), \quad H_2 \sim (\mathbf{1},\mathbf{2},1/2), \tag{1.5}$$

where the numbers in the parenthesis denote the charge assignments under the $\mathrm{SU}(2)_1 \times \mathrm{SU}(2)_2 \times \mathrm{U}(1)_X$ group.

The kinetic part of the most general Lagrangian invariant under a $\mathrm{SU}(2)_1 \times \mathrm{SU}(2)_2 \times \mathrm{U}(1)_X$ gauge group, $\mathcal{L}_{221}$, reads

$$\mathcal{L}_{221}^{\mathrm{kin}} \;=\; \cdots \;-\; \overline{F}_1 \not{D} F_1 \;-\; \overline{F}_2 \not{D} F_2 \;-\; (D_\mu H_1)^\dagger (D^\mu H_1) \;-\; (D_\mu H_2)^\dagger (D^\mu H_2) \;+\; \cdots, \quad (1.6)$$

where we show only the terms relevant for the mass spectrum of the gauge bosons and their couplings to the fermions, since the full Lagrangian is rather lengthy. According to the transformation properties of the particle content in eq. (1.5), the covariant derivatives of the fermions F_1, F_2 and scalars H_1, H_2 can be written as

$$D_\mu F_i = \partial_\mu F_i + \left[-\delta^{ij} \frac{i g_j}{2} (W_j)^a_\mu \tau_a + \frac{i g_X}{2} B_\mu \right] F_i, \quad (1.7)$$

$$D_\mu H_i = \partial_\mu H_i + \left[-\delta^{ij} \frac{i g_j}{2} (W_j)^a_\mu \tau_a - \frac{i g_X}{2} B_\mu \right] H_i, \quad (1.8)$$

where the matrices τ_a, corresponding the generators of a SU(2) group, are the usual Pauli matrices, and g_1, g_2, g_X are the coupling constants associated with the gauge group factors $\mathrm{SU}(2)_1$, $\mathrm{SU}(2)_2$, $\mathrm{U}(1)_X$ respectively.

Now, let us assume that the symmetry is spontaneously broken via non-zero VEVs of the neutral components of the scalar fields H_i:

$$\langle H_i \rangle = \frac{1}{\sqrt{2}} v_i \begin{pmatrix} 0 \\ 1 \end{pmatrix}. \quad (1.9)$$

After contracting the vector fields $(W_i)^a_\mu$ with the Pauli matrices τ_a, substituting the VEVs from eq. (1.9) and the covariant derivatives from eq. (1.8) into the expression for the Lagrangian in eq. (1.6), the scalar field kinetic term containing gauge boson mass terms becomes

$$\begin{aligned} -\sum_i (D_\mu H_i)^\dagger (D^\mu H_i) = \cdots &- \frac{1}{4} g_1^2 v_1^2 \mathrm{W}^+_\mu \mathrm{W}^{-\mu} - \frac{1}{8} v_1^2 (-g_1 (W_1)_{3\mu} + g_X B_\mu)(-g_1 (W_1)^{3\mu} + g_X B^\mu) \\ &- \frac{1}{4} g_2^2 v_2^2 \mathrm{W}'^+_\mu \mathrm{W}'^{-\mu} - \frac{1}{8} v_2^2 (-g_2 (W_2)_{3\mu} + g_X B_\mu)(-g_2 (W_2)^{3\mu} + g_X B^\mu) + \cdots \end{aligned} \quad (1.10)$$

where we display only the terms proportional to v_i^2 and we have introduced

$$\mathrm{W}^\pm_\mu = \frac{1}{\sqrt{2}} \left((W_1)^1_\mu \mp i (W_1)^2_\mu \right), \qquad \mathrm{W}'^\pm_\mu = \frac{1}{\sqrt{2}} \left((W_2)^1_\mu \mp i (W_2)^2_\mu \right). \quad (1.11)$$

The mass terms for the linear combinations $\mathrm{W}^\pm_\mu$, $\mathrm{W}'^\pm_\mu$ can be written in a convenient matrix form

$$\begin{pmatrix} \mathrm{W}^{\pm\mu} & \mathrm{W}'^{\pm\mu} \end{pmatrix} \begin{pmatrix} M^2_{\mathrm{W}} & 0 \\ 0 & M^2_{\mathrm{W}'} \end{pmatrix} \begin{pmatrix} \mathrm{W}^\pm_\mu \\ \mathrm{W}'^\pm_\mu \end{pmatrix} \quad (1.12)$$

with masses $M_{\mathrm{W}} = g_1 v_1/2$, $M_{\mathrm{W}'} = g_2 v_2/2$. Since the mass matrix in eq. (1.12) is diagonal, the flavour eigenstates[3] $\mathrm{W}^\pm_\mu$, $\mathrm{W}'^\pm_\mu$ of our simple example align with the mass eigenstates of the

[3]It is possible to show, that the linear combinations $\mathrm{W}^\pm_\mu$, $\mathrm{W}'^\pm_\mu$ transform as $\delta \mathrm{W}^\pm_\mu = \pm i\omega \mathrm{W}^\pm_\mu$, $\delta \mathrm{W}'^\pm_\mu = \pm i\omega \mathrm{W}'^\pm_\mu$ under U(1) gauge transformation, where ω corresponds to an infinitesimal shift. They thus correspond to flavour eigenstates of the Lagrangian $\mathcal{L}_{221}$ with charges ± 1 of the remaining unbroken U(1) symmetry.

Lagrangian. The theory described by the Lagrangian $\mathcal{L}_{221}$ will thus contain two pairs of charged gauge bosons $\mathrm{W}^{\pm}$, $\mathrm{W}'^{\pm}$, with independent masses M_{W}, $M_{\mathrm{W}'}$ respectively. In general, the mass matrix is not diagonal, flavour eigenstates mix and the mass matrix needs to be diagonalized to obtain the mass eigenstates.

Similarly, the mass terms of the remaining fields, $(W_1)^{3\mu}$, $(W_2)^{3\mu}$ and B^{μ}, can be written as

$$\begin{pmatrix} (W_1)^3_\mu & (W_2)^3_\mu & B_\mu \end{pmatrix} \begin{pmatrix} g_1^2 v_1^2 & 0 & g_1 g_X v_1^2 \\ 0 & g_2^2 v_2^2 & g_2 g_X v_2^2 \\ g_1 g_X v_1^2 & g_2 g_X v_2^2 & g_X^2 (v_1^2 + v_2^2) \end{pmatrix} \begin{pmatrix} (W_1)^{3\mu} \\ (W_2)^{3\mu} \\ B^{\mu} \end{pmatrix} . \tag{1.13}$$

Assuming, that the symmetry of the group $\mathrm{SU}(2)_2$ is broken at much higher scale than that of the group $\mathrm{SU}(2)_1$, $v_1^2/v_2^2 \to 0$, the mass matrix in eq. (1.13) can be diagonalized by an orthogonal mixing matrix parametrized by two mixing angles[4]

$$\mathrm{t}_{\phi_1} = g_1 \sqrt{\frac{1}{g_X^2} + \frac{1}{g_2^2}}, \quad \mathrm{t}_{\phi_2} = \frac{g_2}{g_X}. \tag{1.14}$$

The mass matrix from eq. (1.13) can be diagonalized and written as

$$\begin{pmatrix} \gamma_\mu & \mathrm{Z}_\mu & \mathrm{Z}'_\mu \end{pmatrix} \begin{pmatrix} 0 & 0 & 0 \\ 0 & g_X^2 v_1^2 \frac{\mathrm{s}^2_{\phi_1}}{\mathrm{c}^2_{\phi_2}} & 0 \\ 0 & 0 & g_X^2 v_2^2 \frac{1}{\mathrm{c}^2_{\phi_1}} \end{pmatrix} \begin{pmatrix} \gamma^\mu \\ \mathrm{Z}^\mu \\ \mathrm{Z}'^\mu \end{pmatrix} . \tag{1.15}$$

The theory described by the Lagrangian $\mathcal{L}_{221}$ will thus on top of two charged gauge boson pairs also contains three neutral gauge bosons γ, Z, Z′, out of which one is massless and two are massive with independent masses M_{Z}, $M_{\mathrm{Z}'}$ respectively. In the limit $v_1^2/v_2^2 \to 0$, the mass of the Z′ boson will be much larger than the one of the Z boson, $M_{\mathrm{Z}}^2/M_{\mathrm{Z}'}^2 \to 0$. The mass eigenstates of the Lagrangian γ^μ, Z^μ, Z'^μ can be expressed in terms of the $(W_1)^{3\mu}$, $(W_2)^{3\mu}$, B^μ fields as

$$\begin{aligned} \gamma^\mu &= -\mathrm{c}_{\phi_1}(W_1)^{3\mu} - \mathrm{s}_{\phi_1}\mathrm{c}_{\phi_2}(W_2)^{3\mu} + \mathrm{s}_{\phi_1}\mathrm{s}_{\phi_2} B^\mu, \\ \mathrm{Z}^\mu &= -\mathrm{s}_{\phi_1}(W_1)^{3\mu} - \mathrm{c}_{\phi_1}\mathrm{c}_{\phi_2}(W_2)^{3\mu} + \mathrm{c}_{\phi_1}\mathrm{s}_{\phi_2} B^\mu, \\ \mathrm{Z}'^\mu &= \qquad\qquad - \quad \mathrm{s}_{\phi_2}(W_2)^{3\mu} + \quad \mathrm{c}_{\phi_2} B^\mu. \end{aligned} \tag{1.16}$$

The inverse mapping from $\{\gamma^\mu, \mathrm{Z}^\mu, \mathrm{Z}'^\mu\}$ into $\{(W_1)^{3\mu}, (W_2)^{3\mu}, B^\mu\}$ can be obtained simply by transposing the corresponding mixing matrix since the mapping is orthogonal.

Let us now have a look at the couplings of the Z′-boson to the SM fermions. By making use of the expression for the covariant derivative in eq. (1.7) and by changing the basis from $\{(W_1)^{3\mu}, (W_2)^{3\mu}, B^\mu\}$ to $\{\gamma, \mathrm{Z}, \mathrm{Z}'\}$, the kinetic term for the fermions F_i becomes

$$-\sum_i \frac{1}{2}\overline{F}_i \not{D} F_i = \cdots - \frac{i}{4} g_1 \mathrm{s}_{\phi_2} \mathrm{Z}'_\mu \overline{F_1^-} \gamma^\mu F_1^- - \frac{i}{4} g_2 \mathrm{c}_{\phi_2} \mathrm{Z}'_\mu \overline{F_2^-} \gamma^\mu F_2^- + \cdots , \tag{1.17}$$

where F_i^- denotes the negatively charged component of the fermion doublet

$$F_i = \begin{pmatrix} F_i^0 \\ F_i^- \end{pmatrix} . \tag{1.18}$$

[4]Recall the shorthand notation introduced in the previous section $\mathrm{s}_\phi = \sin\phi$, $\mathrm{c}_\phi = \cos\phi$, $\mathrm{t}_\phi = \tan\phi$.

Note that the U(1) charge of the components of a fermion doublet can be calculated as the sum of the third components of $SU(2)_1$ and $SU(2)_2$ isospin plus the $U(1)_X$ charge. The Z′-boson, will couple to the charged components of the fermion doublets F_1, F_2 with different strengths as a result of the fact that F_1, F_2 are doublets under different gauge groups. The couplings of Z′-boson to the neutral components of fermion doublets F_i, as well as the couplings of the W′-boson can be obtained in a similar fashion.

In conclusion, in a theory with a $SU(2)_1 \times SU(2)_2 \times U(1)_X$ gauge group one extra neutral gauge boson, Z′, and two extra charged gauge bosons, $W'^{\pm}$, appear as compared to a theory with a $SU(2) \times U(1)$ gauge group. The masses of the additional gauge bosons will be functions of the scalar field VEVs, the couplings g_1, g_2, g_X and mixing angles constructed out of the ratios of these couplings. We will show, in one of the following sections, that the dominant contributions to the couplings of the Z′-, W′-bosons in the extensions of the SM with extended electroweak sector by an additional SU(2) group can be expressed in terms of the electroweak coupling, g_W, the Weinberg angle θ_W and one additional mixing angle in the form of the Lagrangian in eqs. (1.1), (1.2).

1.3 G(221) models

While the recent discovery of non-zero neutrino masses [46, 47], possibly generated by a see-saw mechanism and the prospect of parity restoration point in the direction of a left-right (LR) symmetric group containing a $SU(2)_R$, the large hierarchy in the mass spectrum of the SM fermions motivates fermion un-unified (UU) or generation non-universal (NU) groups $SU(2)_2$ and $SU(2)_1$, broken at high and low (SM-like) vacuum expectation values u and v. In general, a large variety of models with a second SU(2) subgroup exist. Often denoted as G(221) models, they also appear naturally in larger unification groups like SO(10) and E_6 and in many string theory compactifications.

The G(221) class, thus, comprises of models with an extended gauge group. More specifically, the electroweak part of the SM gauge group, $SU(2)_L \times U(1)_Y$, is in G(221) models replaced by the $SU(2)_1 \times SU(2)_2 \times U(1)_X$ gauge group. As discussed in the previous section, the particle content of G(221) models is consequently richer than that of the SM. The fermionic content is usually unchanged, however, some of the models may need additional fermion fields assuring the cancellation of gauge anomalies[5] and thus their renormalizability. The gauge sector contains three additional gauge bosons, the neutral Z′-boson and W′-boson with electric charge either $+1$ or -1. The particle content is also extended to contain extra scalars breaking the additional SU(2) symmetry.

1.3.1 Symmetry breaking in G(221) models

In Nature a local $U(1)_{\rm em}$ symmetry is observed. So that the G(221) models describe the experiment, the $SU(2)_1 \times SU(2)_2 \times U(1)_X$ group has to be broken down to the $U(1)_{\rm em}$ group. This symmetry breaking is usually realized in two steps and at two energy scales. In the first step, $SU(2)_1 \times SU(2)_2 \times U(1)_X$ is broken down to the gauge group of the SM, which in the second step is broken down to $U(1)_{\rm em}$. The representations and the VEVs of the scalars are arranged such that the masses of additional vector bosons are large enough neither to have any measurable impact on low-energy observables nor to have been already observed at collider experiments. On the other hand, the VEV of the scalar field triggering the first stage symmetry breaking, realized at a large

[5] One usually assumes that the additional fermion fields needed for anomaly cancellation are very heavy and decouple.

energy scale, can be chosen such that the masses of additional Z′- and W′-bosons are still low enough to be within the reach of the LHC.

G(221) models can be classified according to their symmetry breaking pattern [48]. Identification of $\mathrm{SU}(2)_1$ with the one of the SM implies in the simplest scenarios the breaking scheme $\mathrm{SU}(2)_2{\times}\mathrm{U}(1)_X{\to}\mathrm{U}(1)_Y$ at the scale u through a Higgs doublet (D) or triplet (T). This scheme applies not only to LR [49], but also to leptophobic (LP), hadrophobic (HP) and to fermiophobic (FP) models [50]. In contrast, identification of $\mathrm{U}(1)_X$ with the hypercharge group of the SM as in the UU [51] and NU [52] models leads to the breaking scheme $\mathrm{SU}(2)_1{\times}\mathrm{SU}(2)_2{\to}\,\mathrm{SU}(2)_L$ through a Higgs bi-doublet at the scale u. This classification can be summarized as:

- *right-handed* models (pattern 1): LR, LP, HP and FP models
  $\mathrm{SU}(2)_1 \equiv \mathrm{SU}(2)_L$, $\mathrm{SU}(2)_L{\times}\mathrm{SU}(2)_2{\times}\mathrm{U}(1)_X \to \mathrm{SU}(2)_L{\times}\mathrm{U}(1)_Y \to\ \mathrm{U}(1)_{\mathrm{em}}$

- *left-handed* models (pattern 2): UU, NU models
  $\mathrm{U}(1)_X \equiv \mathrm{U}(1)_Y$, $\mathrm{SU}(2)_1{\times}\mathrm{SU}(2)_2{\times}\mathrm{U}(1)_Y \to \mathrm{SU}(2)_L{\times}\mathrm{U}(1)_Y \to\ \mathrm{U}(1)_{\mathrm{em}}$

where we employ different model category names[6] as compared to the classification in [48]. The W′-bosons of *left-handed* models couple only to left-handed fermions, while in the *right-handed* models the couplings of the W′-boson to the left-handed SM fermions, induced by a mixing of the W′-boson and the SM W-boson, is strongly constrained by low energy observables and precision data.

Table 1.1: The charge assignments of the SM fermions under the $G(221)$ gauge groups [48]. Unless otherwise specified, the charge assignments apply to all three generations.

Cat.	Model	$SU(2)_1$	$SU(2)_2$	$U(1)_X$
left-handed	un-unified (UU)	$\begin{pmatrix} u_L \\ d_L \end{pmatrix}$	$\begin{pmatrix} \nu_L \\ e_L \end{pmatrix}$	Y_{SM} for all fermions.
	non-universal (NU)	$\begin{pmatrix} u_L \\ d_L \end{pmatrix}_{1^{\mathrm{st}},2^{\mathrm{nd}}}, \begin{pmatrix} \nu_L \\ e_L \end{pmatrix}_{1^{\mathrm{st}},2^{\mathrm{nd}}}$	$\begin{pmatrix} u_L \\ d_L \end{pmatrix}_{3^{\mathrm{rd}}}, \begin{pmatrix} \nu_L \\ e_L \end{pmatrix}_{3^{\mathrm{rd}}}$	Y_{SM} for all fermions.
right-handed	left-right (LR)	$\begin{pmatrix} u_L \\ d_L \end{pmatrix}, \begin{pmatrix} \nu_L \\ e_L \end{pmatrix}$	$\begin{pmatrix} u_R \\ d_R \end{pmatrix}, \begin{pmatrix} \nu_R \\ e_R \end{pmatrix}$	$\frac{1}{6}$ for quarks, $-\frac{1}{2}$ for leptons.
	leptophobic (LP)	$\begin{pmatrix} u_L \\ d_L \end{pmatrix}, \begin{pmatrix} \nu_L \\ e_L \end{pmatrix}$	$\begin{pmatrix} u_R \\ d_R \end{pmatrix}$	$\frac{1}{6}$ for quarks, Y_{SM} for leptons.
	hadrophobic (HP)	$\begin{pmatrix} u_L \\ d_L \end{pmatrix}, \begin{pmatrix} \nu_L \\ e_L \end{pmatrix}$	$\begin{pmatrix} \nu_R \\ e_R \end{pmatrix}$	Y_{SM} for quarks, $-\frac{1}{2}$ for leptons.
	fermiophobic (HP)	$\begin{pmatrix} u_L \\ d_L \end{pmatrix}, \begin{pmatrix} \nu_L \\ e_L \end{pmatrix}$		Y_{SM} for all fermions.

[6] For reference, the original model category names, as in [48], are listed in the parentheses.

Table 1.1 shows the transformation properties, or charge assignments, of the SM fermions under the $SU(2)_1$, $SU(2)_2$ and $U(1)_X$ groups, where $f_{L(R)}$ denotes left(right)-handed fermions of the SM, $P_{L(R)}f$. In the UU model, the universality of quark and lepton couplings postulated in the SM is removed and quarks and leptons are in doublet representations of different SU(2) groups. The NU model, on the other hand, questions the universality of couplings across generations of fermions. A special role is attributed to the 3$^{\text{rd}}$ generation of SM fermions which transform as doublets under one group, while the 1$^{\text{st}}$ and 2$^{\text{nd}}$ generation transform as doublets under the other SU(2). The LR model extends the particle content by 3 families of right-handed neutrinos such that the right-handed fermions can be put under the doublet representation of one of the SU(2) groups similar to the left-handed SM fermions. In the LP model, only the right-handed quarks transform as doublets and the right-handed neutrinos are absent. The W$'$ in this model is leptophobic, i.e. its couplings to the left- and right-handed leptons are suppressed. Similarly, the W$'$ couplings to quarks and fermions are suppressed in the HP and FP models, respectively. The details of the scalar sector in G(221) models are shown in Table 1.2.

Table 1.2: These tables display the model-specific scalar field representations and VEVs that achieve the symmetry breaking of G(221) models [48].

First stage breaking		
	Rep.	Multiplet and VEV
LR-D, LP-D, HP-D, FP-D	$\Phi \sim (1, 2, \frac{1}{2})$	$\Phi = \begin{pmatrix} \phi^+ \\ \phi^0 \end{pmatrix}$, $\langle\Phi\rangle = \frac{1}{\sqrt{2}} \begin{pmatrix} 0 \\ u_{\text{D}} \end{pmatrix}$
LR-T, LP-T, HP-T, FP-T	$\Phi \sim (1, 3, 1)$	$\Phi = \frac{1}{\sqrt{2}} \begin{pmatrix} \phi^+ & \sqrt{2}\phi^{++} \\ \sqrt{2}\phi^0 & -\phi^+ \end{pmatrix}$, $\langle\Phi\rangle = \frac{1}{\sqrt{2}} \begin{pmatrix} 0 & 0 \\ u_{\text{T}} & 0 \end{pmatrix}$
UU, NU	$\Phi \sim (2, \overline{2}, 0)$	$\Phi = \begin{pmatrix} \phi^0 + \pi^0 & \sqrt{2}\pi^+ \\ \sqrt{2}\pi^- & \phi^0 - \pi^0 \end{pmatrix}$, $\langle\Phi\rangle = \frac{1}{\sqrt{2}} \begin{pmatrix} u & 0 \\ 0 & u \end{pmatrix}$

Second stage breaking		
	Rep.	Multiplet and VEV
LR-D, LP-D, HP-D, FP-D	$H \sim (2, \overline{2}, 0)$	$H = \begin{pmatrix} h_1^0 & h_1^+ \\ h_2^- & h_2^0 \end{pmatrix}$, $\langle H\rangle = \frac{v}{\sqrt{2}} \begin{pmatrix} c_\beta & 0 \\ 0 & s_\beta \end{pmatrix}$
LR-T, LP-T, HP-T, FP-T	$H \sim (2, \overline{2}, 0)$	$H = \begin{pmatrix} h_1^0 & h_1^+ \\ h_2^- & h_2^0 \end{pmatrix}$, $\langle H\rangle = \frac{v}{\sqrt{2}} \begin{pmatrix} c_\beta & 0 \\ 0 & s_\beta \end{pmatrix}$
UU, NU	$H \sim (1, 2, \frac{1}{2})$	$H = \begin{pmatrix} h^+ \\ h^0 \end{pmatrix}$, $\langle H\rangle = \frac{v}{\sqrt{2}} \begin{pmatrix} 0 \\ 1 \end{pmatrix}$

Parameterizing the model dependence in terms of the tangent of the mixing angle $\tan\phi = g_X/g_2$ (LR, LP, HP, FP) or g_2/g_1 (UU, NU) at the first breaking stage, the ratio of the squared Higgs VEVs $x = u^2/v^2$, and the alignment angle β of the light Higgs fields in the case of the first breaking pattern, Hsieh *et al.* have been able to perform a global analysis of low-energy and electroweak precision data with an effective Lagrangian approach [48] which resulted essentially in lower bounds on the masses of the Z$'$- and W$'$-bosons. The global constraints have been obtained on the basis of a number of theoretical assumptions, in particular generation-diagonal, perturbative

gauge couplings (smaller than $\sqrt{4\pi}$), minimal (doublet, triplet or bi-doublet) Higgs sectors with a hierarchy of VEVs ($u \gg v$), validity of the Appelquist-Carazzone decoupling theorem [53], and negligible influence of additional fermions required, *e.g.*, for the cancellation of gauge anomalies. Fixed reference observables were the electromagnetic fine structure constant α, the Fermi constant G_F determining v^2, and the mass of the SM Z boson $M_{\rm Z}$ fixing the tangent of the weak mixing angle $s_\theta/c_\theta = g_Y/g_L$. Similar to the SM analysis of the Particle Data Group (PDG) [44], the two (three) free parameters were fit to 37 observables, of which the most important ones were the total hadronic cross section at the Z pole, the b-quark forward-backward asymmetry, the neutrino-nucleon deep inelastic scattering cross section, and the parity-violating weak charge of Caesium 133. Low-energy constraints like BR($b \to s\gamma$) requiring information on the extended flavor structure of the models (*e.g.* the right-handed CKM matrix) were voluntarily omitted. Fixing the top quark and light Higgs-boson masses to their SM best-fit values had little influence on the results, which led to lower bounds on the Z' and W' masses ranging from 0.3 to 3.6 TeV depending on the particular G(221) model.

In the following sections, we summarize the properties of the Z′- and W′-bosons predicted in models from the *left-* and *right-handed* categories. In the first step we show how their couplings to the SM fermions [48], expressed in terms of g_1, g_2, g_X can be rewritten in terms of the SM electroweak coupling g_W, the Weinberg angle θ_W and extra G(221) parameters instead. We then show the constraints on these models derived from low-energy observables in mass vs. coupling planes, instead of v^2/u^2 vs. coupling planes used in [48].

1.3.2 *Left-handed* models

The models in the *left-handed* category are the UU (un-unified) and NU (non-universal) models. Their symmetry breaking can be described by the first and second stage mixing angles[7].

$$\mathrm{t}_\phi = \frac{g_2}{g_1}, \quad \mathrm{t}_\theta = \frac{g_W}{g_Y}, \tag{1.19}$$

where

$$g_W = \left(\frac{1}{g_1^2} + \frac{1}{g_2^2}\right)^{-1/2}, \quad g_Y = g_X. \tag{1.20}$$

The electric charge is given by

$$\frac{1}{e^2} = \frac{1}{g_1^2} + \frac{1}{g_2^2} + \frac{1}{g_X^2}, \tag{1.21}$$

and the gauge couplings g_1, g_2, g_X can be written in terms of the mixing angles ϕ, θ and the electric charge as follows

$$g_1 = \frac{e}{\mathrm{s}_\phi \mathrm{s}_\theta}, \quad g_2 = \frac{e}{\mathrm{c}_\phi \mathrm{s}_\theta}, \quad g_X = \frac{e}{\mathrm{c}_\theta}. \tag{1.22}$$

The expression for the masses of the Z′- and W′-bosons and their couplings to the SM fermions contain only two extra free parameters. The first stage symmetry breaking mixing angle ϕ and the VEV u. All the other parameters, can be identified with the (free) parameters of the SM which can be extracted from experiment. For example, the second stage mixing angle θ must be equal to the Weinberg angle θ_W within the precision of measurement and the second stage VEV v can be obtained from the measurement of the W-bosons mass[8]. Similarly, had the Z′- or W′-boson been

[7] Two mixing angles are sufficient for the description of the symmetry breaking only in the presence of a hierarchy of VEVs ($u \gg v$).

[8] Note that the experimentally observed W-boson is in the G(221) models the lighter mass eigenstate of the W_1 and W_2 system.

observed, one could use its mass $M_{\mathrm{Z}'(\mathrm{W}')}$ to fix the value of the first stage breaking VEV u. Instead of parametrizing the W′- and Z′-boson masses and couplings by $\{\phi, u\}$ they can be parametrized by $\{t = \mathrm{t}_\phi, M_{\mathrm{W}'(\mathrm{Z}')}\}$.

In *left-handed* models, it is found that the Z′- and W′-bosons are almost degenerate, $M^2_{\mathrm{Z}'}/M^2_{\mathrm{W}'} = 1 + \mathcal{O}(v^2/u^2)$ [48]. Thus, hereafter, when referring to the Z′- or W′-boson predicted by *left-handed* models we will use the symbol M to denote both of their masses

$$M^2 = M^2_{\mathrm{W}'(\mathrm{Z}')} = \frac{1}{4}\left(g_1^2 + g_2^2\right)u^2 + \frac{\mathrm{s}^2_\phi}{4} g_2^2 v^2 + \mathcal{O}(v^4/u^4). \tag{1.23}$$

The expressions for the Z′- and W′-boson couplings in terms of $\{t = \mathrm{t}_\theta, M\}$ can be obtained in the following way. The couplings in terms of the gauge couplings g_1, g_2, g_X, the mixing angles θ, ϕ and the squared ratio of the VEVs u and v, extracted from [48], are listed in Tables A.1 and A.2 in Appendix A. In the first step, we substitute eqs. (1.22) and (1.20) into the expression for the full CC and NC Lagrangian in eq. (A.1) in Appendix A. In the second step, we solve eq. (1.23) for the VEV u expressed in terms of the resonance mass M and the mixing angle ϕ, which we consequently substitute into the Lagrangian in eq. (A.1). In the UU model this leads to

$$\begin{aligned}
C^{\mathrm{W}'}_{q,L} &= \frac{1}{t} - \mathrm{c}_\theta \epsilon(t, M), & C^{\mathrm{W}'}_{q,R} &= 0,\\
C^{\mathrm{Z}'}_{q,L} &= T_3(f)\mathrm{c}_\theta \frac{1}{t} + (T_3(f) + Q(f)s^2_\theta)\epsilon(t, M), & C^{\mathrm{Z}'}_{q,R} &= Q(f)\mathrm{s}^2_\theta \epsilon(t, M),\\
C^{\mathrm{W}'}_{l,L} &= -t - \mathrm{c}_\theta \epsilon(t, M), & C^{\mathrm{W}'}_{l,R} &= 0,\\
C^{\mathrm{Z}'}_{l,L} &= -T_3(f)\mathrm{c}_\theta t + (T_3(f) + Q(f)\mathrm{s}^2_\theta)\epsilon(t, M), & C^{\mathrm{Z}'}_{l,R} &= Q(f)\mathrm{s}^2_\theta \epsilon(t, M).
\end{aligned} \tag{1.24}$$

Similarly, in the NU model the couplings read

$$\begin{aligned}
C^{\mathrm{W}'}_{1^{\mathrm{st}}(2^{\mathrm{nd}}),L} &= \frac{1}{t} - \mathrm{c}_\theta \epsilon(t, M), & C^{\mathrm{W}'}_{1^{\mathrm{st}}(2^{\mathrm{nd}}),R} &= 0,\\
C^{\mathrm{Z}'}_{1^{\mathrm{st}}(2^{\mathrm{nd}}),L} &= T_3(f)\mathrm{c}_\theta \frac{1}{t} + (T_3(f) + Q(f)s^2_\theta)\epsilon(t, M), & C^{\mathrm{Z}'}_{1^{\mathrm{st}}(2^{\mathrm{nd}}),R} &= Q(f)\mathrm{s}^2_\theta \epsilon(t, M),\\
C^{\mathrm{W}'}_{3^{\mathrm{rd}},L} &= -t - \mathrm{c}_\theta \epsilon(t, M), & C^{\mathrm{W}'}_{3^{\mathrm{rd}},R} &= 0,\\
C^{\mathrm{Z}'}_{3^{\mathrm{rd}},L} &= -T_3(f)\mathrm{c}_\theta t + (T_3(f) + Q(f)\mathrm{s}^2_\theta)\epsilon(t, M), & C^{\mathrm{Z}'}_{3^{\mathrm{rd}},R} &= Q(f)\mathrm{s}^2_\theta \epsilon(t, M),
\end{aligned} \tag{1.25}$$

where q and l in the subscript of C denote SM quarks and leptons, while $1^{\mathrm{st}}(2^{\mathrm{nd}})$ and 3^{rd} denote the first(second) and third generation of SM fermions. Furthermore $T_3(f)$ is the sum of the third components of the $\mathrm{SU}(2)_1$ and $\mathrm{SU}(2)_2$ isospin[9], $Q(f)$ the electric charge and the CKM mixing matrix has been omitted[10]. The $\epsilon(t, M)$ function collects terms proportional to t/M^2 and thus strongly suppressed. Note that the value of t does not necessarily have to be positive and all the couplings, including the $\epsilon(t, M)$ function, are odd in t. The Z′- and W′-bosons predicted by *left-handed* models are both left-handed. That is, similar to the SM W-boson, the right-handed W′ couplings are equal to zero. On the other hand the right-handed Z′ couplings are strongly suppressed, in contrast to the SM Z-boson whose right-handed couplings are sizable.

The exclusion limits, derived from low-energy and electroweak precision data [48], in the $\{t, M\}$ plane are displayed in Figure 1.1. *Left-handed* models are quite constrained, in particular new

[9]The sum of the third components of $\mathrm{SU}(2)_1$ and $\mathrm{SU}(2)_2$ isospin for SM fermions in G(221) models can be identified with the third component of the $SU(2)_L$ isospin in the SM.

[10]To restore the CKM matrix one just needs to multiply the W′-boson couplings to the SM quarks by V_{CKM}.

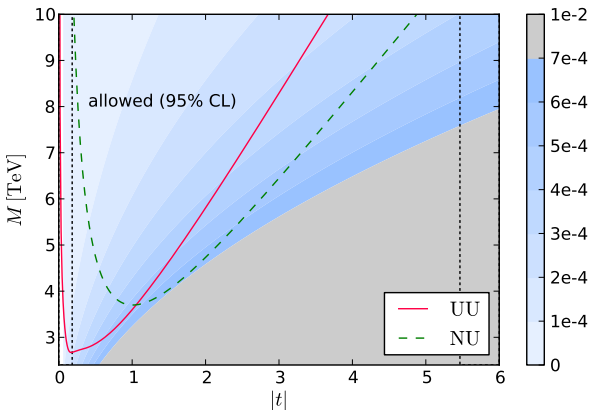

Figure 1.1: Exclusion limits for *left-handed* models. The full and the dashed line represent the 95% confidence level contours, the area outside of the area bounded by the dotted lines represents the regions where at least one of the gauge couplings becomes non-perturbative. The shaded contours represent values of $\epsilon(t, M)$.

resonances in the NU model are excluded up to 3.6 TeV, while their mass in the UU model can go down to 2.5 TeV. However, there is still a significant portion of the allowed parameter space reachable at the LHC with $\sqrt{s} = 14$ TeV, as we shall see in Section 1.4.1.

For completeness, we also show the dependence of ratios of various W′- and Z′-bosons couplings over the corresponding SM W- and Z-boson couplings on the t parameter with the $\epsilon(t, M)$ set to zero by hand. Note that if $\epsilon(t, M) = 0$, the tangent of the first stage mixing angle t is the only free parameter in the expressions for the couplings. The values of $\epsilon(t, M)$ in the t vs. M plane are shown in Figure 1.1 as contours in shades of gray and blue. To demonstrate the error committed if one neglects the terms in ϵ we show the value of $500\epsilon'$ alongside the couplings in Figure 1.2. $\epsilon'(t)$ is equal to the value of $\epsilon(t, M)$ along the exclusion limit curves in Figure 1.1 and thanks to the direction of the ϵ contours represents a good estimate of the largest possible values for $\epsilon(t, M)$ under the constraints imposed by the exclusion limits. The values of $\epsilon(t, M)$ can reach at most 0.2% of the couplings and thus are negligible. The couplings of Z′, W′ bosons to the SM fermions can be up to 10 times larger or 10 times smaller than the corresponding SM Z, W boson couplings. The regions of perturbativity represented by horizontal dotted lines in Figures 1.1 and 1.2, were constructed from the requirement that the gauge couplings be perturbative (smaller than $\sqrt{4\pi}$) which translates into a condition for $c_\phi, s_\phi > 0.18$ [48].

In conclusion, the *left-handed* models predict new left-handed charged and neutral gauge bosons. The description of their couplings and masses contains two free parameters. Their mass is constrained from low-energy and precision observables up to 2.5 TeV, 3.6 TeV in the UU, NU model respectively. At the LHC, one would search for these new Z′ and W′ bosons in the invariant and transverse mass distributions of $\ell^+\ell^-$, $t\bar{t}$, $\ell^\pm\nu$ and $t\bar{b}$ production at equal masses $M = M_{Z'(W')}$.

1.3.3 *Right-handed* models

The models in the *right-handed* category are the LR (left-right), LP (leptophobic), HP (hadrophobic), and FP (fermiophobic) models. The first stage symmetry breaking can proceed either via a scalar in a doublet (D) or a triplet (T) representation of the $SU(2)_2$ group, $\Phi \sim (1, 2, 1/2)$ or $\Phi \sim (1, 3, 1)$, see Table 1.2. According to this representation, the model abbreviations pick up a

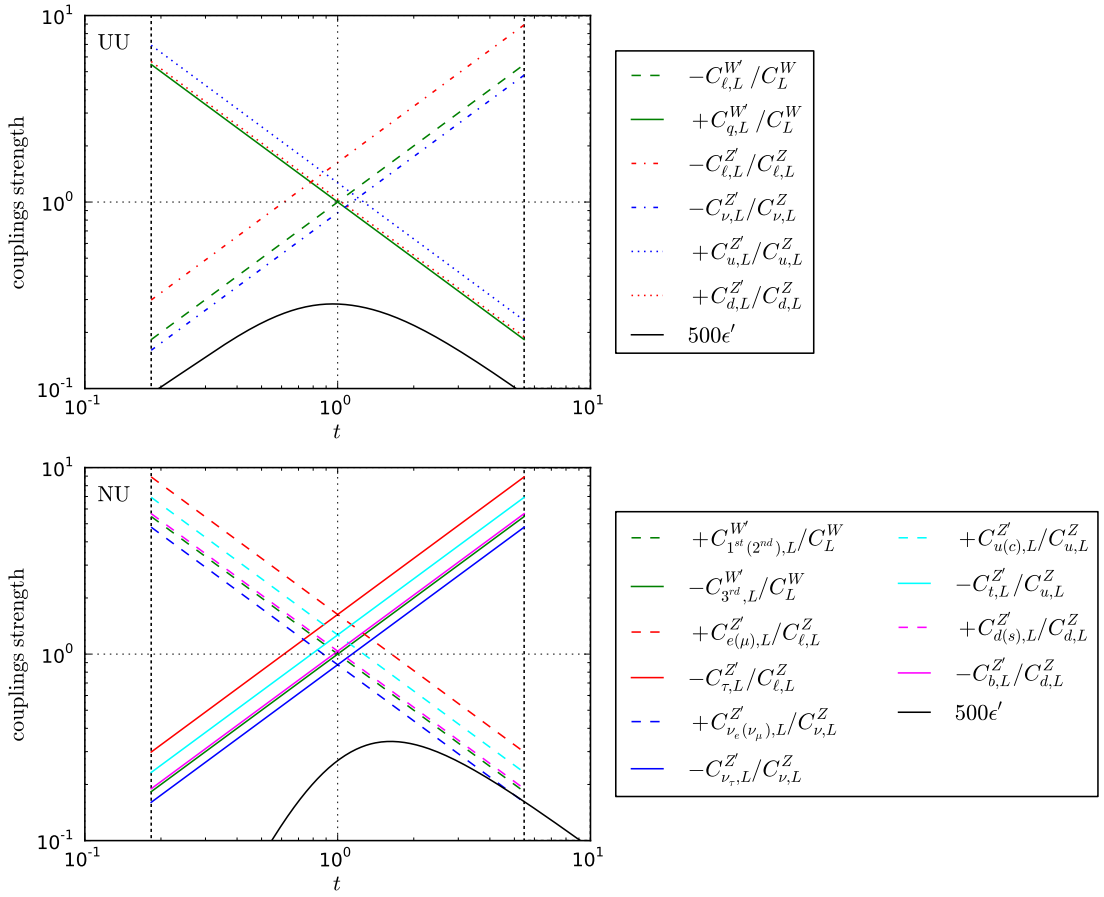

Figure 1.2: Ratios of Z′- and W′-boson couplings over Z- and W-boson couplings to SM fermions as function of the t parameter with $\epsilon(t, M) = 0$. The couplings that are identically equal to zero or are proportional to $\epsilon(t, M)$ are not shown. ϵ' represents the values of $\epsilon(t, M)$ evaluated along the exclusion limits curves. Top: UU model. Bottom: NU model.

suffix -D or -T. For example, the leptophobic model with its first stage symmetry breaking triggered by a triplet, will hereafter be denoted as LP-T.

Independent of whether the first stage scalar field transforms as doublet or triplet, the symmetry breaking of *right-handed* models can be parametrized by the first and second stage mixing angles

$$\mathrm{t}_\phi = \frac{g_X}{g_2}, \quad \mathrm{t}_\theta = \frac{g_W}{g_1}, \tag{1.26}$$

where

$$g_Y = \left(\frac{1}{g_2^2} + \frac{1}{g_X^2}\right)^{-1/2}, \quad g_W = g_1. \tag{1.27}$$

The electric charge is, as for *left-handed* models, given by eq. (1.21) and the gauge couplings g_1, g_2, g_X can be in terms of the mixing angles ϕ, θ and the electric charge written as

$$g_1 = \frac{e}{\mathrm{s}_\theta}, \quad g_2 = \frac{e}{\mathrm{s}_\phi \mathrm{c}_\theta}, \quad g_X = \frac{e}{\mathrm{c}_\phi \mathrm{c}_\theta}. \tag{1.28}$$

Right-handed G(221) models pick up one additional free parameter β, which describes the alignment of the second stage scalar field VEV, see Table 1.2. As compared to two free parameters of *left-handed* models, the *right-handed* ones have three free parameters $\{u, \phi, \beta\}$. Practically, however, it turns out that the sensitivity of Z′- and W′-boson masses and couplings to the SM fermions to the β parameter is very low. We shall see, that for the purpose of this study, two parameters are to a good precision sufficient for their description.

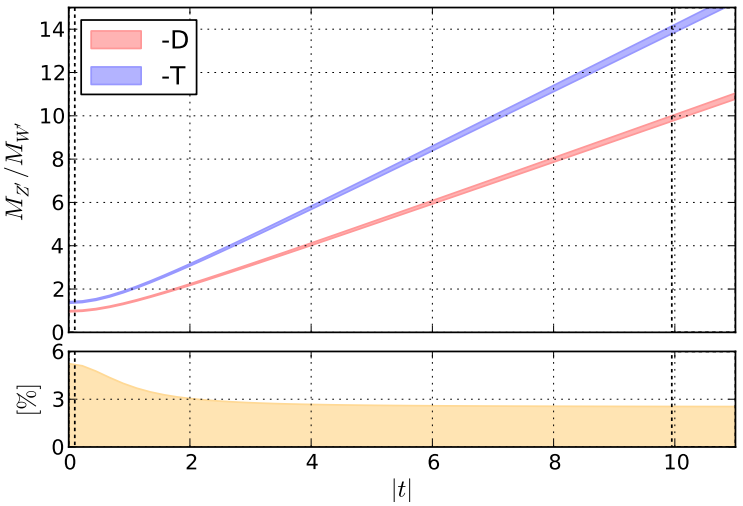

Figure 1.3: Top: Ratio of $M_{Z'}$ mass over $M_{W'}$ mass as a function of t for all allowed values of the remaining free parameters (u, β). The line thickness corresponds to the variation of u and β. Bottom: Line thickness - the maximum of the ratio of the difference of upper and lower line boundaries from the upper plot divided by their average.

In contrast to *left-handed* models, new resonances predicted in *right-handed* models are not degenerate. The series expansion of the ratio of Z′- and W′-boson masses squared around $v^2/u^2 \to 0$ can be in the limit $s^2_{2\beta} \ll u^2$ written as

$$\begin{aligned} \text{-D: } \frac{M^2_{Z'}}{M^2_{W'}} &= (1+t^2) + \frac{v^2}{u^2}\left(\frac{1-(1+t^2)^2}{(1+t^2)}\right) + O(v^4/u^4), \\ \text{-T: } \frac{M^2_{Z'}}{M^2_{W'}} &= 2(1+t^2) + \frac{v^2}{u^2}\left(\frac{1-2(1+t^2)^2}{2(1+t^2)}\right) + O(v^4/u^4). \end{aligned} \tag{1.29}$$

where $t = t_\phi$. The ratio does not depend on the model, only on the first stage scalar field representation – doublet denoted by -D, triplet by -T. We can see, that the second stage VEV alignment β dependence drops out of the approximate expression for the ratio of masses squared, while the first stage scalar field VEV u enters only in the ratio v^2/u^2. The ratio of masses squared as a function of t is shown in Figure 1.3, where we use the full expressions for resonance masses, which we do not show here for brevity. The variation of all the free parameters but t, with the constraint $M_{W'} < 5$ TeV, is contained in the thickness of the line. The mass ratio $M_{Z'}/M_{W'}$ can go up to ~ 10 for models broken by a triplet scalar and up to ~ 14 for models broken by a doublet scalar field. Note that, the W′-boson is always lighter than the Z′-boson and thus is likely to be observed first.

The couplings of the Z′- and W′-bosons to the SM fermions can be in *right-handed* models written as

left-right	lepto-phobic
$C^{\mathrm{W}'}_{q,R} = -\mathrm{t}_\theta \sqrt{\frac{1+t^2}{t^2}} V_R$	$C^{\mathrm{W}'}_{q,R} = -\mathrm{t}_\theta \sqrt{\frac{1+t^2}{t^2}} V_R$
$C^{\mathrm{W}'}_{\ell,R} = -\mathrm{t}_\theta \sqrt{\frac{1+t^2}{t^2}}$	$C^{\mathrm{W}'}_{\ell,R} = 0$

(1.30)

hadro-phobic	fermio-phobic
$C^{\mathrm{W}'}_{q,R} = 0$	$C^{\mathrm{W}'}_{q,R} = 0$
$C^{\mathrm{W}'}_{\ell,R} = -\mathrm{t}_\theta \sqrt{\frac{1+t^2}{t^2}}$	$C^{\mathrm{W}'}_{\ell,R} = 0$

(1.31)

$$
\begin{aligned}
C^{\mathrm{W}'}_{q,L} &= -\epsilon^{\mathrm{W}'}(t, M_{\mathrm{W}'}, \beta) V_{\mathrm{CKM}} \\
C^{\mathrm{W}'}_{\ell,L} &= -\epsilon^{\mathrm{W}'}(t, M_{\mathrm{W}'}, \beta)
\end{aligned}
\tag{1.32}
$$

$$
\begin{aligned}
C^{\mathrm{Z}'}_{L} &= -\mathrm{s}_\theta X(f) t + \left(T_3(f) + Q(f)\mathrm{s}^2_\theta\right) \epsilon^{\mathrm{Z}'}(t, M_{\mathrm{Z}'}) \\
C^{\mathrm{Z}'}_{R} &= \mathrm{s}_\theta \left(-X(f)t + T_3(f)\frac{1}{t}\right) + Q(f)\mathrm{s}^2_\theta \epsilon^{\mathrm{Z}'}(t, M_{\mathrm{Z}'})
\end{aligned}
\tag{1.33}
$$

where t, $T_3(f)$, $Q(f)$, θ have the same meaning as in the case of *left-handed* models, $X(f)$ is the $U(1)_X$ charge and V_R the right-handed analogue of the CKM mixing matrix in the left-handed sector. The values of the $T_3(f)$ and $X(f)$ fermion charges are shown in Table 1.3. The functions $\epsilon^{\mathrm{W}'}(t, M_{\mathrm{W}'}, \beta)$ and $\epsilon^{\mathrm{Z}'}(t, M_{\mathrm{Z}'})$ collect terms proportional to $\mathrm{s}^2_{2\beta}\sqrt{1+t^2}/(M^2_{\mathrm{W}'}t)$ and $1/(M^2_{\mathrm{Z}'}t)$, respectively. In the allowed regions, under the constraints derived from low energy and precision data, the values of ϵ are strongly suppressed. The expressions for ϵ functions can be found in Appendix A. Note that the couplings, except for the full expressions for ϵ functions, do not explicitly depend on the choice of the first stage scalar field representation. The W′-boson in *right-handed* models is right-handed, that is its couplings to the left-handed SM fermions are suppressed. Furthermore, the W′ boson in the LP model is leptophobic, i.e. does not couple to leptons at all, and the W′ boson in the HP and FP models does not couple to quarks and fermions respectively.

As mentioned earlier, two parameters are sufficient to describe the Z′- and W′-boson masses and their couplings to the SM fermions. The ratio of masses squared as a first approximation doesn't depend on the alignment angle β. Additionally, β enters the expression for couplings only via the $\epsilon^{\mathrm{Z}'(\mathrm{W}')}$ functions which are strongly suppressed. Given a mass $M = M_{\mathrm{Z}'(\mathrm{W}')}$ and a tangent of the first stage mixing angle t, one can generate any realization of one of the *right-handed* models, provided the mass M is large enough and the couplings $C(t)$ stay perturbative. Moreover, according to [54], the β parameter almost completely decouples from the u parameter while it is strongly correlated to the ϕ parameter. Thanks to that, the global constraints in [48] could have been for a given value of ϕ acquired by first computing the value of β and only then fixing the value of u. In the following, we will assume, therefore, that β decouples from u completely and its value can be fully obtained from the value of ϕ, such that it is no longer a free parameter. Had the Z′-(W′-)boson been

Table 1.3: The charge assignments of the SM fermions in *right-handed* models. Note that T_3, here corresponds to the sum of the third components of $SU(2)_1$ and $SU(2)_2$ isospin.

		T_3	X			T_3	X			T_3	X			T_3	X
LR	ν_L	$+\frac{1}{2}$	$-\frac{1}{2}$	LP	ν_L	$+\frac{1}{2}$	$-\frac{1}{2}$	HP	ν_L	$+\frac{1}{2}$	$-\frac{1}{2}$	FP	ν_L	$+\frac{1}{2}$	$-\frac{1}{2}$
	e_L	$-\frac{1}{2}$	$-\frac{1}{2}$		e_L	$-\frac{1}{2}$	$-\frac{1}{2}$		e_L	$-\frac{1}{2}$	$-\frac{1}{2}$		e_L	$-\frac{1}{2}$	$-\frac{1}{2}$
	u_L	$+\frac{1}{2}$	$+\frac{1}{6}$		u_L	$+\frac{1}{2}$	$+\frac{1}{6}$		u_L	$+\frac{1}{2}$	$+\frac{1}{6}$		u_L	$+\frac{1}{2}$	$+\frac{1}{6}$
	d_L	$-\frac{1}{2}$	$+\frac{1}{6}$		d_L	$-\frac{1}{2}$	$+\frac{1}{6}$		d_L	$-\frac{1}{2}$	$+\frac{1}{6}$		d_L	$-\frac{1}{2}$	$+\frac{1}{6}$
	ν_R	$+\frac{1}{2}$	$-\frac{1}{2}$		ν_R	0	0		ν_R	$+\frac{1}{2}$	$-\frac{1}{2}$		ν_R	0	0
	e_R	$-\frac{1}{2}$	$-\frac{1}{2}$		e_R	0	-1		e_R	$-\frac{1}{2}$	$-\frac{1}{2}$		e_R	0	-1
	u_R	$+\frac{1}{2}$	$+\frac{1}{6}$		u_R	$+\frac{1}{2}$	$+\frac{1}{6}$		u_R	0	$+\frac{2}{3}$		u_R	0	$+\frac{2}{3}$
	d_R	$-\frac{1}{2}$	$+\frac{1}{6}$		d_R	$-\frac{1}{2}$	$+\frac{1}{6}$		d_R	0	$-\frac{1}{3}$		d_R	0	$-\frac{1}{3}$

observed, one could use its mass $M_{Z'(W')}$ to fix the value of the first stage breaking VEV u for every value of the first stage mixing angle ϕ. We are thus free to parametrize the couplings of *right-handed* Z′- and W′-bosons to the SM fermions models using either $\{t = t_\phi, M_{Z'}\}$ or $\{t = t_\phi, M_{W'}\}$. Because the masses are not degenerate, these parametrizations are not equivalent and in the following we use $\{t, M_{Z'}\}$ to parametrize the Z′-boson couplings and $\{t, M_{W'}\}$ the couplings of the W′.

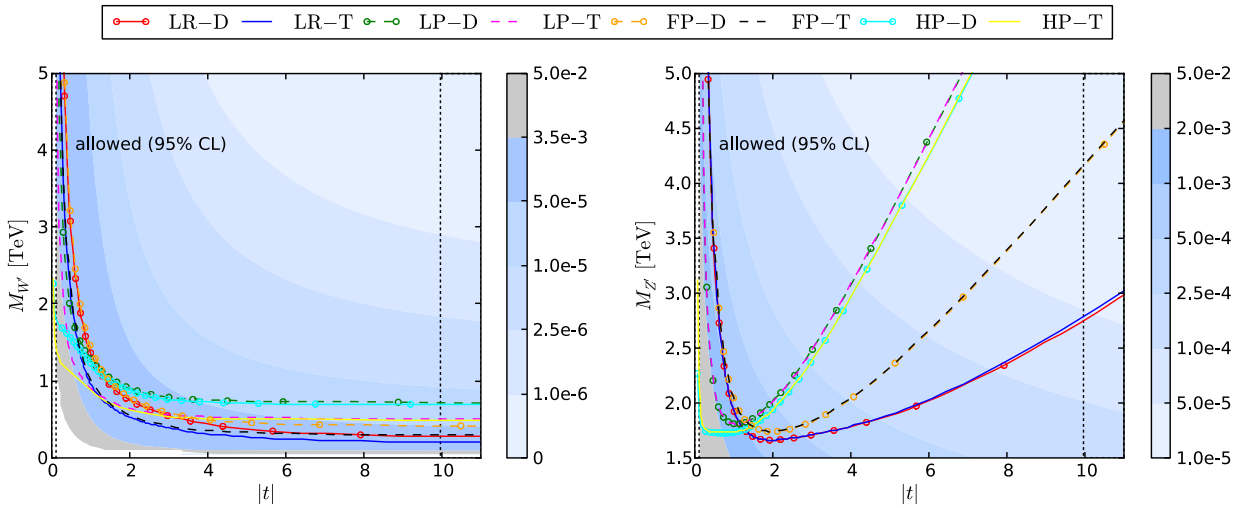

Figure 1.4: Exclusion limits in $\{t, M_{Z'}\}$ and $\{t, M_{W'}\}$ planes for *right-handed* models. The dashed or full lines with or without markers represent the 95% confidence level contours, the dotted lines correspond to the boundaries of the region in which all the gauge couplings are perturbative. The blue shaded contours represent the values of $\epsilon^{Z'(W')}$.

The exclusion limits in the $\{t, M_{Z'}\}$ and $\{t, M_{W'}\}$ planes, derived from low-energy and electroweak precision data [48], are displayed in Figure 1.4. We observe that the *right-handed* models are less constrained than the *left-handed* models and the lowest allowed mass $M_{Z'}$ is 1.6 TeV in the LR model, 1.7 TeV in the LP, HP and FP models. The W′-boson lower mass constraint has a

stronger model dependence and varies between 0.3 TeV and 0.7 TeV[11].

Because the observables requiring information on the extended flavour structure of the models, like BR($b \to s\gamma$), were voluntarily omitted in the global fit to the low energy and precision observables, the exclusion limits in Figure 1.4 do not depend on the right-handed mixing matrix V_R. Moreover the right-handed mixing matrix is not predicted by the gauge structure of these models and we are thus free to fix the value of all its entries. In the numerical study, contained in Section 1.4, we will assume $V_R = V_{CKM}$. To correct for the lack of constraints from the extended flavour structure, which have been shown to be quite restrictive but strongly dependent on the right-handed mixing matrix [55], we will assume that a W′ with a mass below 1.5 TeV is excluded.

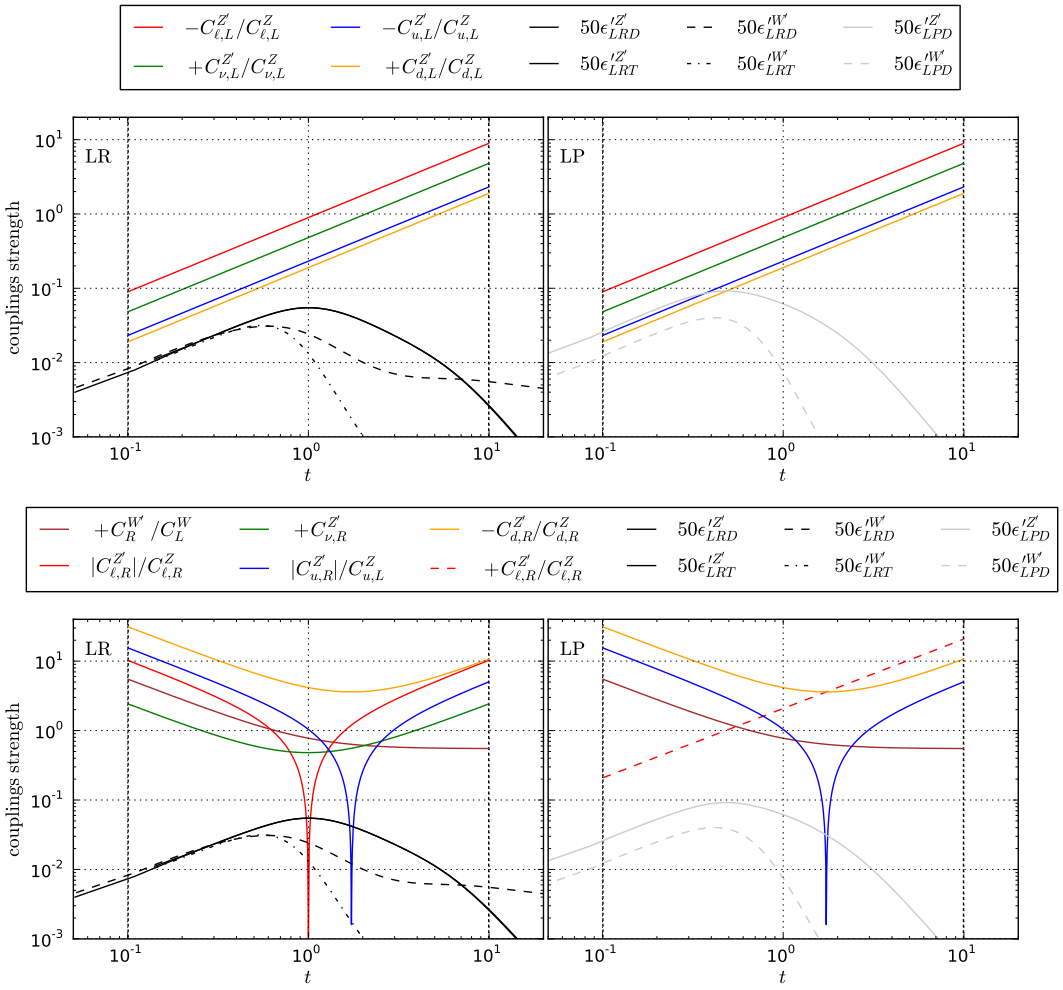

Figure 1.5: Ratios of couplings of Z′- and W′-bosons to Z- and W-bosons couplings to SM fermions as function of the t parameter with $\epsilon(t, M) = 0$. The couplings that are identically equal to zero or are proportional to $\epsilon(t, M)$ are not displayed. ϵ' represents the values of $\epsilon(t, M)$ evaluated along the exclusion limits curves. Note that all the couplings as well as the ϵ function are odd in t. Top: Left-handed couplings in both LR and LP models. Bottom: Right-handed couplings.

The dependence of ratios of various W′- and Z′-bosons couplings over the corresponding SM

[11] See Table 7 in [48] for a complete list of lower mass constraints.

W- and Z-boson couplings on the t parameter with the $\epsilon^{\mathrm{Z}'(\mathrm{W}')} = 0$ for LR and LP models is shown in Figure 1.5. The couplings in HP and FP models can be obtained from the LP model couplings. The values of the terms collected in $\epsilon(t, M)$ in the t vs. M plane are shown in Figure 1.4 as contours in shades of gray and blue. To show the maximum contribution of terms collected in the $\epsilon^{\mathrm{Z}'(\mathrm{W}')}$ functions to the Z' and W' couplings, we have calculated them along the exclusion limit curves in Figure 1.4 and show the value of $50\epsilon(t, M)$ in Figure 1.5. Their value can exceed 2% of some of the W'-boson couplings in the LP, HP and FP models, while their value can be even larger than some Z'-boson couplings in the points of the parameter space in which the right-handed lepton or right-handed quark couplings change the sign.

Note that the right-handed neutrino ν_R is a necessary element of the particle content of the LR model. The gauge structure of the LR model, however, doesn't predict most of the properties of ν_R, like its mass or decay width, and one would need additional free parameters to be able to study their phenomenology. In the LP model, the right-handed neutrino is absent and moreover the W'-boson is leptophobic. Therefore, we have decided not to investigate the lepton plus missing transverse energy final state within *right-handed* models. For examples of phenomenological studies on and experimental searches of a purely right-handed W' decaying into a charged lepton and a right-handed neutrino the reader is referred to [56, 57, 58, 59].

The LR and LP models predict non-degenerate Z'- and W'-bosons, $M_{\mathrm{Z}'} > M_{\mathrm{W}'}$. Their masses and couplings can be described by two free parameters. In Section 1.4, we shall investigate their impact on the transverse dilepton mass as well as the third-generation quark pair production.

1.4 LHC phenomenology

After the discovery of a particle consistent with the Higgs boson at the LHC, the search for new physics is one of the top priorities. New Z' and W' bosons with significant couplings to quarks and leptons are most easily seen as resonances in the invariant and transverse mass spectrum of the Drell-Yan process with dilepton and lepton plus missing transverse energy final states or in the invariant mass distribution of third-generation quark pair production. In this section we study the impact of the presence of Z'- and W'-bosons predicted in G(221) models on the production of $\ell^+\ell^-$, $\ell^\pm\nu$, $\mathrm{t\bar{t}}$ and $\mathrm{t\bar{b}}$ at the LHC.

We assume that the LHC will operate after the 2013-2014 shutdown at its design center-of-mass energy of $\sqrt{s} = 14$ TeV and accumulate an integrated luminosity of 10 to 100 fb^{-1}, so that cross sections down to 10^{-2} fb can be observed. In the SSM [10], which is often taken as a benchmark scenario, the Z' and W' bosons would then be accessible up to masses of 5 TeV [20], while with the present CMS (ATLAS) data masses below 2.96 (2.86) [21, 22] and 3.35 (2.55) TeV [23, 24] are excluded in the electron and muon channels.

In the first step we study new physics contributions to the total cross section for the production of W' and Z' bosons decaying into leptons and third-generation quarks in the regions allowed by low-energy and electroweak precision data shown in Sections 1.3.2 and 1.3.3. We then correlate the new physics contributions in different channels among each other. We show that the total cross sections, while experimentally easily accessible, provide individually only partial information about the model realized in Nature. In contrast, correlations of these cross sections in the neutral and charged current channels may well lead to a unique identification [16].

All the simulations have been performed with the Monte Carlo program `Pythia 6.4` [60], which we have supplemented by terms accounting for the interferences of new and SM charged spin-1 bosons. While the latter can have a significant influence on the shape of the resonance region, their impact on the total cross sections is small. The masses of the t and b quarks and SM Z and W

bosons are fixed to their PDG values [44], and we use the CTEQ6 LO analysis of parton density functions (PDFs) [61]. For a study of the PDF uncertainties on SM and new weak gauge boson production cross sections we refer the reader to Ref. [62]. Following the ATLAS leptonic analyses [24, 22], we require electrons to have transverse energy $E_T > 25$ GeV and lie within the rapidity ranges $|\eta| < 1.37$ or $1.52 < |\eta| < 2.47$. For $\ell\nu$ final states, a missing energy $E_T^{\text{miss}} > 25$ GeV is imposed. In the third-generation quark channels, the ATLAS collaboration reconstruct jets with the anti-k_T algorithm [63] and a radius of $R = 0.4$ and require them to have $E_T > 20$ GeV and $|\eta| < 4.5$ [64]. The total cross sections are then still largely dominated by SM backgrounds, which we suppress by imposing an invariant or transverse mass larger than 75% of the new gauge boson mass.

The invariant mass M_I and transverse mass M_T were defined in eqs. (1.3) and (1.4). To be able to compute the invariant mass we have to know the momenta of both final states which we do in the case that both final state particles are either charged (charged leptons, jets) or their momentum can be fully reconstructed from their decay products (top quarks). If one final state particle is neutral its longitudinal component of the missing momentum cannot be reconstructed because of the collision fragments directed along the beam axis. One, therefore, resorts to measuring the transverse mass instead.

The shape of the invariant mass distribution of a single neutral boson is of a Breit-Wigner form peaked at the mass of the boson with a half-width proportional to its decay width, while the transverse mass distribution of a single charged boson develops a Jacobian peak at the mass of the boson mediating the interaction[12]. In the case that two bosons interfere[13] the shape of the peaks may be significantly distorted. Generally, the contribution of the interference between the two peaks has the opposite sign to the sign of the interference outside of the peaks and its overall sign depends on the relative sign of the couplings[14].

Monte Carlo generators including next-to-leading order (NLO) QCD corrections exist, but only for leptonically decaying Z′ and W′ bosons [66, 67], so that we have not made use of them in this study for consistency. The impact of NLO QCD corrections to the electroweak top-pair production [68] is investigated in the next chapter.

1.4.1 Cross sections

For each model and for each point of its discretized parameter space constrained by the corresponding exclusion limits we have generated samples consisting of 30000 events, each event describing a fixed order LO production of a single Z′ or a single W′ bosons decaying into a lepton pair, a top quark pair, a lepton and a neutrino or a top and bottom quark separately. The lepton-neutrino pair production was simulated only for *left-handed* models, since the left-handed couplings of the W′-boson in *right-handed* models are strongly suppressed. Furthermore, at a hadron collider the total cross section of the W′-boson production in HP and FP models is strongly suppressed. We expect the effect of parton shower in the high invariant mass region to be negligible, because corrections to the transverse momentum of final state particles induced by a near-collinear radiation are very small as compared to the transverse momentum of highly boosted final state pair. Therefore, the

[12] Also note that transverse mass distribution contains more information than the transverse momentum distribution of the outgoing lepton as it contains the full information about the transverse momentum of the boson in the play – the peak is sharper [65].

[13] The interference is not necessarily present – in the case one boson decays into states that are differently polarized than the decay products of the other boson, then these final states are not considered as undistinguishable and thus there is no interference.

[14] The couplings of W′- and Z′-bosons to the SM fermions can in general be both positive or negative.

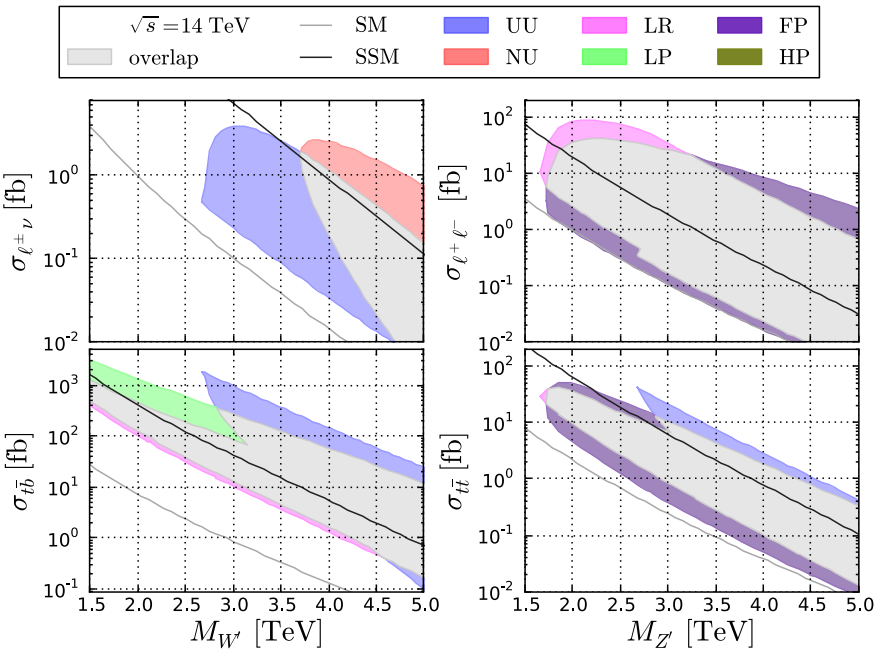

Figure 1.6: Total CC (left) and NC (right) cross sections in the lepton (top) and third-generation quark (bottom) channels.

effects of the parton shower were not simulated. We have, however, verified this assumption on a small control sample.

In Figure 1.6 we show the resulting total CC (left) and NC (right) cross sections in the lepton (top) and third-generation quark (bottom) channels. In all models, including the SSM shown for comparison, they are by up to two orders of magnitude larger than the SM background (which depends on $M_{\mathrm{W}',\mathrm{Z}'}$ due to the transverse and invariant mass cutoff, respectively), but still exceed 10^{-2} fb for masses up to 5 TeV. The shaded areas correspond to the ranges in parameter space still allowed after the global analysis of low-energy and LEP data. As one can observe, they exhibit a large overlap (grey). So while the cross sections are experimentally easily accessible, the pre-LHC constraints are clearly not strong enough to allow for an unambiguous identification of the gauge group possibly realized in Nature. The same applies to the Higgs sector of the LR (pink), LP (green), HP (purple), and FP (olive) models, for which regions with doublets and triplets are coded with the same color, as they overlap almost completely. For these models, we make no predictions for the lepton-neutrino channel, as we do not have any information about the right-handed neutrino sector. Applying a b-tag to the quark channels would reduce their cross sections by the corresponding efficiency of about 60%[15] [64]. For completeness, we also show predictions for the LHC operating at $\sqrt{s} = 8$ TeV in Figure 1.7.

1.4.2 Cross section correlations

In the previous section, we have shown that new resonances predicted in G(221) models are at the LHC operating at $\sqrt{s} = 14$ TeV reachable up to masses $4 - 5$ TeV but their prediction regions of new physics contributions to the cross section of the Z′, W′ production and their subsequent decay

[15] 60% for each b quark in the final state.

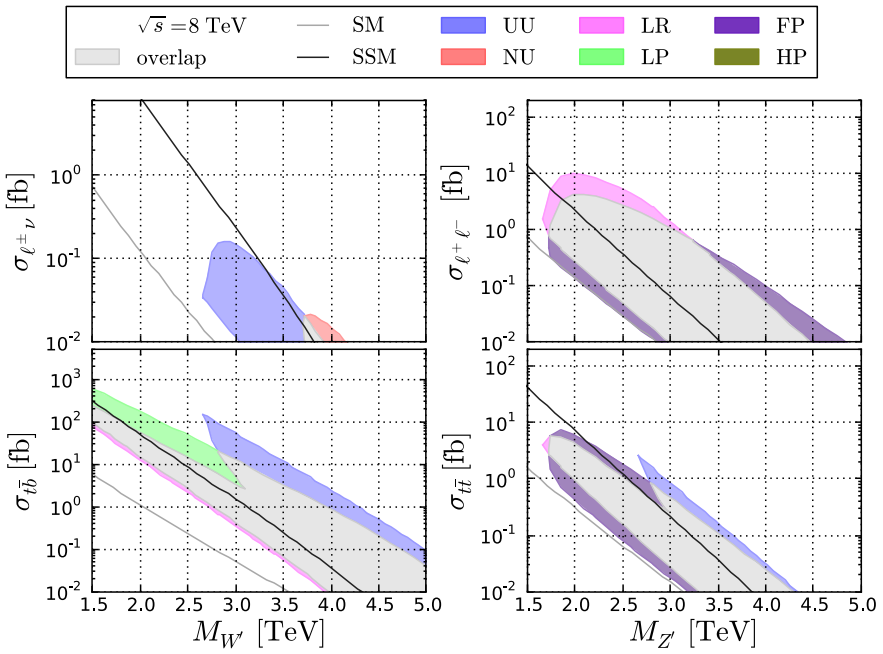

Figure 1.7: Total CC (left) and NC (right) cross sections in the lepton (top) and third-generation quark (bottom) channels.

into a fermionic final state exhibit a large overlap and for significant portions of their parameter spaces are not distinguishable.

The $\ell^+\ell^-$ and $t\bar{t}$ production, mediated by the Z′, and $\ell^\pm\nu$ and $t\bar{b}$ production, mediated by the W′ are correlated. Looking at the cross section correlation in these channels may thus lead to more conclusive predictions. For each model and for each point of its discretized parameter space we have calculated the total cross section for the relevant final states and plot them in the σ_a vs. σ_b planes, where $a, b \in \{\ell^+\ell^-, t\bar{t}, \ell^\pm\nu, t\bar{b}\}$. In Figure 1.8 we show the resulting cross section correlations for the UU and NU models. The blue and red solid curves correspond to the $M = M_{Z'(W')} = 5$ TeV iso-curves for UU and NU models respectively, while the dashed curves correspond to the $M < 5$ TeV iso-curves.

The cross section correlations regions still exhibit a large overlap (grey) among UU and NU models as well as with the SSM cross section correlation curve. It is crucial, however, to observe that for most of the cross section correlations the fixed mass contours intersect in a single point. Constraining the masses of one of the new gauge bosons to its measured value may shrink the cross section correlation regions and limit their overlap. Note that, knowing one of the masses is sufficient, since in the *left-handed* models the Z′ and W′ are degenerate, and in the *right-handed* models their masses are strongly correlated. Similar observations can be made for the cross section correlations in the *right-handed* models.

Let us now assume one of these bosons to have been observed in at least one channel and its mass to have been measured from the invariant mass of a lepton (e, μ), $t\bar{t}$, or $t\bar{b}$ pair or the Jacobian peak of the transverse mass of a single lepton and missing transverse energy as 3.0 ± 0.1 TeV or 4.0 ± 0.1 TeV with a conservative error estimate [20]. Estimating the mass uncertainty ΔM from the resonance width Γ and the number of events N with $\Delta M = \Gamma/\sqrt{N}$ shows that in the G(221) models studied here the statistical error will often be smaller by up to a factor of ten with respect

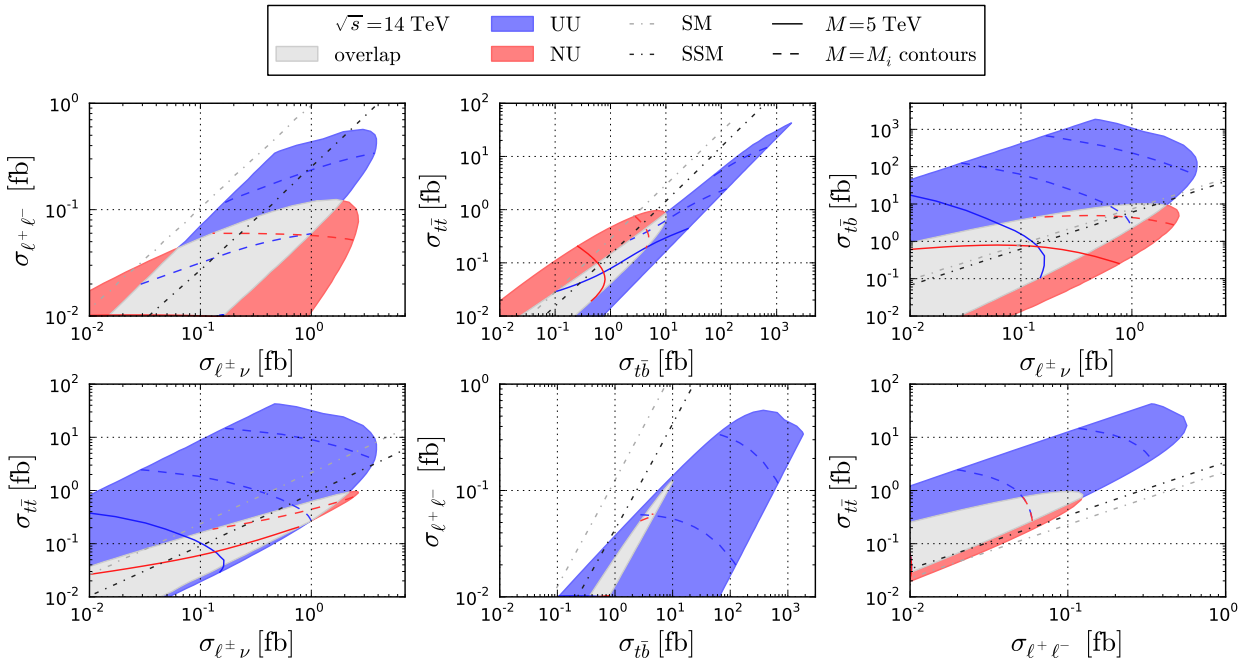

Figure 1.8: Correlations of CC and NC lepton (e, μ) and third-generation quark cross sections in *left-handed* models.

to the conservative error estimate we consider. It will then become comparable to the experimental resolution of currently about 2% and ultimately 0.5%.

In Figure 1.9 we show the total cross section correlations assuming either a known mass of $M_{W'} = 3.0 \pm 0.1$ TeV (top row, center row) or of $M_{Z'} = 3.0 \pm 0.1$ TeV (top row, bottom row). The shaded areas correspond now to the regions of parameter space allowed by the global fit and in addition the uncertainty in the mass of the observed gauge boson. Should the uncertainty be only 0.05 instead of 0.1 TeV, the width of these bands shrinks by more than a factor of two, turning them almost into sharp lines. As the plots in the first line always involve the lepton-neutrino channel and as masses below 3.6 TeV are already excluded for the NU model [48] (cf. also Figure 1.6), we show there only predictions for the UU model, in which $M_{W'} \simeq M_{Z'}$ (see above). With signal cross cross sections that are one to three orders of magnitude larger than those of the SM and do not overlap with those of the SSM for which we also assume $M_{W'} = M_{Z'}$, it would therefore be easily identifiable. The plots in the other two lines do not involve the lepton-neutrino channel, and we can therefore show predictions for all G(221) models except for the excluded NU model and the HP and FP models, which are only accessible in the NC channels. It is clear that the overlap is very much reduced compared to Figure 1.6, making a unique identification of the underlying gauge group possible in almost all cases. Even doublet (D) and triplet (T) Higgs fields can now be distinguished, but this requires the observation of at least one CC channel and/or knowledge of the W' mass. The NC channels are obviously most useful if the Z' mass is known (bottom right) and exhibit then already by themselves a large discriminatory power of the gauge group. It would in particular be sufficient to measure the $t\bar{t}$ and $\ell^+\ell^-$ cross sections with a precision of about 30%.

The position of these measurements in the correlation plane would then also give information on the remaining model parameters, in particular the mixing angle ϕ at the first breaking stage (cf. the red iso-lines in the bottom-right plots of Figures 1.9 and 1.10).

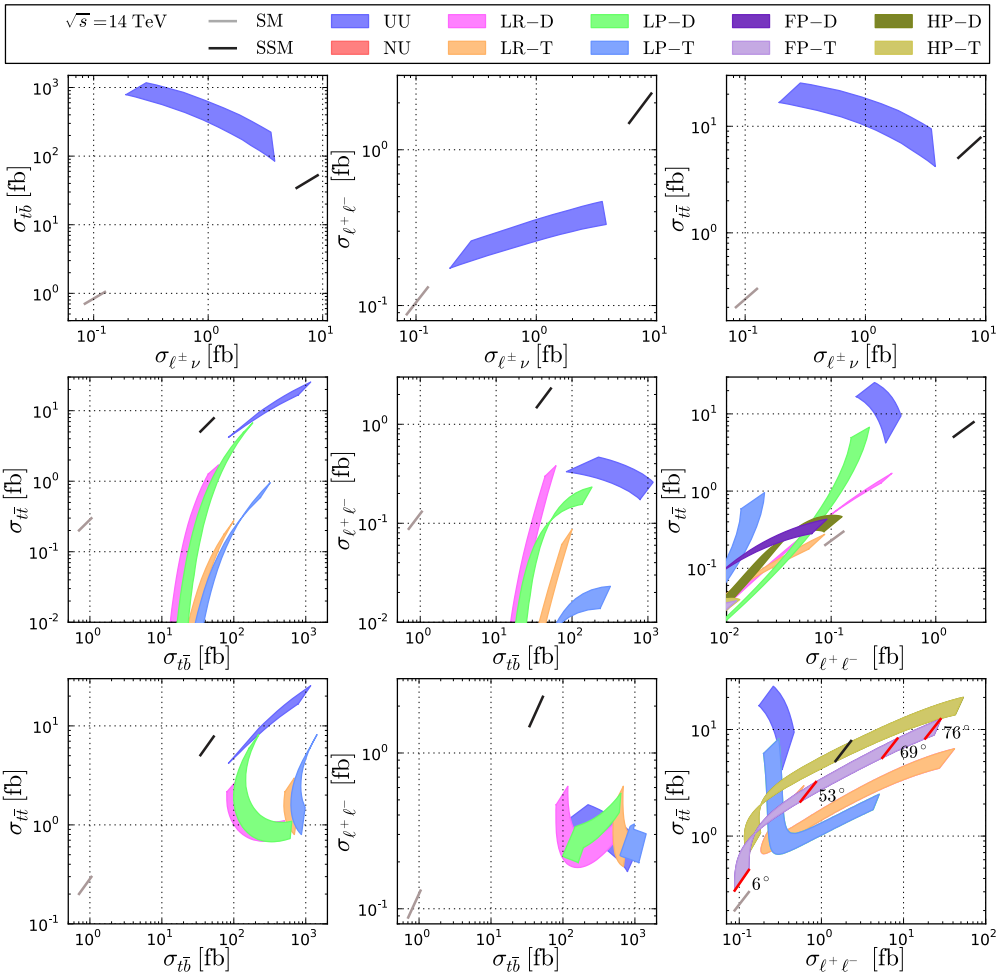

Figure 1.9: Correlations of CC and NC lepton (e, μ) and third-generation quark cross sections for fixed $M_{W'} = 3.0 \pm 0.1$ TeV (top row, center row) and $M_{Z'} = 3.0 \pm 0.1$ TeV (top row, bottom row).

A similar analysis is performed in Fig 1.10, where the W' (top row, center row) and Z' (top row, bottom row) mass is now assumed to be 4.0 ± 0.1 TeV, respectively. This larger mass naturally leads to cross sections that are reduced by about one order of magnitude with respect to those in Figure 1.9, but they remain observable and larger than the SM background. For this higher mass, the NU model is no longer excluded by the global analysis and therefore added to the plots. Correlating the lepton-neutrino with the $t\bar{b}$ and/or NC channels (top) makes it then clearly distinct from the UU model. Since the third generation couples differently from the other two in the NU model, its predictions for third-generation quark cross sections lead to almost constant lines or point-like areas when correlated with the lepton cross sections or each other.

Conversely, agreement of the experimental measurements with the SM predictions in Figs. 1.6-1.10 would allow to considerably constrain the parameter space of the different G(221) models or even to exclude the corresponding new gauge boson masses altogether.

For completeness, we also show the cross section correlations for the LHC operating at $\sqrt{s} = 8$ TeV. The cross sections for resonances with a mass of 4 TeV turn out to be too small and we therefore fix the mass to 3 ± 0.1 TeV in Figure 1.11. The NU model can thus not be identified with

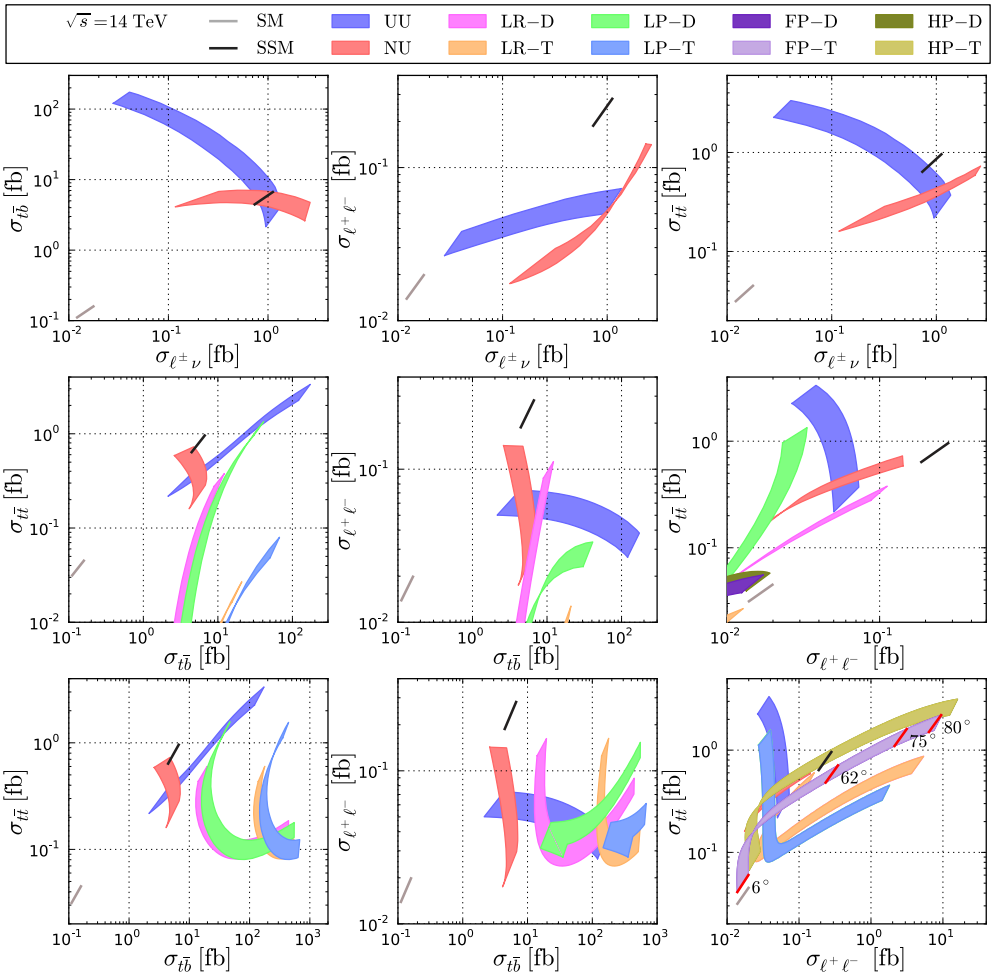

Figure 1.10: Correlations of CC and NC lepton and third-generation quark cross sections for fixed $M_{W'} = 4.0 \pm 0.1$ TeV (top row, center row) and $M_{Z'} = 4.0 \pm 0.1$ TeV (top row, bottom row).

data taken at 8 TeV. Inspecting Figure 1.11, new gauge bosons with a mass of 3 TeV in the UU model could already be distinguished from the SSM if one of the third generation quark channels is measurable (top). If both the neutral and charged current channels are measurable, one can also distinguish it from the LR-D and LP-D models without making any assumptions on the right-handed neutrino (center). Distinguishing different doublet (LR-D, LP-D, ...) and triplet (LR-T, LP-T, ...) models is partly possible using the $(\sigma_{t\bar{t}}, \sigma_{t\bar{b}})$ correlation (bottom left). Furthermore, depending on the precision of the Z' mass measurement, it might also be feasible when correlating the neutral current lepton channel with the $t\bar{t}$ channel (bottom right) and then even lead to a first measurement of the mixing angle ϕ.

1.5 Conclusions

We have investigated the implications of an extended SM gauge symmetry at the LHC. Models with an additional SU(2) group predict the existence of additional neutral and charged gauge bosons, namely the Z′- and W′-boson, and we have explored their impact on common LHC signals

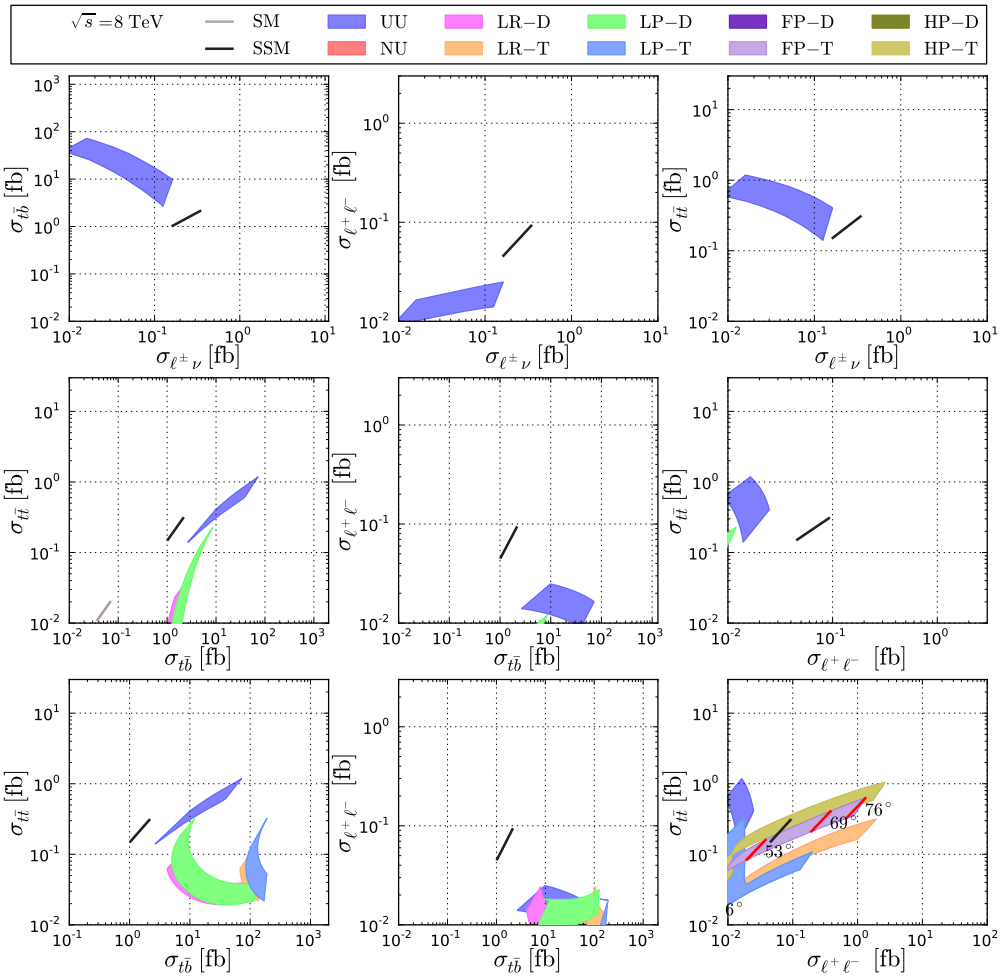

Figure 1.11: Same as Figure 1.9 for LHC at $\sqrt{s} = 8$ TeV.

such as the dilepton, lepton plus missing transverse energy, top-pair and $t\bar{b}$ production. We have concentrated on a class of models with the electroweak gauge symmetry based on the SU(2)× SU(2)×U(1) gauge group, motivated experimentally, e.g., by the observation of neutrino masses and theoretically as an intermediate step towards the grand unification of the SM gauge groups.

We have shown how the Z′- and W′-boson couplings can be parametrized by a set of two (three) common parameters and presented their exclusion limits derived from low-energy and precision data. The total cross sections of the predicted charged and neutral gauge bosons decaying into leptons and third-generation quarks were confirmed to be accessible at the LHC up to masses of 5 TeV within the range of parameters allowed by a recent global analysis of low-energy and LEP constraints.

We have proposed a novel and powerful method to distinguish general SU(2)× SU(2)×U(1) models. Individually, the total cross sections did not allow for the unique identification of the underlying G(221) model. With a Monte Carlo simulation and after applying realistic experimental cuts, we demonstrated that this does become possible by correlating the charged and neutral current cross sections of leptons and third-generation quarks, assuming only that the mass of either the W′ or the Z′ boson has been measured with a conservative uncertainty. The mixing angle of the

high-energy symmetry breaking stage will then also become measurable. The correlations of two observables work nicely here because we only have two (three) free parameters describing all the G(221) models. In the general case of models with more parameters the identification of suitable subsets of correlated observables would represent a first step towards a global analysis of the parameter space.

Chapter 2

QCD corrections to the electroweak top-pair production beyond the Standard Model

Even long after its discovery, at the $p\bar{p}$ collider Tevatron in 1995, the top quark remains a very popular subject of particle physics research. With a mass $m_t = 173.2 \pm 0.9$ GeV [69] close to the electroweak symmetry breaking scale, it is by far the heaviest of all known particles. Due to its very short lifetime, it decays before it can hadronize. This offers a unique opportunity to study the properties of a bare quark, including effects due to its spin via angular correlations of its decay products. It may well provide an effective probe for the electroweak symmetry breaking mechanism and the physics beyond the SM.

At hadron colliders, top quarks can be produced either in pairs, $pp(\bar{p}) \to t\bar{t}$ or as single tops, $pp(\bar{p}) \to t\bar{b}$, $pp(\bar{p}) \to t\bar{q}$, and $pp(\bar{p}) \to tW$. At the LHC, running at its design energy $\sqrt{s} = 14$ TeV and luminosity of 10 fb^{-1}/yr, we expect over 10^6 top-pairs and almost as many single tops produced yearly. Therefore, precision measurements of the top quark properties, such as the mass, the production cross section and kinematic distributions become feasible and any deviations from the SM predictions will hint at physics beyond the SM.

While leading order (LO) predictions in theories beyond the SM usually suffice for devising new physics search strategies or even for deriving the exclusion limits in the parameter spaces of new physics scenarios, an accurate determination of the model parameters requires precise predictions that go beyond the leading order accuracy. Should the new physics be observed, higher-order predictions will most likely play a vital role in the identification of the underlying theory.

Ideally, precise predictions for the production cross sections should be combined with simulations of parton shower effects, multi-parton interactions, and the underlying event – the effects that are always present at hadron colliders. This calls for the use of multi purpose Monte Carlo generators such as `Pythia` [60] or Herwig [70], which, however, provide only LO accuracy for hard scattering processes.

A framework that allows to combine NLO QCD computations with the parton shower is the so-called POWHEG [71] approach. The `POWHEG BOX` [72] is a public tool providing all general building blocks of this method, but requires the user to individually implement process specific pieces such as matrix elements for the hard scattering process at NLO QCD accuracy.

In this manuscript we present the calculation of 1-loop corrections to the top-pair production at hadron colliders in SM extensions featuring an additional Z' boson and its implementation in

POWHEG BOX. The NLO corrections to the top-pair production have been previously studied within a specific model in [73] or for a class of models predicting strongly coupled neutral resonances mediating the top-pair production in [74]. Before the completion of our calculation, a similar calculation of Z′-boson production and its decay into a pair of the top quarks has appeared in [75]. In this publication, a similar set of 1-loop corrections is calculated including the decay of the top-quark at NLO accuracy. As compared to our work, the calculation by Melnikov et. al. is a fixed order calculation, while we offer an implementation in a Monte Carlo event generator compatible with the parton shower algorithm.

This chapter is organized as follows. The calculation of the LO matrix elements is discussed in Section 2.2. Section 2.3 details the calculation of next-to-leading (NLO) corrections consisting of virtual and real contributions, including explanations of the common techniques employed in calculations of 1-loop corrections. The parton shower algorithm and the issue of matching NLO QCD calculation with the parton shower by virtue of the POWHEG method is discussed in Section 2.4. Subsequently, in Section 2.5 we briefly address the issue of automation of higher-order calculations. Finally, the numerical results for the electroweak top-pair production at NLO QCD accuracy at the LHC are presented in Section 2.6.

2.1 Introduction

The top-pair production in hadronic collisions can be calculated according to the standard factorization formula [76]

$$\sigma^{\mathrm{t\bar{t}}}_{h_1,h_2}(s_{\mathrm{had}}, m_{\mathrm{t}}^2) = \sum_{ij} \int_{(2m_{\mathrm{t}})^2}^{s_{\mathrm{had}}} d\hat{s} L_{ij}(\hat{s}, \mu_f^2) \hat{\sigma}_{ij}(\hat{s}, m_{\mathrm{t}}^2, \mu_f^2) \ , \tag{2.1}$$

in which the interactions at low-momentum and high-momentum transfer factorize. The low-momentum transfer part, the process independent partonic luminosity L_{ij} naively describes the probability of finding, in the hadrons h_1 and h_2 (where $h_1, h_2 = \mathrm{p}, \mathrm{p}$ at the LHC), an initial state involving partons i and j with the given partonic center of mass system energy squared $\hat{s}$. The high-momentum transfer part, the hard scattering of the partons i and j ($i, j \in \{q, \overline{q}, \mathrm{g}\}$) at a partonic center of mass energy $\hat{s}$ is described by the partonic cross section $\hat{\sigma}_{ij}$. The integration ranges extend from the threshold at which two top quarks t with mass m_{t} can be produced up to the collider hadronic center of mass energy squared s_{had}. Both the partonic cross section and the luminosities depend on the factorization scale μ_f which fixes the energy scale at which the factorization is realized and is usually set to the partonic energy $\hat{s}$[1].

In principle, the partonic luminosities are calculable in QCD. In practice, this is a non-perturbative calculation, since the QCD coupling becomes large at energy scales close to the proton mass and below. This difficulty is sidestepped by extracting the L_{ij} from experiment [62, 77, 78, 79]. On the other hand, owing to the fact that the QCD coupling is perturbative at the scale of the hard interaction, the expansion of the hard partonic cross section $\hat{\sigma}_{ij}$ can be calculated in perturbation theory. Since the partonic luminosities are universal and their scale dependence well known we will concern ourselves only with the calculation of the partonic cross section.

At the lowest or leading order of perturbation theory, in terms of the couplings parametrizing the strength of the strong and electroweak interactions mediating the top-pair production, denoted α_S and α_W respectively, the partonic cross section $\hat{\sigma}_{ij}^{\mathrm{LO}}$ in the Standard Model can be split into

[1] For more details on the factorization scale μ_f and its choice, the reader is referred to Section 2.3.3.

two parts

$$\hat{\sigma}^{\mathrm{LO}} = \hat{\sigma}_S^{\mathrm{LO}}(\alpha_S^2) + \hat{\sigma}_W^{\mathrm{LO}}(\alpha_W^2) \tag{2.2}$$

where the indices i, j of the incoming partons were suppressed and we keep explicit only the dependence on the coupling constants. $\hat{\sigma}_S^{\mathrm{LO}}$ denotes the partonic cross section of gluon mediated subprocesses in the channels gg and $q\overline{q}$, see Figure 2.1 (a)-(c) and Figure 2.1 (d) respectively. $\hat{\sigma}_W^{\mathrm{LO}}$ contains the contributions from the subprocesses mediated by electroweak gauge bosons, photon γ and Z-boson, initiated by $q\overline{q}$, see Figure 2.1 (e) and (f).

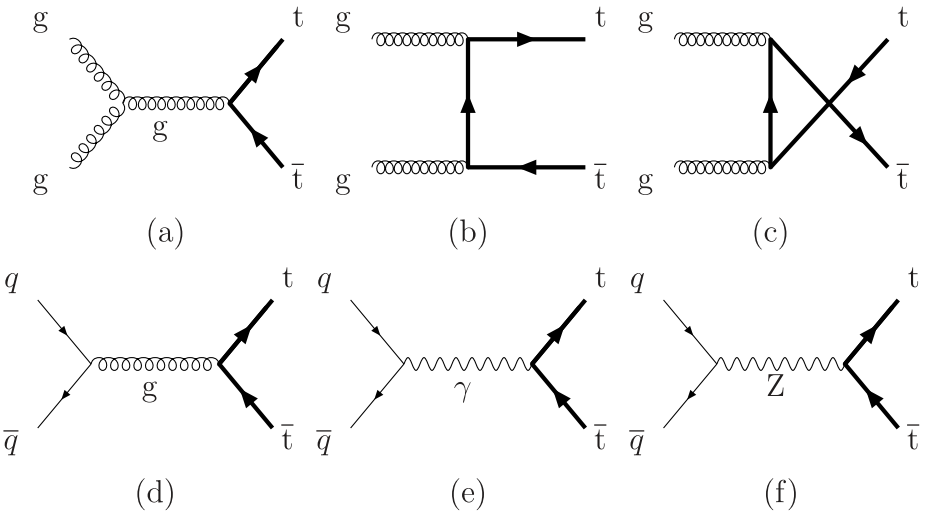

Figure 2.1: Leading order Feynman diagrams for top-pair production. gg-channel at the order $\mathcal{O}(\alpha_S^2)$ (a)–(c), $q\overline{q}$-channel at the order $\mathcal{O}(\alpha_S^2)$ (d) and $q\overline{q}$-channel at the order $\mathcal{O}(\alpha_W^2)$ (e), (f). Thick fermion lines correspond to massive fermions, thin ones to massless fermions.

Higher order corrections to the top-pair production comprise the terms beyond the leading order perturbative expansion in eq. (2.2). Since two coupling constants enter the top-pair production, α_S and α_W, the partonic cross section will have a simultaneous perturbative expansion in both of these couplings. Next-to-leading corrections to the partonic cross section refer to the terms containing one additional power of one of the coupling constants α_S or α_W. The perturbative expansion of the top-pair production partonic cross section up to the NLO reads

$$\hat{\sigma} = \hat{\sigma}_{2;0}(\alpha_S^2) + \hat{\sigma}_{0;2}(\alpha_W^2) + \hat{\sigma}_{3;0}(\alpha_S^3) + \hat{\sigma}_{2;1}(\alpha_S^2\alpha_W) + \hat{\sigma}_{1;2}(\alpha_S\alpha_W^2) + \hat{\sigma}_{0;3}(\alpha_W^3) \tag{2.3}$$

where the integer indices $m;n$ respectively denote the powers of α_S and α_W. The expansion is ordered by the size of the overall coupling[2]. The terms $\hat{\sigma}_{2;0}$, $\hat{\sigma}_{0;2}$ correspond to the LO partonic cross sections $\hat{\sigma}_S^{\mathrm{LO}}$, $\hat{\sigma}_W^{\mathrm{LO}}$ from eq. (2.2) respectively. Both $\hat{\sigma}_S^{\mathrm{LO}}$ and $\hat{\sigma}_W^{\mathrm{LO}}$ at next-to-leading order receive QCD as well as electroweak corrections (EW). The QCD and EW corrections to $\hat{\sigma}_S^{\mathrm{LO}}$ are contained in the terms $\hat{\sigma}_{3;0}$ and $\hat{\sigma}_{2;1}$, while the QCD and EW corrections to $\hat{\sigma}_W^{\mathrm{LO}}$ in the terms $\hat{\sigma}_{1;2}$ and $\hat{\sigma}_{0;3}$ respectively. Diagrammatically speaking, since every line in a Feynman diagram has to couple at its two endpoints, each of them yielding an additional factor $\alpha_{S(W)}^{1/2}$, the NLO corrections involve the calculation of squared amplitudes corresponding to the interferences of diagrams with one additional line. Throughout this manuscript we often refer to the term $\hat{\sigma}_{m;n}$ in the perturbative

[2] $1 > \alpha_S > \alpha_W$.

expansion as the partonic cross section at order $\mathcal{O}(\alpha_S^m \alpha_W^n)$, e.g. $\hat{\sigma}_{1;2}(\alpha_S \alpha_W^2)$ will be referred to as the partonic cross section at order $O(\alpha_S \alpha_W^2)$.

For the purpose of this calculation, we consider final state top quarks as stable particles produced on-shell, despite their short lifetime. We can allow ourselves to make such an approximation thanks to the fact that general purpose Monte Carlo event generators can handle the top quark decay at leading order accuracy automatically. More detailed discussion on top quark decay can be found in Section 2.4.3. For an example on how the top quark decay can be accounted for in full generality at NLO accuracy within the framework of NLO Monte Carlo event generators, we refer to [80].

Cross sections and distributions including QCD effects of $\mathcal{O}(\alpha_S^3)$ were computed in [81, 82, 83, 84]. From the electroweak side, the one-loop corrections at $\mathcal{O}(\alpha_S^2 \alpha_W)$ were investigated in [85] for the subclass of the infrared-free non-photonic contributions. In these calculations contributions including the interference of QCD and electroweak interactions were neglected. A study of non-photonic EW corrections with the gluon-Z interference effects was done more recently in [86, 87, 88, 89]. Finally, a subset of the full EW corrections, corresponding to the QED corrections was calculated in [90]. The 1-loop corrections to the top-pair production in the SM are thus complete.

In theories beyond the Standard Model predicting the existence of an additional neutral vector boson, denoted Z′, the partonic cross section of the top-pair production is modified. In the following we assume that the Z′ couplings to the SM fermions are flavour diagonal[3], as is the case of the Z′ bosons predicted in G(221) models. The Feynman rule for the $q\overline{q}$ vertex featuring such a Z′-boson can be written as [44]

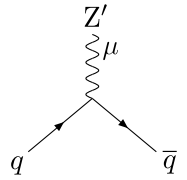

$$i(2\pi)^4 \tfrac{g_W}{c_{\theta_W}} \gamma^\mu (C^{Z'}_{q,L} P_L + C^{Z'}_{q,R} P_R) = i(2\pi)^4 \tfrac{g_W}{4c_{\theta_W}} \gamma^\mu \left(a^q_{Z'} + b^q_{Z'} \gamma_5 \right)$$

where $C^{Z'}$ couplings[4] have been introduced in eq. (1.2) and $P_{R,L} = (1 \pm \gamma_5)/2$. Furthermore, γ^μ and γ_5 are the usual Dirac matrices, $g_W^2 = 4\pi\alpha_W$, the vector and axial-vector couplings $a^q_{Z'}$, $b^q_{Z'}$ in general depend on the quark flavour and we have introduced a short-hand notation $s_\theta = \sin\theta$, $c_\theta = \cos\theta$.

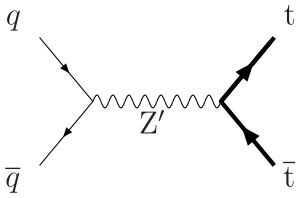

Figure 2.2: Leading order Feynman diagrams for the new physics contribution to the top-pair production.

In SM extensions predicting new neutral currents, the partonic cross section of the top-pair production at leading order receives a contribution from the Z′ boson mediated subprocesses in

[3]The couplings of the Z′-boson across the families of SM fermions are prohibited.

[4]Note that throughout this chapter we parametrize Z′ bosons couplings to the SM fermions by the vector and axial-vector couplings $a_{Z'}$ and $b_{Z'}$, instead of the left- and right-handed couplings $C_L^{Z'}$ and $C_R^{Z'}$.

the $q\bar{q}$ channel, see Figure 2.2. Since the Z′ boson couples to the SM fermions via the electroweak coupling α_W, the new physics contribution to the top-pair production will be contained in the $\hat{\sigma}_W^{\mathrm{LO}}$ part of the partonic cross section, while in the same SM extension the $\hat{\sigma}_S^{\mathrm{LO}}$ is not altered.

Similarly, at next-to-leading order, neutral currents beyond the SM affect only the partonic cross section at orders $\mathcal{O}(\alpha_S^2\alpha_W)$, $\mathcal{O}(\alpha_S\alpha_W^2)$, $\mathcal{O}(\alpha_W^3)$ but not at order $\mathcal{O}(\alpha_S^3)$. In this work, we concentrate on the simplest but presumably most relevant term in the perturbative expansion of the top-pair production cross section, the term $\hat{\sigma}_{1;2}(\alpha_W^2\alpha_S)$ corresponding to the NLO QCD corrections to the EW top-pair production. Even though, the term $\hat{\sigma}_{2;1}(\alpha_S^2\alpha_W)$ is more likely to yield a larger correction than the term $\hat{\sigma}_{1;2}(\alpha_S\alpha_W^2)$, simply because $\alpha_S^2\alpha_W > \alpha_S\alpha_W^2$, the QCD corrections to the EW top-pair production are more likely to be relevant for new physics searches at the LHC due to the resonant role of the Z′ boson. Besides, while the procedure for the calculation of NLO corrections at order $\mathcal{O}(\alpha_S\alpha_W^2)$ is model independent, provided that the Z′ couplings to the SM quarks are kept general, as in the above mentioned Feynman rule, the NLO corrections at orders $\mathcal{O}(\alpha_S^2\alpha_W)$ and $\mathcal{O}(\alpha_W^3)$ are strongly model dependent due to the rich structure of the Higgs sector in models beyond the SM, see for example [91, 92].

In the following sections we will investigate how the presence of an additional Z′-boson impacts the EW top-pair production. We will detail the calculation of the LO matrix element, and its virtual and real QCD corrections.

2.2 Leading-order electroweak top-pair production

In SM extensions containing an additional Z′ boson, the partonic cross section of the top-pair production can be split into two parts, the cross section $\hat{\sigma}_{2;0} = \hat{\sigma}_S^{\mathrm{LO}}$ of the subprocesses mediated by the strong interaction and the cross section $\hat{\sigma}_{0;2} = \hat{\sigma}_W^{\mathrm{LO}}$ of the subprocesses mediated by the electroweak interaction. The existence of the Z′ boson does not affect the $\hat{\sigma}_S^{\mathrm{LO}}$ cross section, which is the same as in the SM and has been long known in the literature. In this section we describe the calculation of the partonic cross section $\hat{\sigma}_W^{\mathrm{LO}}$, often referred to as the Born or the tree-level contribution.

Let us start by considering a general $2 \to 2$ hadron scattering. The momentum conservation for the hard process can be written as

$$x_1K_1 + x_2K_2 = p_1 + p_2 \ , \tag{2.4}$$

where K_1, K_2 are the momenta of the incoming hadrons h_1, h_2 and x_1, x_2 are the momentum fractions of the incoming partons, while p_1, p_2 the momenta of the outgoing particles. In the following discussion, we will often use the partonic momenta

$$k_1 = x_1K_1 \ , \ k_2 = x_2K_2 \tag{2.5}$$

instead of the hadronic momenta and the partonic momentum fractions K_i, x_i. The hadronic and partonic center of mass energy squared can be defined in terms of hadronic and partonic momenta as

$$s_{\mathrm{had}} = -(K_1 + K_2)^2 \ , \ \hat{s} = -(k_1 + k_2)^2 \ . \tag{2.6}$$

Note that in calculations throughout this chapter we use the Pauli metric in which the dot product of momenta has an overall minus sign as compared to the Bjorken-Drell metric[5].

[5]For a detailed discussion on the relevance of the choice of the metric and a recipe on how to convert between formulae employing different metrics, the reader is encouraged to consult [93].

To fully characterize the 2-parton phase space, we introduce the set of variables

$$\mathbf{\Phi}_2 = \{x_1, x_2; p_1, p_2\} \ . \tag{2.7}$$

These are constrained by the momentum conservation, eq. (2.4), and by the on-shell conditions $p_i^2 = -m_i^2$ for final state particles where m_i is the mass of the particle with momentum p_i.

The total cross section at leading order is given by

$$\sigma^{\mathcal{B}} = \int d\mathbf{\Phi}_2 f_1(x_1) f_2(x_2) \mathcal{B}(\mathbf{\Phi}_2) \tag{2.8}$$

where $\mathcal{B}$ denotes the LO amplitude squared, summed and averaged over initial spin and color, including an appropriate flux factor. Furthermore, f_i are the parton distribution functions (PDFs) and the integration measure $d\mathbf{\Phi}_2$ is defined as

$$d\mathbf{\Phi}_2 = dx_1 dx_2 d\Phi_2(k_1 + k_2; p_1, p_2) \ , \tag{2.9}$$

in which $d\Phi_2$ is the usual 2-body phase space

$$d\Phi_2(q; p_1, p_2) = (2\pi)^4 \delta^4 \left(q - \sum_{i=1}^{2} p_i \right) \prod_{i=1}^{2} \frac{d^3 p_i}{(2\pi^3) 2p_i^0} \ . \tag{2.10}$$

The parton luminosities L_{ij} in eq. (2.1) are given by a convolution of PDFs f_i and f_j of the incoming partons:

$$L_{ij}(x, \mu_f^2) = x \int_0^1 dy \int_0^1 dz \delta(x - yz) f_i(y, \mu_f^2) f_j(z, \mu_f^2). \tag{2.11}$$

Throughout this chapter, however, we rather use the product of parton distribution functions $\mathcal{L}$ defined as

$$\mathcal{L} = \mathcal{L}(x_1, x_2) = f_1(x_1) f_2(x_2) \ . \tag{2.12}$$

Note that, as in eq. (2.8), we often suppress the dependence of PDFs and partonic cross sections on the factorization scale, in which case it is implicit.

While it is possible to express partonic cross sections in terms of the scalar products of independent momenta of the process, it is often more convenient to use Mandelstam variables $\hat{s}$, $\hat{t}$ and $\hat{u}$ instead. $\hat{s}$ was defined in eq. (2.6) and the definitions of $\hat{t}$ and $\hat{u}$ read

$$\hat{t} = -(k_1 - p_1)^2 = -(k_2 - p_2)^2 \ , \qquad \hat{u} = -(k_1 - p_2)^2 = -(k_2 - p_1)^2 \ . \tag{2.13}$$

The Mandelstam variables $\hat{s}$, $\hat{t}$ and $\hat{u}$ are not all independent and one can easily show that

$$\hat{s} + \hat{t} + \hat{u} = \sum_i m_i^2 \tag{2.14}$$

where we sum over all the external particles, provided they are on-shell.

The amplitude squared of the Born contribution to the EW top-pair production comprises of nine terms obtained by interfering the diagrams in Figure 2.1 (e), (f) and Figure 2.2. Feynman rules, spin and polarization sums used in the calculations of amplitudes squared are listed in Appendix B. The incoming partons are considered massless, while the outgoing top quarks on-shell

$$k_i^2 = 0 \ , \quad p_i^2 = -m_{\mathrm{t}}^2 \ . \tag{2.15}$$

The independent scalar products can be expressed in terms of Mandelstam variables as

$$k_1 \cdot k_2 = -\frac{1}{2}\hat{s} \ , \quad k_1 \cdot p_1 = \frac{1}{2}(\hat{t} - m_{\mathrm{t}}^2) \ , \quad k_2 \cdot p_1 = \frac{1}{2}(\hat{u} - m_{\mathrm{t}}^2) \ , \tag{2.16}$$

and the Mandelstam variables sum to

$$\hat{s} + \hat{t} + \hat{u} = 2m_{\mathrm{t}}^2 \ . \tag{2.17}$$

The full expression for the matrix element is rather lengthy but for completeness we show the expression for a general interference term, $\mathcal{B}_q(B, B')$:

$$\begin{aligned}\mathcal{B}_q(B,B') = \frac{2\alpha_W^2}{\hat{s}^2 D_B D_{B'} s_W^4} \Big\{ & \hat{s}(\hat{t}-\hat{u}) \left(A_B^q B_{B'}^q + A_{B'}^q B_B^q\right) \left(A_B^{\mathrm{t}} B_{B'}^{\mathrm{t}} + A_{B'}^{\mathrm{t}} B_B^{\mathrm{t}}\right) + \\ & \left(A_B^q A_{B'}^q + B_B^q B_{B'}^q\right) \left[\left(\hat{t}^2 + \hat{u}^2 + 4\hat{s}m_{\mathrm{t}}^2 - 2m_{\mathrm{t}}^4\right) A_B^{\mathrm{t}} A_{B'}^{\mathrm{t}} + \left(\hat{t}^2 + \hat{u}^2 - 2m_{\mathrm{t}}^4\right) B_B^{\mathrm{t}} B_{B'}^{\mathrm{t}}\right] \Big\} \\ & \Big\{ \left[(\hat{s} - M_B^2)(\hat{s} - M_{B'}^2) + m_B m_{B'} \Gamma_B \Gamma_{B'}\right] + i \left[(\hat{s} - M_B^2) m_{B'} \Gamma_{B'} - (\hat{s} - M_{B'}^2) m_B \Gamma_B\right] \Big\} \ , \end{aligned} \tag{2.18}$$

where $B, B' \in \{\gamma, \mathrm{Z}, \mathrm{Z}'\}$ and the index q denotes incoming massless partons and

$$\begin{aligned} D_\gamma &= \frac{1}{\hat{s}^2}, & A_\gamma^q &= s_W Q_q, & A_\gamma^{\mathrm{t}} &= s_W Q_u, & B_\gamma^q &= 0, & B_\gamma^{\mathrm{t}} &= 0, \\ D_{\mathrm{Z}} &= \frac{1}{(\hat{s} - M_{\mathrm{Z}}^2)^2 + m_{\mathrm{Z}}^2 \Gamma_{\mathrm{Z}}^2}, & A_{\mathrm{Z}}^q &= \frac{a_{\mathrm{Z}}^q}{4c_W}, & A_{\mathrm{Z}}^{\mathrm{t}} &= \frac{a_{\mathrm{Z}}^u}{4c_W}, & B_{\mathrm{Z}}^q &= \frac{b_{\mathrm{Z}}^q}{4c_W}, & B_{\mathrm{Z}}^{\mathrm{t}} &= \frac{b_{\mathrm{Z}}^u}{4c_W}, \\ D_{\mathrm{Z}'} &= \frac{1}{(\hat{s} - M_{\mathrm{Z}'}^2)^2 + m_{\mathrm{Z}'}^2 \Gamma_{\mathrm{Z}'}^2}, & A_{\mathrm{Z}'}^q &= \frac{a_{\mathrm{Z}'}^q}{4c_W}, & A_{\mathrm{Z}'}^{\mathrm{t}} &= \frac{a_{\mathrm{Z}'}^{\mathrm{t}}}{4c_W}, & B_{\mathrm{Z}'}^q &= \frac{b_{\mathrm{Z}'}^q}{4c_W}, & B_{\mathrm{Z}'}^{\mathrm{t}} &= \frac{b_{\mathrm{Z}'}^{\mathrm{t}}}{4c_W}, \end{aligned} \tag{2.19}$$

where Q_u, Q_d are the electric charges of up- and down-type quark respectively, the Z-boson couplings to the SM fermions are equal to $a_{\mathrm{Z}}^u = 1 - 8/3 s_{\theta_W}^2$, $a_{\mathrm{Z}}^d = 4/3 s_{\theta_W}^2 - 1$, $b_{\mathrm{Z}}^u = 1$, $b_{\mathrm{Z}}^d = -1$ and $a_{\mathrm{Z}'}^q$, $b_{\mathrm{Z}'}^q$ are the model dependent vector and axial-vector couplings of the Z′ boson to a SM quark $q \in \{\mathrm{d}, \mathrm{u}, \mathrm{s}, \mathrm{c}, \mathrm{b}, \mathrm{t}\}$. Note in eq. (2.19), that the Z-boson couplings are family universal and the superscript u refers to up-type quarks, while different generations of the SM fermions can couple to Z′-boson with different strengths, and the superscript t refers to the top quark couplings only.

The expression for the total Born matrix element can be written in terms of general interference terms as

$$\mathcal{B} = \sum_q \left(\mathcal{B}_q(\gamma,\gamma) + \mathcal{B}_q(\mathrm{Z},\mathrm{Z}) + \mathcal{B}_q(\mathrm{Z}',\mathrm{Z}') + \sum_{B \neq B'} \mathcal{B}_q(B,B') \right) \ , \tag{2.20}$$

where we sum over all the possible light quarks in the initial state $q \in \{\mathrm{d}, \mathrm{u}, \mathrm{s}, \mathrm{c}, \mathrm{b}\}$. Note that, in general, the expression for an interference term $\mathcal{B}_q$ has an imaginary part, but since $\mathcal{B}_q(B,B) \in \mathbb{R}$ and $\mathcal{B}_q(B',B) = \mathcal{B}_q(B,B')^*$ the total amplitude is real.

The amplitudes squared of the Born contribution in 4- and D-dimensions[6], have been calculated automatically using the tool chain QGRAF/DIANA → FORM [94, 95, 96] interfaced via a Python [97] script which we have developed for this purpose. A detailed description of this calculation chain and its automation can be found in Section 2.5.

[6]The Born matrix element calculated in D-dimensions will be required for the renormalization of the virtual contribution.

2.3 Next-to-leading order QCD corrections to the electroweak top-pair production

The calculation of NLO corrections comprises the calculation of interferences of Feynman diagrams with one additional line, as compared to the diagrams of the Born contribution. According to how this line is attached to tree-level diagrams, NLO contributions can be split into two distinct classes. The virtual and the real corrections.

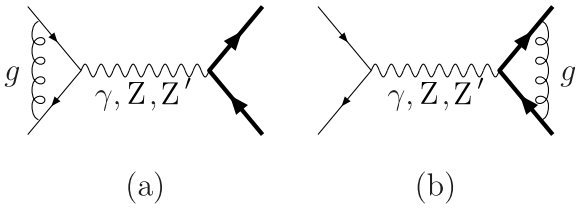

Figure 2.3: Virtual diagrams contributing to the top-pair production at order $\mathcal{O}(\alpha_S \alpha_W^2)$.

Virtual contributions are characterized by an additional internal exchange of particles. That is for a $2 \to 2$ process, the Feynman diagrams of virtual contributions also have two incoming and two outgoing external lines. The additional line is internal and leads to a single closed loop. Hereafter, we will often refer to the diagrams of virtual contribution as the 1-loop diagrams. The 1-loop diagrams of the top-pair production at the order $\mathcal{O}(\alpha_S \alpha_W^2)$ are displayed in Figure 2.3. Note that also box-like diagrams, depicted in Figure 2.4 are allowed but do not contribute at order $\mathcal{O}(\alpha_S \alpha_W^2)$, because their interference with tree-level diagrams is proportional to a trace over a single colour matrix which is traceless. A careful reader must have noticed that an interference of a 1-loop diagram with another 1-loop diagram in Figure 2.3 does not correspond to the order $\mathcal{O}(\alpha_S \alpha_W^2)$ but to the order $\mathcal{O}(\alpha_S^2 \alpha_W^2)$ instead. This is because the interferences of 1-loop diagrams have two additional internal lines and two loops in total. In order to obtain the corrections at order $\mathcal{O}(\alpha_S \alpha_W^2)$, one has to interfere 1-loop diagrams with tree-level diagrams. Because the final state of the tree-level and 1-loop diagrams is the same, the virtual contribution has to be added to the Born matrix element coherently.

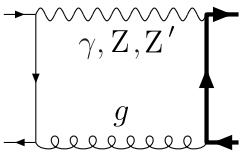

Figure 2.4: Box-like virtual diagrams that are allowed but do not contribute to the top-pair production at order $\mathcal{O}(\alpha_S \alpha_W^2)$. Note that they will contribute at order $\mathcal{O}(\alpha_S^2 \alpha_W)$.

In the case of real contributions the additional line is external. The real contribution to a $2 \to 2$ process, therefore, is a $2 \to 3$ process. At NLO, real contributions do not contain any closed loops, in contrast with virtual contributions, and the amplitude squared is obtained by interfering real diagrams with real diagrams. A subset of real diagrams is shown in Figure 2.5. Real contributions have a different final state, as compared to the tree-level and virtual contributions, therefore, it has to be added to the total partonic cross section incoherently.

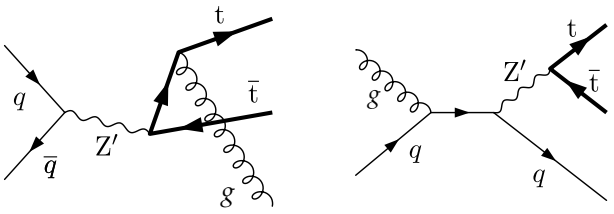

Figure 2.5: A subset of diagrams contributing to the real part of the NLO top-pair production.

In this section, we present the calculation of the real and virtual corrections to top-pair production at order $\mathcal{O}(\alpha_S \alpha_W^2)$. We demonstrate that virtual corrections suffer from ultra-violet (UV) and infra-red (IR) divergences which can be regulated in dimensional regularization. We then show how we evaluate the loop integrals by reducing them to a small set of master integrals which we subsequently calculate using the differential equations method [98]. Finally, we show that the UV divergences can be treated by the procedure called renormalization. The treatment of the IR divergences is postponed to Section 2.3.3.

2.3.1 Virtual contributions

Virtual contributions are characterized by an additional internal line and contain closed loops. Since the particle on this additional line is virtual and because energy-momentum conservation does not provide any constraint on it, its four-momentum can take on any value and one has to integrate over all the possibilities. In the points where the modulus of this four-momentum, also referred to as the loop momentum, approaches zero or infinity the amplitude of the virtual contribution may become singular.

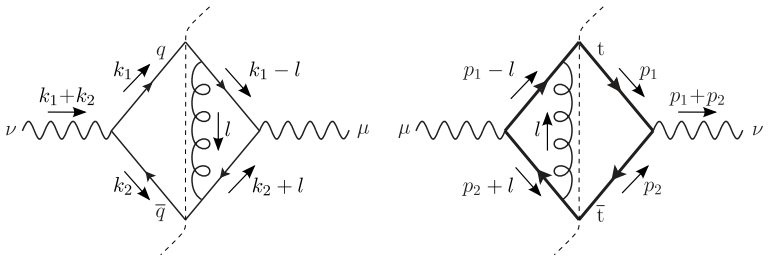

Figure 2.6: Left: 1-loop initial state fermion line. Right: 1-loop final state fermion line.

Let us illustrate this on two examples related to the EW top-pair production: the trace of the fermion line of a tree-level diagram interfered with a 1-loop diagram featuring a gluon exchange in the initial (final) state, depicted on the left (right) diagram of Figure 2.6. The amplitudes squared of these fermion lines will contain loop integrals

$$I^{\mathrm{i}} = \int \frac{d^4l}{(2\pi)^2} \frac{f^{\mathrm{i}}(l,k_1,k_2)}{l^2(k_1-l)^2(k_2+l)^2} = \int \frac{d^4l}{(2\pi)^2} \frac{f^{i}(l,k_1,k_2)}{l^2(l^2-2k_1\cdot l)(l^2+2k_2\cdot l)} \ , \tag{2.21}$$

$$\begin{aligned} I^{\mathrm{f}} &= \int \frac{d^4l}{(2\pi)^2} \frac{f^{\mathrm{f}}(l,p_1,p_2)}{l^2[(p_1-l)^2+m_{\mathrm{t}}^2][(p_2+l)^2+m_{\mathrm{t}}^2]} \\ &= \int \frac{d^4l}{(2\pi)^2} \frac{f^{f}(l,p_1,p_2)}{l^2(l^2-2p_1\cdot l)(l^2+2p_2\cdot l)} \ , \end{aligned} \tag{2.22}$$

where $I^{\mathrm{i(f)}}$ denotes a loop integral in the fermion line with a gluon exchange in the initial (final) state. The $1/q^2$ factors come from the propagator denominators of the gluon and (initial) final state quarks (after) before the emission of the gluon. Furthermore, $f^{\mathrm{i(f)}}$ are functions of scalar products of the momenta l, k_1, k_2, p_1 and p_2[7]. Considering various forms of the functions $f^{\mathrm{i(f)}}$ can lead to explicit un-integrable singularities.

Assume that the function f^{i} does not depend on the loop momentum. If the virtual gluon is soft, i.e., $l \to 0$, the integrand of I^{i} can be approximated by

$$-\frac{1}{(2\pi)^2}\frac{1}{l^2 2k_1\cdot l 2k_2\cdot l} \tag{2.23}$$

and the loop integral will be logarithmically divergent as $l \to 0$, because there are four powers of l in the denominator. These divergences are called the soft infrared (IR) divergences since they come from the low-momentum region of the loop integral and are caused by the soft emission of a particle. The loop integral I^{i} is also divergent when the loop momentum becomes collinear to the momentum of one of the incoming partons. If $l \sim k_1$, for example, which also implies $l^2 \to 0$, then the integrand of I^{i} is approximately proportional to

$$-\frac{1}{(2\pi)^2}\frac{1}{l^2 l^2 2k_1\cdot k_2}\ . \tag{2.24}$$

The loop integral is again logarithmically divergent. The divergences originating from the configurations in which the loop momentum is collinear with one of the external momenta are referred to as collinear IR divergences. The loop integral I^{i} is thus IR divergent. The loop integral I^{f} also has soft divergences but no collinear divergences, due to the fact that $l^2 \to m_{\mathrm{t}}^2$ if $l \sim p_1$.

Now let us consider the loop integral I^{f}. In the case when the function f^{f} coincides with one of the propagator denominators, e.g. $f^{\mathrm{f}} = l^2 - 2p_1\cdot l$. In the region where $l \to \infty$, the integrand is proportional to $1/l^4$ and leads to a logarithmically divergent loop integral. The divergence in this case comes from the high-momentum region and is denoted as the ultraviolet (UV) divergence.

UV divergences are properly taken care of by the renormalization procedure, while the soft divergences cancel in the sum of real and virtual contributions to the cross section. Final state collinear divergences cancel in inclusive quantities, when integrated over the final state phase space or with a jet definition. Initial state collinear divergences are absorbed into the PDFs via the procedure of mass factorization.

Although the divergences are subtracted out in the final physical answer, it is useful to require that divergent integrals be mathematically manageable in the intermediate stages of the calculation. This can be achieved via dimensional regularization. As we have seen in the previous section, the criterion that the loop integrals in eqs. (2.21) and (2.22) diverge is closely related to the dimension of the integral. A generic loop integral

$$\int \frac{d^4 l}{(2\pi)^2}\frac{1}{l^n} \tag{2.25}$$

is in 4 dimensions UV divergent for $n \leq 4$ and IR divergent for $n \geq 4$. In $D < 4$ dimensions, the same integral is UV finite while in $D > 4$ it is IR finite. If we keep the dimension D of the loop momentum in the integral general, the divergences will manifest as $1/(D-4)$ poles and the loop integral becomes divergent only as D approaches 4. UV divergent as $D \to 4$ from the minus direction, IR divergent as $D \to 4$ from the plus direction. Keeping the number of dimensions general in the calculation of virtual contributions thus regularizes UV and IR divergences.

[7] In general, there will be also loop integrals with uncontracted l^μ, l^ν on the numerator, so-called tensor integrals, which we ignore at the moment.

Let us define our theory in a D-dimensional Minkowski space. The integration momentum l, is now a D-dimensional momentum, $l^\mu = (l^0, l^1, \ldots, l^{D-1})$. The metric $g^{\mu\nu}$ is such that $g^\mu_\mu = D$. The integration measure is defined as

$$\int \frac{d^4 l}{(2\pi)^2} \to \mu_r^{4-D} \int \frac{d^D l}{(2\pi)^{(D-2)}} \ , \tag{2.26}$$

where we have introduced a mass scale μ_r which preserves the coupling constants dimensionless.

We also need to extend the Dirac algebra into D-dimensions. The index μ of γ^μ now runs over $(0, \ldots, D-1)$. If one naively follows the definition of a Clifford algebra in arbitrary dimensions, one would normalize the γ matrices such that $Tr\{\gamma^\mu \gamma^\nu\} = 2^{D/2} g^{\mu\nu}$. This, however, is not necessary as it is sufficient that our D-dimensional generalization reduces to the usual formula in $D = 4$, and we are free to choose the normalization to be $Tr\{\gamma^\mu \gamma^\nu\} = 4g^{\mu\nu}$ [99]. The γ_5 matrix in 4-dimensions is defined as

$$\gamma_5 = -\frac{i}{4!} \epsilon_{\mu\nu\rho\sigma} \gamma^\mu \gamma^\nu \gamma^\rho \gamma^\sigma, \tag{2.27}$$

where $\epsilon_{\mu\nu\rho\sigma}$ is a totally antisymmetric tensor. This is a purely 4-dimensional quantity and its definition cannot be consistently extended into D-dimensions. The treatment of γ_5 in dimensional regularization, thus, requires more attention. In the calculation of virtual corrections to the top-pair production we employ a prescription for γ_5 relying on the algorithms for trace calculations implemented in the computer algebra system FORM [96]. In FORM, it is possible to extend the definition of all relevant objects to D-dimensions, while for the simplification of chains of γ matrices one can use the algorithms valid in 4-dimensions. For a detailed account on the algorithms used implemented in FORM and the γ_5 prescription we use we refer to [100]. We point out, that prescription we use has been shown to be consistent with the procedure of renormalization as well as with the treatment of infrared divergences.

In dimensional regularization, thus, the calculation of 1-loop corrections involves the evaluation of loop integrals such as

$$\mu_r^{4-D} \int \frac{d^D l}{(2\pi)^{(D-2)}} \frac{f(l, k_1, k_2, p_1)}{\mathcal{D}_1^a \mathcal{D}_2^b \ldots} \ , \tag{2.28}$$

where, as previously, f is a function of scalar products of the loop momentum l and external momenta of the problem, in our case k_1, k_2 and p_1 (p_2 can be excluded via the momentum conservation). $\mathcal{D}_i$ denote the denominators coming from the propagators of internal particles and, in general, are of the form $\mathcal{D} = (l - q)^2 + m^2$, where $l - q$ is the momentum and m the mass on the corresponding internal line.

The virtual correction to the top-pair production at order $\mathcal{O}(\alpha_S \alpha_W^2)$ contain the interference terms of 1-loop diagrams in Figure 2.3 with the tree-level diagrams in Figure 2.1 (e), (f) and in Figure 2.2, which totals to 18 interference terms plus the charge conjugated combinations. We have calculated the corresponding traces in D-dimensions using the γ_5 treatment described above and the Feynman rules listed in Appendix B. The virtual contribution to the NLO top-pair production partonic cross section can be written as

$$\sigma^{\mathcal{V}} = \int d\mathbf{\Phi}_2 \mathcal{L} \sum_q \mathcal{V}_q(\mathbf{\Phi}_2) = \int d\mathbf{\Phi}_2 \mathcal{L} \left\{ \sum_q \sum_{B,B'} \left[\mathcal{V}_q^{\mathrm{i}}(B, B') + \mathcal{V}_q^{\mathrm{f}}(B, B') \right] + \mathrm{c.c.} \right\} \tag{2.29}$$

where, as in the case of the Born matrix elements, we sum over all the possible light quarks in the initial state $q \in \{\mathrm{d}, \mathrm{u}, \mathrm{s}, \mathrm{c}, \mathrm{b}\}$, and $d\mathbf{\Phi}_2$ and $\mathcal{L}$ were defined in Section 2.2. $\mathcal{V}_q^{\mathrm{i(f)}}(B, B')$ denotes

a general interference term of a 1-loop diagram with a tree diagram involving a s-channel B, B' vector boson respectively and a gluon exchange in the initial (final) state. We sum over all the combinations of B and B' where $B, B' \in \{\gamma, \mathrm{Z}, \mathrm{Z}'\}$. The expression for the interference term $\mathcal{V}_q^{\mathrm{i(f)}}(B, B')$ is rather lengthy at this stage and we show it in the next section. The interference terms $\mathcal{V}_q^{i(f)}$ contain in total 30 different loop integrals. As discussed above, the virtual contribution to the total cross section, $\sigma^{\mathcal{V}}$, at this stage suffers from both UV and IR divergences manifesting as $1/(D-4)$ poles.

Similarly as in the case of the Born matrix elements, the virtual corrections were calculated automatically using the DIANA/QGRAF → FORM tool chain. For more details, see the discussion in Section 2.5.

In the following subsections we show how we evaluate the loop integrals and discuss the details concerning the renormalization procedure used to cure UV divergences.

Evaluation of loop integrals: IBP reduction

Although it is possible to evaluate all the 1-loop integrals in the problem directly, this is not necessary as not all loop integrals are independent. Let us introduce the concept of auxiliary topologies [101]. An auxiliary topology is a set of independent propagator denominators $\mathcal{A} = \{\mathcal{D}_1, \ldots, \mathcal{D}_n\}$ of a size equal to the number of independent scalar products in the problem involving the loop momentum – scalar products of the loop momentum l with itself and with all the independent external momenta. The propagator denominators have the usual form $\mathcal{D} = (l-q)^2 + m^2$, where $l-q$ is the momentum and m the mass of the corresponding particle in the loop. At 1-loop, all these scalar products can be expressed in terms of the denominators from the auxiliary topology [102]. The notion of auxiliary topologies, thus, allows us to rewrite the functions $f^{\mathrm{i(f)}}$ from eqs. (2.21) and (2.22) in terms of the propagator denominators and write all loop integrals in the following form

$$I(a, b, \ldots) = \mu_r^{4-D} \int \frac{d^D l}{(2\pi)^{(D-2)}} \frac{1}{\mathcal{D}_1^a \mathcal{D}_2^b \ldots} \,, \tag{2.30}$$

in which only propagator denominators appear in the integrand. The indices a, b, ... denote the denominator powers and can in general acquire positive or negative integer values. The denominators with zero powers do not appear in the loop integral and the denominators with negative powers appear in the numerator.

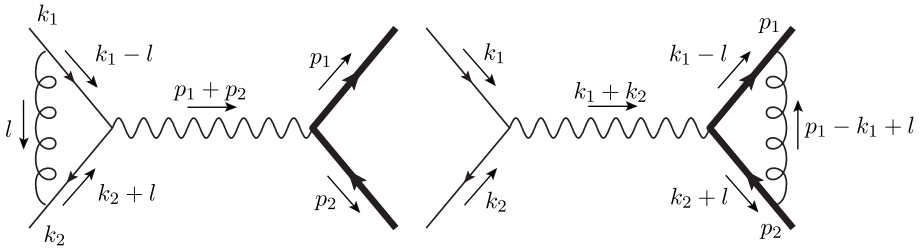

Figure 2.7: The momenta distribution in 1-loop diagrams of the top-pair production at order $\mathcal{O}(\alpha_S \alpha_W^2)$.

Let us assume that the momenta in 1-loop diagrams, entering the virtual contribution of the top-pair production at order $\mathcal{O}(\alpha_S \alpha_W^2)$, are distributed as in Figure 2.7. Since the propagator denominators in the two diagrams differ in the mass of the fermions in the loop, we will need two

sets of independent denominators, two auxiliary topologies, to rewrite all the 1-loop integrals into the form of eq. (2.30). From the loop momentum l and three independent external momenta k_1, k_2, p_1[8] one can form four scalar products $l\cdot l$, $l\cdot k_1$, $l\cdot k_2$, $l\cdot p_1$ containing the loop momentum. Both diagrams in Figure 2.7, however, feature only three propagator denominators containing a loop momentum. In order to be able to construct auxiliary topologies corresponding to these diagrams one has to complete the sets of propagator denominators figuring in these diagrams by one linearly independent denominator. We have chosen the auxiliary topologies in the following way

$$\mathcal{A}_1 = \{\mathcal{D}_{1,1} = l^2, \mathcal{D}_{1,2} = (k_1 - l)^2, \mathcal{D}_{1,3} = (k_2 + l)^2, \mathcal{D}_{1,4} = (p_1 - k_1 + l)^2\}, \tag{2.31}$$

$$\mathcal{A}_2 = \{\mathcal{D}_{2,1} = l^2, \mathcal{D}_{2,2} = (k_1 - l)^2 + m_\mathrm{t}^2, \mathcal{D}_{2,3} = (k_2 + l)^2 + m_\mathrm{t}^2, \mathcal{D}_{2,4} = (p_1 - k_1 + l)^2\}, \tag{2.32}$$

where the $\mathcal{A}_1$ and $\mathcal{A}_2$ auxiliary topologies of the left and right diagrams in the Figure 2.7 were respectively completed by the denominators $\mathcal{D}_{1,4}$ and $\mathcal{D}_{2,1}$. The scalar products $l\cdot l$, $l\cdot k_1$, $l\cdot k_2$, $l\cdot p_1$ can be written in terms of the denominators $\mathcal{D}_{1,i}, \mathcal{D}_{2,i} \in \mathcal{A}_1 \cup \mathcal{A}_2$ as follows

$$l\cdot l = \mathcal{D}_{1,1} = \mathcal{D}_{2,1}\ , \tag{2.33}$$

$$l\cdot k_1 = \frac{1}{2}\left(\mathcal{D}_{1,1} - \mathcal{D}_{1,2}\right) = \frac{1}{2}\left(\mathcal{D}_{2,1} - \mathcal{D}_{2,2} + m_\mathrm{t}^2\right)\ , \tag{2.34}$$

$$l\cdot k_2 = \frac{1}{2}\left(\mathcal{D}_{1,3} - \mathcal{D}_{1,1}\right) = \frac{1}{2}\left(\mathcal{D}_{2,3} - \mathcal{D}_{1,1} - m_\mathrm{t}^2\right)\ , \tag{2.35}$$

$$l\cdot p_1 = \frac{1}{2}\left(\hat{t} + \mathcal{D}_{1,4} - \mathcal{D}_{1,2}\right) = \frac{1}{2}\left(\hat{t} + \mathcal{D}_{2,4} - \mathcal{D}_{2,2} + m_\mathrm{t}^2\right)\ . \tag{2.36}$$

All loop integrals figuring in the virtual contributions of top-pair production at order $\mathcal{O}(\alpha_S\alpha_W^2)$ can be thus written as

$$I_{\mathcal{A}_1}(i_1,i_2,i_3,i_4) = \mu_r^{4-D}\int \frac{d^Dl}{(2\pi)^{D-2}}\frac{1}{\mathcal{D}_{1,1}^{i_1}\mathcal{D}_{1,2}^{i_2}\mathcal{D}_{1,3}^{i_3}\mathcal{D}_{1,4}^{i_4}}\ , \tag{2.37}$$

$$I_{\mathcal{A}_2}(i_1,i_2,i_3,i_4) = \mu_r^{4-D}\int \frac{d^Dl}{(2\pi)^{D-2}}\frac{1}{\mathcal{D}_{2,1}^{i_1}\mathcal{D}_{2,2}^{i_2}\mathcal{D}_{2,3}^{i_3}\mathcal{D}_{2,4}^{i_4}}\ , \tag{2.38}$$

where i_1, i_2, i_3, i_4 have integers values.

Loop integrals are not independent of each other but related by Integration By Parts (IBP) identities. In dimensional regularization the integral over a total derivative is zero. Let I' be an integrand of (2.37) or (2.38). Then the equation

$$\int \frac{d^Dl}{(2\pi)^{D-2}}\frac{\partial}{\partial l^\mu}\left[q^\mu I'(i_1,i_2,i_3,i_4)\right] = 0 \tag{2.39}$$

can be used for the derivation of IBP identities. The momentum q can be either the loop momentum or one of the independent external momenta. If the auxiliary topology is constructed out of n loop momenta and $m+1$ external lines one can build $n(n+m)$ identities for every integral [103].

The differentiation in eq. (2.39) will typically generate loop integrals with indices shifted by integer values and multiplied by a coefficient composed out of the external momenta invariants, dimension D and the denominator powers i_i. It is useful to introduce step operators $\mathbf{N}^{+(-)}$ which raise (lower) the denominator power in the loop integral at position N, e.g. $\mathbf{3}^+I(i_1,i_2,i_3,i_4) =$

[8] p_2 can be expressed in terms of k_1, k_2, p_1 via the momentum conservation.

$I(i_1, i_2, i_3 + 1, i_4)$. The IBP identities for auxiliary topologies $\mathcal{A}_1$ and $\mathcal{A}_2$ read

$$\begin{aligned}
&\left[(D - 2i_1 - i_2 - i_3 - i_4) - (\mathbf{2}^+ i_2 + \mathbf{3}^+ i_3)\mathbf{1}^- - \mathbf{4}^+ i_4(\mathbf{1}^- + \hat{t})\right] I_{\mathcal{A}_1}(i_1, i_2, i_3, i_4) = 0 \ , \\
&\big[(i_2 - i_1) + \mathbf{1}^+ i_1 \mathbf{2}^- - \mathbf{2}^+ i_2 \mathbf{1}^- + \mathbf{3}^+ i_3(\mathbf{2}^- - \mathbf{1}^- + \hat{s}) \\
&\qquad\qquad - \mathbf{4}^+ i_4(\mathbf{2}^- - \mathbf{1}^- + \hat{t})\big] I_{\mathcal{A}_1}(i_1, i_2, i_3, i_4) = 0 \ , \\
&\big[(i_1 - i_3) - \mathbf{1}^+ i_1 \mathbf{3}^- - \mathbf{2}^+ i_2(\mathbf{1}^- - \mathbf{3}^- + \hat{s}) + \mathbf{3}^+ i_3 \mathbf{1}^- \\
&\qquad\qquad + \mathbf{4}^+ i_4(\mathbf{1}^- - \mathbf{3}^- + \hat{t})\big] I_{\mathcal{A}_1}(i_1, i_2, i_3, i_4) = 0 \ , \\
&\big[(i_2 - i_4) + \mathbf{1}^+ i_1(\mathbf{2}^- - \mathbf{4}^- - \hat{t}) + \mathbf{2}^+ i_2 \mathbf{4}^- + \mathbf{3}^+ i_3(\mathbf{2}^- - \mathbf{4}^- + \hat{s}) \\
&\qquad\qquad + \mathbf{4}^+ i_4 \mathbf{2}^-\big] I_{\mathcal{A}_1}(i_1, i_2, i_3, i_4) = 0 \ ,
\end{aligned} \tag{2.40}$$

$$\begin{aligned}
&\Big[(D - 2i_1 - i_2 - i_3 - i_4) - (\mathbf{2}^+ i_2 + \mathbf{3}^+ i_3)(\mathbf{1}^- - m_{\mathrm{t}}^2) - \mathbf{4}^+ i_4(\mathbf{1}^- + \hat{t})\Big] I_{\mathcal{A}_2}(i_1, i_2, i_3, i_4) = 0 \ , \\
&\Big[(i_2 - i_1) + \mathbf{1}^+ i_1(\mathbf{2}^- - m_{\mathrm{t}}^2) - \mathbf{2}^+ i_2(\mathbf{1}^- + m_{\mathrm{t}}^2) + \mathbf{3}^+ i_3(\mathbf{2}^- - \mathbf{1}^- + \hat{s} - m_{\mathrm{t}}^2) \\
&\qquad\qquad - \mathbf{4}^+ i_4(\mathbf{2}^- - \mathbf{1}^- + \hat{t})\big] I_{\mathcal{A}_2}(i_1, i_2, i_3, i_4) = 0 \ , \\
&\Big[(i_1 - i_3) - \mathbf{1}^+ i_1(\mathbf{3}^- - m_{\mathrm{t}}^2) - \mathbf{2}^+ i_2(\mathbf{1}^- - \mathbf{3}^- + \hat{s} - m_{\mathrm{t}}^2) + \mathbf{3}^+ i_3(\mathbf{1}^- + m_{\mathrm{t}}^2) \\
&\qquad\qquad + \mathbf{4}^+ i_4(\mathbf{1}^- - \mathbf{3}^- + \hat{t})\big] I_{\mathcal{A}_2}(i_1, i_2, i_3, i_4) = 0 \ , \\
&\Big[(i_2 - i_4) + \mathbf{1}^+ i_1(\mathbf{2}^- - \mathbf{4}^- - \hat{t} - m_{\mathrm{t}}^2) + \mathbf{2}^+ i_2(\mathbf{4}^- - 2m_{\mathrm{t}}^2) + \mathbf{3}^+ i_3(\mathbf{2}^- - \mathbf{4}^- + \hat{s} - 2m_{\mathrm{t}}^2) \\
&\qquad\qquad + \mathbf{4}^+ i_4 \mathbf{2}^-\big] I_{\mathcal{A}_2}(i_1, i_2, i_3, i_4) = 0 \ .
\end{aligned} \tag{2.41}$$

The IBP identities, in general, form a homogeneous system of linear equations with the integrals as unknowns. By solving it, one can obtain the expressions of some of the loop integrals in terms of other loop integrals. One can easily see that IBP identities in eqs. (2.40) and (2.41) form an under-determined system. It is thus impossible to find a solution for all loop integrals and the integrals whose value cannot be determined from the system are called the master integrals. In conclusion, the IBP identities can be used to express most of the loop integrals in the system in terms of a small set of master integrals.

The procedure of solving systems of IBPs is called reduction. There exist different reduction methods. In one method a general solution of an infinite system of identities is attempted, i.e. a solution valid for any integer values of the denominator powers. This solution has the form of a combination of identities which, lowering and raising exponents, transform the loop integrals into linear combinations of carefully chosen master integrals [104, 105]. Up to now, this method has been based on laborious human analysis because a general algorithm is not known[9]. In the other method, the so called Laporta algorithm [107], the values of denominator powers and thus the system of equations is constrained and solved by the usual Gauss elimination algorithm. The Laporta algorithm can be fully automated and there exist implementations such as AIR [108] or Reduze [101, 109], which are publicly available.

In the Laporta algorithm, the abstract propagator denominator powers $i_1, \ldots$ are substituted by tuples of integer values, called seeds. For a set of seeds one generates a system of equations which is consequently solved by eliminating integrals via backsubstitution. Let $\sum_i c_j I_j = 0$ be an

[9]There exists a proof that the number of master integrals in any system is finite, but the proof is not constructive and so it does not provide a method of reduction [106].

equation from the system, it is then transformed into $I_l = \sum_{i \neq l} c'_j I_j$ and I_l is substituted in all the other equations in the system.

In general, it is desirable for the solution of a reduction to be composed of expressions of integrals in terms of simpler integrals. Therefore, it is usually the most complex integral that is put on the l.h.s. before it is backsubstituted. The definition of the complexity of the loop integrals is one of the basic ingredients of the Laporta algorithm. Naively, a loop integral with less denominators is likely going to be easier to evaluate than a loop integral with more denominators, thus, the sum of positive denominator powers is usually one of the characteristics of the loop integrals entering the definition of the complexity. Note that because the system is constrained, there may be unsolved integrals which do not belong to the set of master integrals. These integrals would have been reduced had the set of seeds been larger. The order in which the equations are chosen for elimination greatly affects the performance of the algorithm. The set of master integrals in a problem and thus its solution, however, neither depends on the details of the complexity definition nor on the order in which the equations are processed, provided that the set of unsolved integrals consists only of the master integrals.

In the calculation of $\mathcal{O}(\alpha_W^2 \alpha_S)$ virtual corrections to the top-pair production we have used the Laporta algorithm to solve the IBPs in eqs. (2.40) and (2.41) to reduce the amplitude squared containing 30 distinct loop integrals in terms of only 3 master integrals

$$I_{\mathcal{A}_2}(0,1,0,0), I_{\mathcal{A}_2}(0,1,1,0), I_{\mathcal{A}_1}(0,1,1,0) \tag{2.42}$$

where the first integral in the list is usually referred to as the massive tadpole (one-point function), the second one as the massive bubble and the last one as the massless bubble (two-point functions). For this purpose, we have used the publicly available tool Reduze version 2 [109]. For details on how Reduze 2 was interfaced with the QGRAF/DIANA $\rightarrow$ FORM tool chain, we refer to Section 2.5.

The solution of the full system of IBPs of the auxililiary topologies $\mathcal{A}_1$ and $\mathcal{A}_2$ in eqs. (2.40) and (2.41) is too lengthy to be shown here. For illustration, however, we show how the loop integral I^{i} from eq. (2.21) with f^{i} independent of the loop momentum, the so-called massless triangle, can be reduced to a massless bubble:

$$I^{\mathrm{i}}\big|_{f^{\mathrm{i}}=1} = I_{\mathcal{A}_1}(1,1,1,0) = \frac{2}{\hat{s}} \left(\frac{1}{D-4} + 1 \right) I_{\mathcal{A}_1}(0,1,1,0) \ , \tag{2.43}$$

where we have expanded around $D \rightarrow 4$.

Evaluation of loop integrals: Virtual contributions after the reduction

The expression for virtual contributions in eq. (2.29) is assembled from interference terms $\mathcal{V}_q^{\mathrm{i}}$ and $\mathcal{V}_q^{\mathrm{f}}$. After the reduction to master integrals, the expressions for $\mathcal{V}_q^{\mathrm{i(f)}}$ are relatively short. There are in total 18 interference terms of loop and tree-level diagrams $\mathcal{V}_{q;1,0}^{\mathrm{i(f)}}$, displayed in Figures 2.3, 2.1 (e) and (f), 2.2. There are also 18 charge conjugated interference terms $\mathcal{V}_{q;0,1}^{\mathrm{i(f)}}$[10]. Observe that, if the couplings are real, $\mathcal{V}_{q;1,0}^{\mathrm{i(f)}}(B,B') = \mathcal{V}_{q;1,0}^{\mathrm{i(f)}}(B',B)^* = \mathcal{V}_{q;0,1}^{\mathrm{i(f)}}(B,B')^*$.

[10]Note the $1 \leftrightarrow 0$ permutation in the subscript of $\mathcal{V}_q^{\mathrm{i(f)}}$. The subscript $1,0$ refers to interferences of 1-loop and tree-level diagrams, while $0,1$ to interferences of tree-level and 1-loop diagrams.

The expression for the general interference terms of the auxiliary topology $\mathcal{A}_1$, featuring gluon exchange in the initial state after the reduction reads:

$$\mathcal{V}_q^{\rm i} = \mathcal{V}_{q;1,0}^{\rm i}(B,B') = \mathcal{N}\frac{\alpha_S}{2\pi}\frac{C_F}{(2\pi)^2}\frac{2\alpha_W^2}{\hat{s}^2 D_B D_{B'} s_W^4}\left(A_B^q A_{B'}^q + B_B^q B_{B'}^q\right) F(B,B') \\ \left\{A_B^{\rm t} A_{B'}^{\rm t}\left[\mathcal{E}_A^1 I_{\mathcal{A}_1}(0,1,1,0)\right] + B_B^{\rm t} B_{B'}^{\rm t}\left[\mathcal{E}_B^1 I_{\mathcal{A}_1}(0,1,1,0)\right]\right\}\ , \quad (2.44)$$

while the general interference terms of the auxiliary topology $\mathcal{A}_2$, featuring gluon exchange in the final state after the reduction can be written as

$$\mathcal{V}_q^{\rm f} = \mathcal{V}_{q;1,0}^{\rm f}(B,B') = \mathcal{N}\frac{\alpha_S}{2\pi}\frac{C_F}{(2\pi)^2}\frac{2\alpha_W^2}{\hat{s}^2 D_B D_{B'} s_W^4}\left(A_B^q A_{B'}^q + B_B^q B_{B'}^q\right) F(B,B') \\ \left\{A_B^{\rm t} A_{B'}^{\rm t}\left[\mathcal{E}_A^2 I_{\mathcal{A}_2}(0,1,0,0) + \mathcal{E}_A^3 I_{\mathcal{A}_2}(0,1,1,0)\right]\right. \\ \left. + B_B^{\rm t} B_{B'}^{\rm t}\left[\mathcal{E}_B^2 I_{\mathcal{A}_2}(0,1,0,0) + \mathcal{E}_B^3 I_{\mathcal{A}_2}(0,1,1,0)\right]\right\} \quad (2.45)$$

where the overall normalization $\mathcal{N}$ reads

$$\mathcal{N} = (4\pi)^{\frac{4-D}{2}}\Gamma(3-D/2)\left(\frac{\mu_r^2}{m_{\rm t}^2}\right)^{\frac{4-D}{2}}\ . \quad (2.46)$$

In the expressions above we have introduced

$$F(B,B') = \left\{\left[(s-M_B^2)(s-M_{B'}^2) + m_B m_{B'}\Gamma_B\Gamma_{B'}\right]\right. \\ \left. + i\left[(s-M_B^2)m_{B'}\Gamma_{B'} - (s-M_{B'}^2)m_B\Gamma_B\right]\right\}, \quad (2.47)$$

and the coefficients $\mathcal{E}_{A(B)}^i$ have, in $D = 4-2\epsilon$ dimensional space, the following expansions around $\epsilon \to 0$:

$$\mathcal{E}_A^1 = \frac{1}{\epsilon}f(3,1,2) + f(7/8,1/8,1/4) + \epsilon f(1,1/4,1/2), \quad (2.48)$$

$$\mathcal{E}_B^1 = \frac{1}{\epsilon}f(-1,1,-2) + f(-5/8,1/8,-5/4) + \epsilon f(-1/2,1/4,-1), \quad (2.49)$$

$$\mathcal{E}_A^2 = \frac{1}{8m_{\rm t}^2 S}\left\{\frac{1}{\epsilon}8(\hat{t}+\hat{u})f(3,1,1) - 2g(5,2,8,1) - \epsilon g(2,-2,-2,-2)\right\}, \quad (2.50)$$

$$\mathcal{E}_B^2 = \frac{\hat{t}+\hat{u}}{4m_{\rm t}^2 S}\left\{\frac{1}{\epsilon}4f(-1,1,-2) - f(1,1,2) - \epsilon f(0,-2,0)\right\}, \quad (2.51)$$

$$\mathcal{E}_A^3 = \frac{1}{8S}\left\{\frac{1}{\epsilon}8(\hat{t}+\hat{u})f(3,1,2) - \hat{s}f(7,1,2) - \epsilon\hat{s}f(4,2,0)\right\}, \quad (2.52)$$

$$\mathcal{E}_B^3 = \frac{1}{4S}\left\{\frac{1}{\epsilon}4(\hat{t}+\hat{u})f(-1,1,-2) - Sf(1,-1,6) - \epsilon Sf(4,-2,8)\right\}, \quad (2.53)$$

in which

$$f(a,b,c) = a\hat{s}^2 + b(\hat{t}-\hat{u})^2 + c\hat{s}(\hat{t}+\hat{u}), \quad (2.54)$$

$$g(a,b,c,d) = f\left(a/\hat{s}(\hat{s}^2 + d\hat{t}^2 + d\hat{u}^2), b(\hat{t}+\hat{u}), c\hat{s}\right) + 6d\hat{s}\hat{t}\hat{u}, \quad (2.55)$$

$$S = \hat{s} + 2(\hat{t}+\hat{u}). \quad (2.56)$$

As usual, in eqs. (2.44) and (2.45), $B, B' \in \{\gamma, {\rm Z}, {\rm Z}'\}$ and the couplings A_B, B_B are defined as in eq. (2.19). The interference terms $\mathcal{V}_q^{\rm i(f)}$ in eq. (2.29) are equal to $\mathcal{V}_{q;1,0}^{\rm i(f)}$, while the $\mathcal{V}_{q;0,1}^{\rm i(f)}$ terms contribute to the charge conjugated amplitude.

Evaluation of loop integrals: Master integrals

IBP identities can be used also to obtain differential equations for the master integrals with respect to invariants of the problem, which can be subsequently employed for their evaluation. We illustrate this method for the evaluation of master integrals, often referred to as the differential equation method [98, 110], in the following example. Let us consider an equal mass two-point function, the massive bubble

$$I_{\mathcal{A}_2}(0,1,1,0) = \mu_r^{4-D} \int \frac{d^D l}{(2\pi)^{D-2}} \frac{1}{[(k_1-l)^2+m_{\rm t}^2][(k_2+l)^2+m_{\rm t}^2]} \ . \tag{2.57}$$

By shifting the momenta k_1, k_2, l as

$$k_1 - l \to l', \quad k_2 + l \to p + l', \quad \text{where } p = k_1 + k_2, \tag{2.58}$$

the massive bubble can be rewritten as

$$I_{\mathcal{A}_2}(0,1,1,0) = \mu_r^{4-D} \int \frac{d^D l'}{(2\pi)^{D-2}} \frac{1}{(l'^2+m_{\rm t}^2)[(p+l')^2+m_{\rm t}^2]} \ . \tag{2.59}$$

Using the properties of dimensional regularization and the fact that

$$p^\mu \frac{d}{dp^\mu} = p^\mu \frac{d}{dp^2}\frac{dp^2}{dp^\mu} = p^\mu \frac{d}{dp^2}(2p_\mu) = 2p^2 \frac{d}{dp^2} \ , \tag{2.60}$$

one can write

$$\frac{d}{dp^2} I_{\mathcal{A}_2}(0,1,1,0) = \frac{1}{2} I_{\mathcal{A}_2}(0,2,1,0) - \frac{1}{2p^2} I_{\mathcal{A}_2}(0,1,1,0) - \frac{D-2}{4m_{\rm t}^2 p^2} I_{\mathcal{A}_2}(0,1,0,0) \ . \tag{2.61}$$

This is not a differential equation, since the r.h.s. contains not only the bubble $I_{\mathcal{A}_2}(0,1,1,0)$ but also $I_{\mathcal{A}_2}(0,2,1,0)$, the bubble with one of the propagators squared. $I_{\mathcal{A}_2}(0,2,1,0)$ can, however, be reduced to the sum of a massive bubble and a massive tadpole

$$I_{\mathcal{A}_2}(0,2,1,0) = I_{\mathcal{A}_2}(0,1,2,0) = -\frac{D-3}{p^2+4m_{\rm t}^2} I_{\mathcal{A}_2}(0,1,1,0) - \frac{D-2}{2m_{\rm t}^2(p^2+4m_{\rm t}^2)} I_{\mathcal{A}_2}(0,1,0,0) \ . \tag{2.62}$$

One thus obtains the following differential equation

$$\begin{aligned} \frac{d}{dp^2} I_{\mathcal{A}_2}(0,1,1,0) = -\frac{1}{2}\left[\frac{1}{p^2} - \frac{D-3}{p^2+4m_{\rm t}^2}\right] I_{\mathcal{A}_2}(0,1,1,0) \\ - \frac{D-2}{4m_{\rm t}^2}\left[\frac{1}{p^2} - \frac{1}{p^2+4m_{\rm t}^2}\right] I_{\mathcal{A}_2}(0,1,0,0) \ . \end{aligned} \tag{2.63}$$

The discussion of the solution of this differential equation as well as the evaluation of the other master integrals, the massless bubble $I_{\mathcal{A}_1}(0,1,1,0)$ and massive tadpole $I_{\mathcal{A}_2}(0,1,0,0)$ is beyond the scope of this manuscript. For more details, we refer to the reviews in [98, 111]. For completeness, however, we show the expressions for the master integrals we have used in the calculation. It is convenient to map the center of mass energy $\hat{s}$ on to a dimensionless variable x:

$$\hat{s} \to -m_{\rm t}^2 \frac{(1-x)^2}{x}, \quad x \in \mathbb{R}. \tag{2.64}$$

The Laurent series of the master integrals $I_{\mathcal{A}_1}(0,1,1,0)$, $I_{\mathcal{A}_2}(0,1,0,0)$, $I_{\mathcal{A}_2}(0,1,1,0)$, around $D \to 4$, then up to the order $\mathcal{O}((D-4)^2)$ read[11]

$$
\begin{aligned}
I_{\mathcal{A}_1}(0,1,1,0) = (2\pi)^2 \Bigg\{ & -(D-4)^{-1}\frac{1}{2} + (D-4)^0 \left[\frac{1}{2} + \frac{1}{4}H(0;x) + \frac{1}{2}H(1;x)\right] \\
& + (D-4)^1 \Bigg[-\frac{1}{2} + \frac{1}{8}\zeta(2) - \frac{1}{4}H(0;x) - \frac{1}{8}H(0,0;x) - \frac{1}{4}H(0,1;x) - \frac{1}{2}H(1;x) - \frac{1}{4}H(1,0;x) \\
& \qquad - \frac{1}{2}H(1,1;x)\Bigg] \\
& + (D-4)^2 \Bigg[+\frac{1}{2} - \frac{1}{8}\zeta(2) - \frac{1}{8}\zeta(3) + \frac{1}{4}H(0;x) - \frac{1}{16}H(0;x)\zeta(2) + \frac{1}{8}H(0,0;x) + \frac{1}{16}H(0,0,0;x) \\
& \qquad + \frac{1}{8}H(0,0,1;x) + \frac{1}{4}H(0,1;x) + \frac{1}{8}H(0,1,0;x) + \frac{1}{4}H(0,1,1;x) + \frac{1}{2}H(1;x) \\
& \qquad - \frac{1}{8}H(1;x)\zeta(2) + \frac{1}{4}H(1,0;x) + \frac{1}{8}H(1,0,0;x) + \frac{1}{4}H(1,0,1;x) + \frac{1}{2}H(1,1;x) \\
& \qquad + \frac{1}{4}H(1,1,0;x) + \frac{1}{2}H(1,1,1;x)\Bigg] + \mathcal{O}((D-4)^3)\Bigg\} ,
\end{aligned}
\tag{2.65}
$$

$$
\begin{aligned}
I_{\mathcal{A}_2}(0,1,0,0) = (2\pi)^2 m_{\mathrm{t}}^2 \Bigg\{ & (D-4)^{-1}\frac{1}{2} - (D-4)^0\frac{1}{4} - (D-4)^1\frac{1}{8} + (D-4)^2\frac{1}{16} \\
& + \mathcal{O}((D-4)^3)\Bigg\} ,
\end{aligned}
\tag{2.66}
$$

$$
\begin{aligned}
I_{\mathcal{A}_2}(0,1,1,0) = (2\pi)^2 \Bigg\{ & -(D-4)^{-1}\frac{1}{2} + (D-4)^0 \left[\frac{1}{2} - \frac{1}{4}H(0;x) + \frac{1}{2(1-x)}H(0;x)\right] \\
& + (D-4)^1 \Bigg[-\frac{1}{2} + \frac{1}{4(1-x)}\zeta(2) - \frac{1}{8}\zeta(2) - \frac{1}{4}H(-1,0;x) + \frac{1}{2(1-x)}H(-1,0;x) + \frac{1}{4}H(0;x) \\
& \qquad - \frac{1}{2(1-x)}H(0;x) + \frac{1}{8}H(0,0;x) - \frac{1}{4(1-x)}H(0,0;x)\Bigg] \\
& + (D-4)^2 \Bigg[+\frac{1}{2} - \frac{1}{4(1-x)}\zeta(2) - \frac{1}{4(1-x)}\zeta(3) + \frac{1}{8}\zeta(2) + \frac{1}{8}\zeta(3) + \frac{1}{4(1-x)}H(-1;x)\zeta(2) \\
& \qquad - \frac{1}{8}H(-1;x)\zeta(2) - \frac{1}{4}H(-1,-1,0;x) + \frac{1}{2(1-x)}H(-1,-1,0;x) + \frac{1}{4}H(-1,0;x) \\
& \qquad - \frac{1}{2(1-x)}H(-1,0;x) + \frac{1}{8}H(-1,0,0;x) - \frac{1}{4(1-x)}H(-1,0,0;x) - \frac{1}{4}H(0;x) \\
& \qquad - \frac{1}{8(1-x)}H(0;x)\zeta(2) + \frac{1}{2(1-x)}H(0;x) + \frac{1}{16}H(0;x)\zeta(2) + \frac{1}{8}H(0,-1,0;x) \\
& \qquad - \frac{1}{4(1-x)}H(0,-1,0;x) - \frac{1}{8}H(0,0;x) + \frac{1}{4(1-x)}H(0,0;x) - \frac{1}{16}H(0,0,0;x) \\
& \qquad + \frac{1}{8(1-x)}H(0,0,0;x)\Bigg] + \mathcal{O}((D-4)^3)\Bigg\} ,
\end{aligned}
\tag{2.67}
$$

[11] The expressions for the 1-loop scalar integrals can be for example found in [112].

where ζ is the Euler-Riemann ζ function and we have introduced functions H, denoting the harmonic polylogarithms (HPLs) [113, 114]. Note that the Laurent series is needed up to the order $\mathcal{O}((D-4)^2)$ because the coefficients in front of the loop integrals in the general interference terms of the virtual contribution, eqs. (2.44) and (2.45), contain single and double poles $1/(D-4)$, $1/(D-4)^2$.

The HPLs can be defined as repeated integrations of the following three fundamental[12] *weight functions*:

$$f(-1;t) = \frac{1}{t+1}, \quad f(0;t) = \frac{1}{t}, \quad f(1;t) = \frac{1}{t-1}. \tag{2.68}$$

The *weight functions* have a non-integrable singularity in $t=-1$, $t=0$ and $t=1$ respectively. The related HPLs of weight 1 are

$$\begin{aligned} H(-1;x) &= \int_0^x dt f(-1;t) = \int_0^x \frac{dt}{t+1} = \log(x+1), \\ H(0;x) &= \int_1^x dt f(0;t) = \int_1^x \frac{dt}{t} = \log(x), \\ H(1;x) &= \int_0^x dt f(1;t) = \int_0^x \frac{dt}{t-1} = \log(1-x), \end{aligned} \tag{2.69}$$

where x is a real variable ($x \in R$), in our case defined as in eq. (2.64). Since the logarithms have branch cuts on the real axis for $x \leq -1$, $x \leq 0$, $x \geq 1$, respectively, the three HPLs are real and uniquely defined only for $x > -1$, $x > 0$, and $x < 1$, respectively. Outside these intervals, the logarithms become complex, and a prescription for the approach to the branch cut has to be chosen [115].

A HPL with weight 2 or bigger is defined through a repeated integration of the weight function. If $\mathbf{w}$ is a vector with w components consisting of a sequence of -1, 0, and +1, we define the HPL of weight $w+1$ as follows:

$$H(a,\mathbf{w};x) = \int_0^x dt f(a;t) H(\mathbf{w};t) \ , \quad a = -1, 0, 1, \tag{2.70}$$

with the exception of the case in which the weights are only zeroes, in which case it is defined as

$$H(\mathbf{0}_{w+1};x) = \int_1^x dt f(0;t) H(\mathbf{0}_w;t) = \frac{1}{(w+1)!} \log^{w+1}(x) \ . \tag{2.71}$$

The master integrals in eqs. (2.65), (2.66) and (2.67) have been evaluated in a non-physical negative-energy region $x \leq 0$. For negative x, since the logarithm has a branch cut for negative argument, we must choose how to approach the cut. In order to do that, we add an infinitesimal imaginary part to the variable x. Let us choose the following prescription[13]: $x \to -x' - i0^+$. The HPLs of weight zero then become:

$$\begin{aligned} H(0;x) = \log(x) &\to \log(-x' - i0^+) = H(0;x') - i\pi, \\ H(1;x) &\to -H(-1;x'), \\ H(-1;x) &\to -H(1;x'). \end{aligned} \tag{2.72}$$

[12] Note the minus sign in the weight +1 with respect to the Remiddi-Vermaseren definition of [113].

[13] This choice has to be consistent with the ϵ prescription in the propagators.

The analytic continuation of the HPLs of higher weight can be obtained by making use of the shuffle algebra

$$H(a;x)H(m_p,\ldots,m_1;x) = H(a,m_p,\ldots,m_1;x)+ \\ + H(m_p,a,m_{p-1},\ldots,m_1;x)+\cdots+H(m_p,\ldots,m_1,a;x). \quad (2.73)$$

For example the HPL of weight two $H(1,1;x)$ can be decomposed using the shuffle algebra into a product of two HPLs of weight one:

$$H(1,1;x) = \frac{1}{2}H(1;x)H(1;x). \quad (2.74)$$

Using eqs. (2.72) and the shuffle algebra, the prescription $x \to -x' - i0^+$ maps $H(1,1;x)$ into

$$H(1,1;x) = +\frac{1}{2}H(1;x)^2 \to \frac{1}{2}H(-1;x')^2 = H(-1,-1;x'). \quad (2.75)$$

The HPLs are now consistently defined in a physical region.

The final formula for the virtual contribution to the top-pair production at order $\mathcal{O}(\alpha_S\alpha_W^2)$ is rather lengthy and so we do not show it here. It contains IR and UV divergences and in the following section we will discuss the procedure used to cure UV singularities, the renormalization. The treatment of IR divergences is postponed to Section 2.3.3.

Renormalization

In computing higher order corrections one faces the problem of having to deal with UV divergences. As we have seen in previous sections, these come from the high-momentum region of loop integrals in the amplitudes squared of the interferences of 1-loop and tree-level diagrams. Measurable quantities or physical observables, like cross sections, are always finite, however. In this section we discuss renormalization, a procedure which cures UV divergences by a redefinition of the Lagrangian parameters and fields of the underlying theory, rendering physical observables calculated at higher orders finite.

Any Lagrangian contains two types of objects: fields and parameters (couplings, masses, ...). Let p_0 be a given parameter of the Lagrangian that enters the expression of an observable $O(p_0)$. One could extract p_0 by measuring $O(p_0)$. If $O(p_0) = \infty$, however, as is usually the case of observables calculated at higher orders, the extraction of p_0 is impossible. The bare parameters of the Lagrangian, thus, are not necessarily well defined physical quantities. One may replace the bare parameters of the Lagrangian, $\{p_0\}$, by the renormalized ones by multiplicative renormalization. For each bare parameter p_0 we write

$$p_0 = Z_p p = p + \delta p, \qquad \delta p = \alpha\delta p^{(1)} + \cdots, \quad (2.76)$$

where α is a coupling constant and renormalization constants Z_p are different from 1 by loop corrections. The renormalization constants are, in general, infinite and fixed by a finite set of renormalization conditions. This decomposition is to a large extent arbitrary. The divergent parts are determined directly by the structure of the divergences of the one-loop amplitudes while the finite parts depend on our choice of the renormalization condition which, in turn, defines the renormalization scheme. It turns out, that in a renormalizable theory it is always possible to find renormalization constants Z_p such that the observables depending on the renormalized parameters $O(\{Z_p^{-1}p_0\})$ are finite. To be more precise, the parameter renormalization is sufficient to obtain

finite $\mathcal{S}$-matrix elements if, in addition, wave function renormalization factors for external on-shell particles are included [116].

By virtue of the LSZ-reduction formula, see for example [117], the renormalized amplitude $\mathcal{M}_{\text{ren}}$ can be written in terms of the bare amplitude $\mathcal{M}$ and renormalized parameters $\{p\}$ as

$$\mathcal{M} = \prod_n Z_{\text{WF},n}^{1/2} \mathcal{M}_0(\{p_0\} \to \{Z_p p\}), \tag{2.77}$$

where $\{p_0\}$ is the set of bare Lagrangian parameters and the product runs over all the external particles. $Z_{\text{WF},n}$ is the wave function renormalization constant of the external particle n, in our case $n \in \{q, \text{t}\}$, and Z_p is the renormalization constant for parameter p. In the case of the top-pair production corrections at order $\mathcal{O}(\alpha_S \alpha_W^2)$ neither the coupling constants nor the mass of the top quark m_t, which enter the expression for the amplitude, need to be renormalized. The reason is that the coupling constants as well as the top quark propagator do not receive any corrections. That is, $\mathcal{O}(\alpha_S \alpha_W^2)$ corrections to the top-pair production are LO in α_S and α_W and the diagrams in Figure 2.3 do not contain corrections to the top quark propagator. It is sufficient thus, to perform the wave function renormalization.

We renormalise the incoming light quark wave function in the modified minimal subtraction ($\overline{\text{MS}}$) scheme, while the outgoing top quark wave function in the on-shell (OS) scheme. The corresponding wave function renormalization constants in $D = 4 - 2\epsilon$ dimensional space read [118]

$$\delta Z_{\text{WF},q} = 0, \tag{2.78}$$

$$\delta Z_{\text{WF,t}} = C(\epsilon) \left(\frac{\mu_r^2}{m_\text{t}^2} \right)^\epsilon C_F \left(-\frac{3}{4\epsilon} - \frac{1}{1-2\epsilon} \right), \tag{2.79}$$

where

$$C(\epsilon) = (4\pi)^\epsilon \Gamma(1+\epsilon), \tag{2.80}$$

and

$$Z_{\text{WF},n} = 1 + \frac{\alpha_S}{\pi} \delta Z_{\text{WF},n}. \tag{2.81}$$

The bare matrix element of the NLO top-pair production has the following expansion

$$\mathcal{M} = \cdots + \left(\frac{\alpha_W}{\pi} \right)^2 \mathcal{M}_{0;2} + \cdots + \frac{\alpha_S}{\pi} \left(\frac{\alpha_W}{\pi} \right)^2 \mathcal{M}_{1;2} + \cdots, \tag{2.82}$$

where we show only the terms relevant for the electroweak top-pair production and its QCD corrections. By substituting the expansions (2.81) and (2.82) and the light quark wave function renormalization constant in eq. (2.79) into the expression for the renormalized matrix element in eq. (2.77) we obtain

$$\mathcal{M}^{\text{ren}} = \left(\frac{\alpha_W}{\pi} \right)^2 \mathcal{M}_{0;2} + \frac{\alpha_S}{\pi} \left(\frac{\alpha_W}{\pi} \right)^2 \mathcal{M}_{1;2} + \frac{\alpha_S}{\pi} \left(\frac{\alpha_W}{\pi} \right)^2 \delta Z_{\text{WF,t}} \mathcal{M}_{0;2} + \cdots. \tag{2.83}$$

The renormalized amplitude of the top-pair production at order $\mathcal{O}(\alpha_S \alpha_W^2)$, thus, can be written as

$$\mathcal{M}_{1;2}^{\text{ren}} = \frac{\alpha_S}{\pi} \left(\frac{\alpha_W}{\pi} \right)^2 (\mathcal{M}_{1;2} + \delta Z_{\text{WF,t}} \mathcal{M}_{0;2}). \tag{2.84}$$

Since only the virtual contributions are UV divergent, one can write

$$\mathcal{V}_{\text{ren}} = \mathcal{V} + \frac{\alpha_S}{\pi} \delta Z_{\text{WF,t}} \mathcal{B}, \tag{2.85}$$

where $\mathcal{B}$ is the Born matrix element calculated in D-dimensions and the virtual contribution $\mathcal{V}$ was calculated in one of the previous subsections. $\mathcal{V}_{\text{ren}}$ is UV finite but still contains IR soft and collinear divergences. The treatment of soft and collinear divergences will be discussed in Section 2.3.3.

Final remarks

In this section we have calculated the virtual contribution to the NLO QCD corrections of the electroweak top-pair production. We have calculated the amplitude squared of the interferences of 1-loop diagrams with tree-level diagrams, depicted in Figures 2.3, 2.1 and 2.2, in D dimensions. All loop integrals figuring in the virtual corrections have been reduced to a small set of master integrals using the IBP identities and the Laporta algorithm, and the master integrals have been evaluated using the differential equation method. The bare virtual QCD corrections to the electroweak top-pair production can be written as:

$$\sigma^{\mathcal{V}} = \int d\mathbf{\Phi}_2 \mathcal{L} \sum_q \mathcal{V}_q(\mathbf{\Phi}_2) = \int d\mathbf{\Phi}_2 \mathcal{L} \left\{ \sum_q \sum_{B,B'} \left[\mathcal{V}_q^{\text{i}}(B,B') + \mathcal{V}_q^{\text{f}}(B,B') \right] + \text{c.c.} \right\} \tag{2.86}$$

where we sum over all the possible light quarks in the initial state $q \in \{\text{d}, \text{u}, \text{s}, \text{c}, \text{b}\}$. The expression for the general interference terms $\mathcal{V}_q^{\text{i(f)}}(B,B')$ after the reduction of loop integral to master integrals and before the insertion of master integrals can be found in eqs. (2.44) and (2.45). Moreover, we have treated the UV singularities coming from the high-momentum region of the loop integrals using renormalization.

Note that, while evaluating the loop integrals in D-dimensions we have introduced a *renormalization scale* μ_r to preserve the coupling dimensionless. The total cross section, thus, besides the dependence on the factorization scale μ_f picks up a dependence on the renormalization scale μ_r.

A significant part of the calculation has been performed automatically using publicly available tools interfaced via a Python script that we have developed for this purpose. The details of the automation of the calculation will be described in Section 2.5, where we describe how the individual pieces in a calculation of 1-loop corrections can be calculated automatically.

2.3.2 Real contributions

The real contributions involve the production of an additional final state particle. The NLO real contribution to a $2 \to 2$ process is a $2 \to 3$ process. At NLO, the Feynman diagrams contain an additional external line but no loops, in contrast to the virtual contributions in which the additional line leads to a closed loop. Because the real diagrams have a different final state from the Born contribution the amplitude of the real contribution is obtained by interfering real diagrams with real diagrams.

In the real contribution to the electroweak top-pair production a new channel opens up, as compared to the channels which are already present at LO. While $2 \to 2$ top-pair production at order $\mathcal{O}(\alpha_S \alpha_W^2)$ can be initiated only by $q\overline{q}$, the $2 \to 3$ production of a top-pair and an additional parton can also proceed via the $\text{g}q$ and $\text{g}\overline{q}$ channels. The real diagrams of the electroweak top-pair production are shown in Figures 2.8 and 2.9.

Since the real diagrams do not contain any loops, they are not UV divergent. In general, however, they suffer from soft and collinear singularities. The real contribution in the $q\overline{q}$ channel is IR divergent when the additional gluon becomes soft and/or collinear to one of the incoming

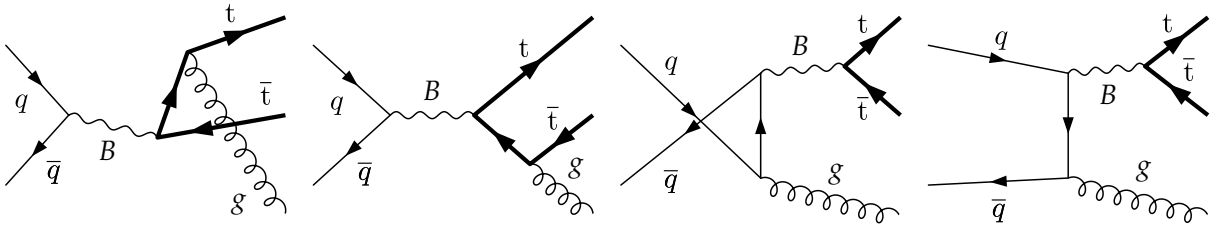

Figure 2.8: Diagrams for $q\overline{q}$ initiated contributions to the real part of $\alpha_S\alpha_W^2$ top-pair production corrections. Note that $B \in \{\gamma, \mathrm{Z}, \mathrm{Z}'\}$.

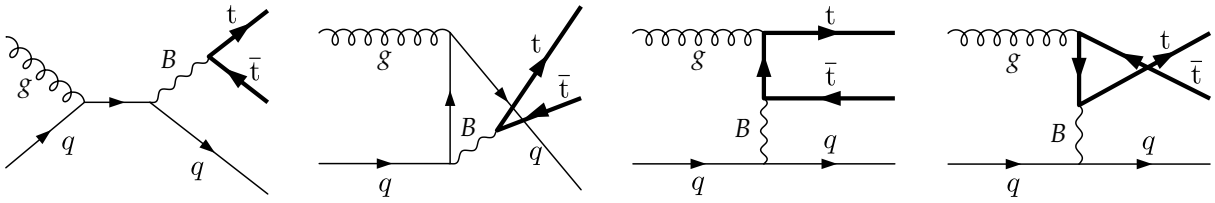

Figure 2.9: Diagrams for gq initiated contributions to the real part of $\alpha_S\alpha_W^2$ top-pair production corrections. Note that $B \in \{\gamma, \mathrm{Z}, \mathrm{Z}'\}$.

partons. The gq and g$\overline{q}$ channels, do not have any soft divergences, but there is a collinear divergence in some of the diagrams with a photon exchange. In particular, there is a collinear divergence in the 3$^{\mathrm{rd}}$ and 4$^{\mathrm{th}}$ diagram in Figure 2.9 when the incoming quark is collinear with the outgoing light quark. The soft divergences in the $q\overline{q}$ channel cancel against the divergences originating from the virtual contribution [119, 120], while the initial state collinear divergences are cancelled by the collinear counterterms of the mass factorization. The initial state collinear divergences in the gq and g$\overline{q}$ channels could also be treated with the mass factorization, had photon been included into the definition of proton. In addition new photon-initiated subprocesses to top-pair production would have to be taken into account. Due to time constraints, however, we have not performed the mass factorization of the g$q(\overline{q})$ channels and we regulate the corresponding IR divergences for the time being by giving a non-zero mass to the photon. The cancellation of soft divergences and the mass factorization will be in more detail discussed in Section 2.3.3.

Let k_1, k_2 be the momenta of the incoming partons, p_1, p_2 the momenta of the outgoing t, $\overline{\mathrm{t}}$ quarks, respectively, and q the momentum of the additional outgoing parton, a gluon in the $q\overline{q}$ channel and a light quark in the gq, g$\overline{q}$ channels. Five independent scalar products are needed to fully describe the kinematics of this $2 \to 3$ process and we choose the following invariants to parametrize them

$$\begin{aligned} \hat{s} &= -(k_1+k_2)^2, & \hat{t}_1 &= -(k_2-p_2)^2 + p_2^2\ , & \hat{t}' &= -(k_2-q)^2\ , \\ & & \hat{u}_1 &= -(k_1-p_2)^2 + p_2^2\ , & \hat{u}' &= -(k_1-q)^2\ . \end{aligned} \tag{2.87}$$

The real contribution contains in total 144 interference terms in the $q\overline{q}$ channel and as many in

the $\mathrm{g}q(\overline{q})$ channels. The total real contribution can be written as

$$\sigma^{\mathcal{R}} = \int d\mathbf{\Phi}_3 \mathcal{L}\mathcal{R} = \int d\mathbf{\Phi}_3 \mathcal{L} \sum_q \sum_{\mathrm{ch}} \Bigg[\mathcal{R}_{q,\mathrm{ch}}(\gamma,\gamma) + \mathcal{R}_{q,\mathrm{ch}}(\mathrm{Z},\mathrm{Z}) + \mathcal{R}_{q,\mathrm{ch}}(\mathrm{Z}',\mathrm{Z}') + \sum_{B\neq B'} \mathcal{R}_{q,\mathrm{ch}}(B,B') \Bigg], \quad (2.88)$$

where we integrate over the three particle phase space $d\mathbf{\Phi}_3$ and $B, B' \in \{\gamma, \mathrm{Z}, \mathrm{Z}'\}$. Moreover, we sum over all the possible light quarks in the initial state $q \in \{\mathrm{d},\mathrm{u},\mathrm{s},\mathrm{c},\mathrm{b}\}$ and over the channels $\mathrm{ch} \in \{q\overline{q}, \mathrm{g}q, \mathrm{g}\overline{q}\}$. Let us denote the term obtained by interfering a real diagram of the $q\overline{q}$ channel with a gluon emitted from the external line with momentum p, see the diagrams in Figure 2.8, with a real diagram with a gluon absorbed by the external line with momentum p' as $\mathcal{R}^{p,p'}_{q,q\overline{q}}(B,B')$. Then it is convenient to decompose $\mathcal{R}_{q,q\overline{q}}(B,B')$ into interference terms with gluon exchange only in the initial state, only in the final state or mixed terms:

$$\mathcal{R}_{q,q\overline{q}}(B,B') = \mathcal{R}^{\mathrm{i}}_{q,q\overline{q}}(B,B') + \mathcal{R}^{\mathrm{if}}_{q,q\overline{q}}(B,B') + \mathcal{R}^{\mathrm{fi}}_{q,q\overline{q}}(B,B') + \mathcal{R}^{\mathrm{f}}_{q,q\overline{q}}(B,B'), \quad (2.89)$$

where

$$\mathcal{R}^{\mathrm{i}}_{q,q\overline{q}}(B,B') = \sum_{p,p'\in\{k_1,k_2\}} \mathcal{R}^{p,p'}_{q,q\overline{q}}(B,B'), \quad (2.90)$$

$$\mathcal{R}^{\mathrm{if}}_{q,q\overline{q}}(B,B') = \sum_{p\in\{k_1,k_2\},p'\in\{p_1,p_2\}} \mathcal{R}^{p,p'}_{q,q\overline{q}}(B,B'), \quad (2.91)$$

$$\mathcal{R}^{\mathrm{fi}}_{q,q\overline{q}}(B,B') = \sum_{p\in\{p_1,p_2\},p'\in\{k_1,k_2\}} \mathcal{R}^{p,p'}_{q,q\overline{q}}(B,B'), \quad (2.92)$$

$$\mathcal{R}^{\mathrm{f}}_{q,q\overline{q}}(B,B') = \sum_{p,p'\in\{p_1,p_2\}} \mathcal{R}^{p,p'}_{q,q\overline{q}}(B,B'). \quad (2.93)$$

Because there is no colour flow in the s-channel, the mixed terms $\mathcal{R}^{\mathrm{if}}_{q,q\overline{q}}(B,B')$ and $\mathcal{R}^{\mathrm{fi}}_{q,q\overline{q}}(B,B')$ are zero and the expression for $\mathcal{R}^{\mathrm{i(f)}}_{q,q\overline{q}}(B,B')$ reads:

$$\begin{aligned}\mathcal{R}^{\mathrm{i(f)}}_{q,q\overline{q}}(B,B') = \frac{\alpha_S}{2\pi} C_F \frac{2\alpha_W^2}{\hat{s}^2 D_B^{\mathrm{i(f)}} D_{B'}^{\mathrm{i(f)}} s_W^4} \frac{1}{4c_0^{\mathrm{i(f)}}} \left((\Gamma_B - 2iM_B)^2 + 4c_1^{\mathrm{i(f)}}\right)\left((\Gamma_{B'} + 2iM_{B'})^2 + 4c_1^{\mathrm{i(f)}}\right) \\ \Big\{ A^q_{B'} \left[A^{\mathrm{t}}_{B'} \left(A^q_B A^{\mathrm{t}}_B c_3^{\mathrm{i(f)}} + B^q_B B^{\mathrm{t}}_B c_1^{\mathrm{i(f)}} c_2^{\mathrm{i(f)}} \right) + B^{\mathrm{t}}_{B'} \left(A^q_B B^{\mathrm{t}}_B c_1^{\mathrm{i(f)}} c_2^{\mathrm{i(f)}} + B^q_B A^{\mathrm{t}}_B c_4^{\mathrm{i(f)}} \right) \right] \\ + B^q_{B'} \left[B^{\mathrm{t}}_{B'} \left(A^q_B A^{\mathrm{t}}_B c_1^{\mathrm{i(f)}} c_2^{\mathrm{i(f)}} + B^q_B B^{\mathrm{t}}_B c_4^{\mathrm{i(f)}} \right) + A^{\mathrm{t}}_{B'} \left(A^q_B B^{\mathrm{t}}_B c_3^{\mathrm{i(f)}} + B^q_B A^{\mathrm{t}}_B c_1^{\mathrm{i(f)}} c_2^{\mathrm{i(f)}} \right) \right] \Big\}, \end{aligned} \quad (2.94)$$

where the coefficients $c_l^{\mathrm{i(f)}}(\hat{s},\hat{t}_1,\hat{u}_1,\hat{t}',\hat{u}',m_{\mathrm{t}})$ are listed in Appendix C. The denominators $D^{\mathrm{i(f)}}(B)$ depend on the topology and we have:

$$\begin{aligned} D^{\mathrm{i}}_{\gamma} &= \frac{1}{(\hat{s}+\hat{t}'+\hat{u}')^2}, & D^{\mathrm{f}}_{\gamma} &= \frac{1}{\hat{s}^2}, \\ D^{\mathrm{i}}_{\mathrm{Z}} &= \frac{1}{(\hat{s}+\hat{t}'+\hat{u}'-M_{\mathrm{Z}}^2)^2 + m_{\mathrm{Z}}^2\Gamma_{\mathrm{Z}}^2}, & D^{\mathrm{f}}_{\mathrm{Z}} &= \frac{1}{(\hat{s}-M_{\mathrm{Z}}^2)^2 + m_{\mathrm{Z}}^2\Gamma_{\mathrm{Z}}^2}, \\ D^{\mathrm{i}}_{\mathrm{Z}'} &= \frac{1}{(\hat{s}+\hat{t}'+\hat{u}'-M_{\mathrm{Z}'}^2)^2 + m_{\mathrm{Z}'}^2\Gamma_{\mathrm{Z}'}^2}, & D^{\mathrm{f}}_{\mathrm{Z}'} &= \frac{1}{(\hat{s}-M_{\mathrm{Z}'}^2)^2 + m_{\mathrm{Z}'}^2\Gamma_{\mathrm{Z}'}^2}. \end{aligned} \quad (2.95)$$

The couplings A_B and B_B are defined as in eq. (2.19).

The expressions for the interference terms in the gq and g$\overline{q}$ channels can be obtained from the interference term $\mathcal{R}_{q,q\overline{q}}(B,B')$ via crossing

$$\mathcal{R}_{q,\mathrm{g}(k_2)q(k_1)} = -\frac{3}{8}\mathcal{R}_{q,q(k_1)\overline{q}(k_2)}(B,B')\big|_{\hat{t}_1\leftrightarrow\hat{u}_1,\hat{t}'\leftrightarrow\hat{u}'} \ , \tag{2.96}$$

$$\mathcal{R}_{q,\mathrm{g}(k_1)q(k_2)} = -\frac{3}{8}\mathcal{R}_{q,q(k_1)\overline{q}(k_2)}(B,B')\big|_{\hat{s}\leftrightarrow\hat{u}',\hat{t}_1\to-(\hat{s}+\hat{t}_1+\hat{u}_1+\hat{t}'+\hat{u}')} \ , \tag{2.97}$$

$$\mathcal{R}_{q,\mathrm{g}q} = \mathcal{R}_{q,\mathrm{g}\overline{q}} \ , \tag{2.98}$$

where the overall minus sign comes from crossing a single external fermion line from the final to the initial state and the factor of 3/8 from the colour average over the initial state, since we replace the initial quark by a gluon. Furthermore, the replacement rules for the invariants can be obtained by renaming the appropriate momenta in eq. (2.87).

The amplitude squared of the real contribution has been calculated automatically. For a detailed discussion of the automation, the reader is referred to Section 2.5.

2.3.3 Treatment of soft and collinear singularities

The partonic cross section of a general $2 \to n$ hadron scattering can be at next-to-leading order schematically written as

$$\sigma^{\mathrm{NLO}} = \int d\mathbf{\Phi}_n \mathcal{L}\mathcal{B} + \int d\mathbf{\Phi}_n \mathcal{L}\mathcal{V} + \int d\mathbf{\Phi}_{n+1}\mathcal{L}\mathcal{R} \tag{2.99}$$

$$= \int_n d\sigma^{\mathcal{B}} + \int_n d\sigma^{\mathcal{V}} + \int_{n+1} d\sigma^{\mathcal{R}} \tag{2.100}$$

where $\mathbf{\Phi}_n$ is a set of variables characterizing the n-particle phase space, similarly as in the case of the leading order cross section[14], and $\mathcal{L}$ is the partonic luminosity introduced in eq. (2.12). The calculation of the Born matrix elements $\mathcal{B}$ as well as the next-to-leading order virtual $\mathcal{V}$ and real $\mathcal{R}$ corrections to the total partonic cross section were discussed in Sections 2.2, 2.3.1 and 2.3.2 respectively. In this section we briefly describe the cancellation of IR soft and collinear singularities among the real and virtual contribution and collinear counterterms.

After renormalization of the 1-loop matrix element all the contributions to the cross section σ are UV finite. The Born contribution is integrable over the IR region of the phase space, but the real and virtual contributions to σ^{NLO} are separately affected by IR divergences produced by soft and collinear partons.

According to the Kinoshita-Lee-Nauenberg (KLN) theorem, in a theory with massless fields, the transition rates are free of any infrared divergence if the summation over the initial and final degenerate states is carried out [119, 120]. In other words, all the soft divergences and the collinear divergences from the final state radiation cancel in the sum of the virtual and real contributions to the partonic cross section. The divergences in the initial state radiation remain uncancelled, because we do not sum over degenerate states in the initial state. They cancel against similar collinear divergences present in the QCD corrections to the quark distribution functions, the collinear counterterms.

Although the soft and final state collinear IR divergences cancel in the sum on the right-hand side of eq. (2.100), the separate pieces have to be regularized before any numerical calculation

[14] For more details, see eqs. (2.7) and (2.9).

can be attempted. As discussed in 2.3.1, the 1-loop virtual contributions can be regularized via dimensional regularization and the divergences appear as $1/(D-4)$ and $1/(D-4)^2$ poles, where D denotes the number of dimensions. In the real part, the divergences appear in the integration over the 1-particle phase-space of the additional external particle. In order to obtain a finite result we need a procedure to explicitly extract and cancel the divergences among the real and virtual corrections and collinear counterterms. One of the approaches is to use a subtraction method based on the Catani-Seymour (CS) dipole formalism. There are other methods like the Frixione-Kunszt-Signer (FKS) dipole subtraction [121] or methods based on phase space slicing, see for example [90].

In the following we briefly discuss the factorization formula in eq. (2.1), to clarify the issue of initial state collinear divergences and their treatment. We then describe the CS dipole formalism and how we have applied it to cross-check the singularity structure of the virtual contribution to the NLO QCD corrections to the electroweak top-pair production. This section is only a brief review, for a more detailed account the reader is invited to consult for example [122, 123].

Factorization

The total cross section of many[15] hadronic collisions can be calculated using the factorization formula

$$\sigma_{\mathrm{pp}\to X} = \sum_{ij} \int f_i(x_1,\mu_f) f_j(x_2,\mu_f) d\hat{\sigma}_{ij\to X}(\mu_f^2) \ , \tag{2.101}$$

where X denotes any hadronic final state, $d\hat{\sigma}_{ij\to X}$ contains the matrix elements and the appropriate phase space. f_i are the parton distribution functions (PDFs) naively describing the probability of finding a parton i with momentum fraction x_i in one of the incoming hadrons.

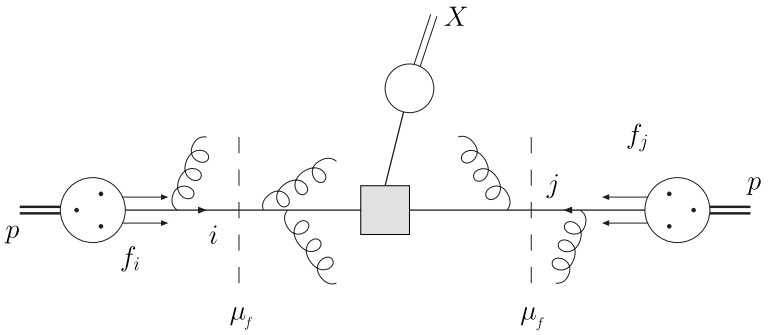

Figure 2.10: A pictorial representation of the factorization formula in eq. (2.101).

The factorization is schematically depicted in Figure 2.10. The central part of the figure, between the dashed vertical lines, represents the high-momentum transfer part described by the short distance cross section $d\hat{\sigma}_{ij\to X}(\mu_f^2)$, which is the renormalized partonic cross section after subtracting the collinear divergences. The remaining parts of Figure 2.10, on the left and right of the dashed vertical lines, represent the low-momentum transfer part of the hadronic collision described by the parton distribution functions. The dashed lines represent the scale of the factorization μ_f – the separation between the high-momentum and low-momentum parts of the hadronic collision.

[15]The factorization has been explicitly proven for DIS process [124] but it is believed to be a universal feature of QCD.

The factorization scale, μ_f, is an abstract quantity, not a physical observable, and we are free to choose its value. In a typical calculation involving a s-channel resonance, the factorization scale is chosen to be equal to the partonic scale of the hard scattering $\hat{s}$ in order to avoid large fixed order logarithms $ln(\hat{s}/\mu_f^2)$ in the hard scattering cross sections. The dependence on the factorization scales becomes smaller when including higher-orders and would vanish if all orders could be included. This is not rigorous, but a reasonable estimate of the scale uncertainty is usually obtained by varying the factorization scale in the interval $\mu_f^2 \in (\hat{s}/4, 4\hat{s})$.

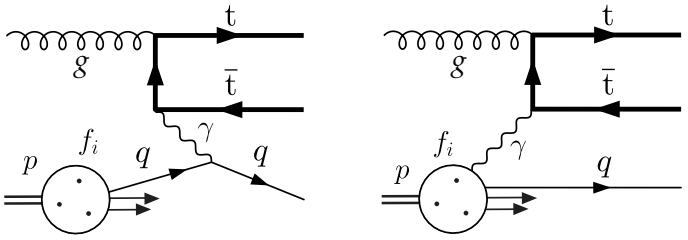

Figure 2.11: Left: $q \to q\gamma$ splitting as a part of the hadronic cross section. Right: $q \to q\gamma$ as a part of PDFs. Note that in this case the photon is integrated in the description of the proton.

Because the factorization scale is not fixed, there is an ambiguity on when the radiation of the extra particle from the initial state happens. Depending on the value of μ_f, the position of the vertical dashed line in Figure 2.10, the additional radiation from the initial state can either be described by the PDFs or the hard part described by the partonic cross section. For example, in Figure 2.11, the splitting of $q \to q\gamma$ in the $2 \to 3$ gq scattering can be considered as the part of the hard process, but it can also happen in the low-momentum non-perturbative regime. Since splittings of this kind are universal, we are free to absorb the associated collinear divergences into the description of the proton into the PDFs, as it is usually done.

In conclusion, the collinear divergences in the initial state are absorbed into the definition of PDFs. In order to obtain a finite partonic cross section, one has to subtract the collinear divergences which have been absorbed into the definition of PDFs, often referred to as collinear counterterms. Thanks to the collinear factorization of QCD amplitudes, this subtraction can be taken care of within the dipole formalism described in the following section.

Dipole subtraction formalism

The NLO contribution to a partonic cross section of a general $2 \to n$ hadron scattering including collinear counterterms can be schematically written as

$$\sigma^{\mathrm{NLO}}(p) = \int_{n+1} d\sigma^{\mathcal{R}}(p) + \int_n (d\sigma^{\mathcal{B}}(p) + d\sigma^{\mathcal{V}}(p)) + \int_n d\sigma^{\mathcal{C}}(p) \tag{2.102}$$

where

$$\int_n d\sigma^{\mathcal{C}}(p) = \int_0^1 dx \int d\sigma^{\mathcal{B}}(xp)\Gamma(x), \tag{2.103}$$

contains the collinear counterterms. As schematically written in eq. (2.103), it can be shown that the collinear counterterm $d\sigma^{\mathcal{C}}$ is given by the convolution of the Born cross section with a process-independent factor $\Gamma(x)$, which is singular in 4 dimensions.

The general idea behind the CS dipole formalism is to introduce an auxiliary cross section $d\sigma^{\mathcal{A}}$ that has the same pointwise singular behaviour (in D dimensions) as $d\sigma^{\mathcal{R}}$. Moreover, $d\sigma^{\mathcal{A}}$

can be chosen simple enough, such that it is analytically integrable in D dimensions over the one-parton subspaces that cause the soft and collinear divergences. Thus, without performing any approximations, $d\sigma^{\mathcal{A}}$ is subtracted from the real contribution and added back to the virtual contribution.

Within the dipole formalism, $d\sigma^{\mathcal{A}}$ is constructed by summing over different contributions, named dipoles. Each dipole contribution describes soft and collinear radiation from a pair of ordered partons. The first parton is called emitter and the second spectator, since only the kinematics of the former lead to the IR singularities. The dipole configurations can be thought of as being obtained by an effective two-step process: using the Born cross section, an n-parton configuration is first produced and the emitter and the spectator, which contains information on the colour and spin correlations of the real cross section $d\sigma^{\mathcal{R}}$, is used to balance momentum conservation. The auxiliary cross section $d\sigma^{\mathcal{A}}$ can be symbolically written as

$$d\sigma^{\mathcal{A}} = \sum_{\text{dipoles}} d\sigma^{\mathcal{B}} \otimes dV_{\text{dipole}} \tag{2.104}$$

where the universal dipole factors dV_{dipole} describe the two-parton decays of the emitters and can be obtained from the QCD factorization formulae in the soft and collinear limits (including the associated colour and spin correlations, as denoted by the symbol $\otimes$). The dipole factors dV_{dipole} are process independent and fully analytically integrable over the one-parton subspaces. The integral over the auxiliary cross section $d\sigma^{\mathcal{A}}$ thus can be written as:

$$\int_{n+1} d\sigma^{\mathcal{A}} = \sum_{\text{dipoles}} \int_n d\sigma^{\mathcal{B}} \otimes \int_1 dV_{\text{dipole}} = \int_n \left[d\sigma^{\mathcal{B}} \otimes \mathbf{I} \right] \ , \tag{2.105}$$

where the universal factor $\mathbf{I}$,

$$\mathbf{I} = \sum_{\text{dipoles}} \int_1 dV_{\text{dipoles}}, \tag{2.106}$$

contains all the poles necessary to cancel those of $d\sigma^{\mathcal{V}}$.

The final NLO partonic cross section can be written as:

$$\begin{aligned}
\sigma^{\text{NLO}}(p) &= \sigma^{\text{NLO}\{n+1\}} + \sigma^{\text{NLO}\{n\}} + \int_0^1 dx \sigma^{\text{NLO}\{n\}}(x; xp) \\
&= \int_{n+1} \left(d\sigma^{\mathcal{R}}(p) - \sum_{\text{dipoles}} d\sigma^{\mathcal{B}}(p) \otimes dV_{\text{dipole}} \right) \\
&\quad + \int_n \left(d\sigma^{\mathcal{B}}(p) + d\sigma^{\mathcal{V}}(p) + d\sigma^{\mathcal{B}}(p) \otimes \mathbf{I} \right) \\
&\quad + \int_0^1 \int_n d\sigma^{\mathcal{B}}(xp) \otimes (\mathbf{P} + \mathbf{K})(x).
\end{aligned} \tag{2.107}$$

The contributions $\sigma^{\text{NLO}\{n+1\}}$ and $\sigma^{\text{NLO}\{n\}}$, with $(m+1)$-parton and m-parton kinematics, respectively, are separately finite and integrable. The integrated dipoles $\mathbf{I}$ now also contain the singular pieces of the collinear counterterms cancelling the initial state collinear divergences in the virtual part. The finite remainder after cancellation of the singularities of the collinear counterterm, so called collinear remnants, are contained in the last term on the r.h.s. of eq. (2.107). This term involves a cross section $\sigma^{\text{NLO}\{n\}}$ with n-parton kinematics and an additional one-dimensional integration with respect to the longitudinal momentum fraction x. This integration arises from the convolution of the Born cross section with $d\sigma^{\mathcal{B}}(xp)$ with x-dependent universal functions $\mathbf{P}$ and $\mathbf{K}$.

The expressions for the dipoles dV_{dipole}, the universal functions $\mathbf{P}$ and $\mathbf{K}$, and the integrated dipoles $\mathbf{I}$ can be found in [122]. If the separate contributions to the NLO cross section, the Born matrix element $\mathcal{B}$, the renormalized virtual corrections $\mathcal{V}$, the real part $\mathcal{R}$ and the full colour structure of the process is known, the calculation of the finite terms in $\sigma^{\text{NLO}\{n+1\}}$, $\sigma^{\text{NLO}\{n\}}$ as well as $\int_0^1 dx \sigma^{\text{NLO}\{n\}}(x; xp)$ can be and has been fully automated, see the discussion in the following section.

To ensure the consistency of the Born matrix element with the virtual part, we have explicitly verified the cancellation of the singularities in $d\sigma^{\mathcal{V}}$ against $d\sigma^{\mathcal{B}} \otimes I$ manually. As we will discuss in one of the following sections, this consistency cross-check has not been automated yet. For completeness, we list the expressions for the integrated dipoles I required for this task.

Before proceeding, let us introduce the square of a colour correlated Born amplitude with n final state partons, $\left|\mathcal{B}^{j,k}\right|^2$, as follows

$$\left|\mathcal{B}^{j,k}\right|^2 = \left[\mathcal{B}^{a_1 \ldots b_j \ldots b_k \ldots a_n}\right]^* T^l_{b_j a_j} T^l_{b_k a_k} \mathcal{B}^{a_1 \ldots a_j \ldots a_k \ldots a_n}, \tag{2.108}$$

where $T^l_{a_j b_j} = (\mathbf{T}_j)^l$ is the colour matrix associated with parton j. For gluon we have $T^l_{cb} = i f_{clb}$, for quark and anti-quark $T^l_{\alpha\beta} = t^l_{\alpha\beta}$, $T^l_{\alpha\beta} = -t^l_{\beta\alpha}$ respectively. The colour correlated Born amplitude is a matrix capturing the colour connections or correlations between the external legs of a given process. For example, in the case of electroweak top-pair production there is no colour connection between the initial and final state partons and so the corresponding elements of the colour correlated Born amplitude are zero, as will be shown in the following section.

The colour charge algebra for the product $(\mathbf{T}_i)^l (\mathbf{T}_j)^l \equiv \mathbf{T}_i \cdot \mathbf{T}_j$ is:

$$\mathbf{T}_i \cdot \mathbf{T}_j = \mathbf{T}_j \cdot \mathbf{T}_i \quad \text{if } i \neq j, \quad T_i^2 = C_i, \tag{2.109}$$

where C_i is the quadratic Casimir operator in the representation of particle i and we have $C_F = (N_c^2 - 1)/(2N_c)$, $C_A = N_c$ where N_c is number of colours.

The integrated dipole $\mathbf{I}$ for a process with two massive final state partons i, j and two initial state partons a, b reads[16]:

$$\mathbf{I} = \mathbf{I}_m + \mathbf{I}_a + \mathbf{I}_b + \mathbf{I}_0, \tag{2.110}$$

where $\mathbf{I}_0$ contains dipoles corresponding to the massless initial state partons, $\mathbf{I}_m$ the dipoles of the massive final state partons and $\mathbf{I}_a = \mathbf{I}_b = 0$ if the colour connection between the initial and final state partons vanish. Dimensional regularized expressions for the singular parts of $\mathbf{I}_m$ and $\mathbf{I}_0$ in $D = 4 - 2\epsilon$ dimensional space read

$$\mathbf{I}_0 = -\frac{\alpha_S}{2\pi} \frac{(4\pi)^\epsilon}{\Gamma(1-\epsilon)} \frac{1}{\mathbf{T}_a^2} \mathbf{T}_a \cdot \mathbf{T}_b \left(\frac{\mu^2}{\hat{s}}\right)^\epsilon \left(\frac{\mathbf{T}_a^2}{\epsilon^2} + \frac{\gamma_a}{\epsilon}\right) + a \leftrightarrow b \tag{2.111}$$

$$\mathbf{I}_m = -\frac{\alpha_S}{2\pi} \frac{(4\pi)^\epsilon}{\Gamma(1-\epsilon)} \frac{1}{\mathbf{T}_j^2} \mathbf{T}_j \cdot \mathbf{T}_k \left(\mathbf{T}_j^2 \left(\frac{\mu^2}{\hat{s}}\right)^\epsilon \frac{\log \rho}{v_{jk}} \frac{1}{\epsilon} + \frac{\gamma_a}{\epsilon}\right) + j \leftrightarrow k \tag{2.112}$$

$$\tag{2.113}$$

where Γ is the usual Euler function and $\gamma_a = 3/2 C_F$ for quarks. Furthermore, ρ and v_{jk} are defined as

$$v_{jk} = \sqrt{1 - \frac{p_j^2 p_k^2}{(p_j p_k)^2}}, \quad \rho = \sqrt{\frac{1 - v_{jk}}{1 + v_{jk}}}. \tag{2.114}$$

[16] See eqs. (6.66), (6.16), (6.18), (6.20), (5.30), (6.28) and (6.32) in [122].

In electroweak top-pair production these simplify to

$$v_{jk} = \frac{(1-x)(1+x)}{1+x^2}, \quad \rho = x, \tag{2.115}$$

in terms of the variable x introduced in eq. (2.64).

After subtracting the Born matrix element, $\mathcal{B}$, multiplied by the singular pieces of integrated dipoles $\mathbf{I}$ from the expression for the renormalized virtual corrections, $\mathcal{V}_{\text{ren}}$, we have obtained a finite expression

$$\mathcal{V}_{\text{fin}} = \mathcal{V}_{\text{ren}} + \mathcal{B} \otimes \mathbf{I}. \tag{2.116}$$

Note that, $\mathcal{V}_{\text{fin}}$ does not constitute the full finite expression for the virtual contribution to the EW top-pair production, because the finite terms of the dipole subtraction are not included. $\mathcal{V}_{\text{fin}}$ does, however, correspond to the virtual amplitude which has to be implemented in the Monte Carlo event generator `POWHEG BOX`, discussed in detail in the following section.

In the following section, we will briefly discuss, among others, how the automation of the treatment of IR soft and collinear divergences is implemented in the Monte Carlo event generator `POWHEG BOX`.

2.4 Implementing next-to-leading order top-pair production in a Shower Monte Carlo

In order to obtain numerical results for the electroweak top quark production and its NLO QCD corrections at hadron colliders, we have implemented the formulae calculated in the previous sections in a Monte Carlo event generator `POWHEG BOX` [72]. The Positive Weight Hardest Emission Generator (POWHEG) method, implemented in the `POWHEG BOX`, allows for a matching of QCD corrections with a parton shower algorithm implemented in various publicly available Shower Monte Carlo (SMC) event generators like `Pythia` [60] or Herwig [70].

SMC codes usually aim at a complete description of particle collisions from the high-energy perturbative domain down to the detector level[17], which is, after all, what is observed by experiments. Fixed order calculations, such as the one presented in the previous section, have by definition a fixed, in most cases, low number of final state particles. This contrasts with the large number of final state particles in hadronic collisions. Moreover, even at next-to-leading order, in some regions of the phase space higher-order terms are particularly enhanced and must be accounted for by resummation.

Besides a large library of SM processes implemented at leading order accuracy, SMC codes include the so-called parton shower algorithm, in which higher-order low-angle radiation of initial and final state particles is generated automatically. Furthermore, they usually also implements the parton-hadron conversion, based on a phenomenological model of hadron formation, and the subsequent decay of unstable hadrons. Although, one could simply convolute the formulae obtained in the previous sections with the parton luminosities, to obtain the total cross section or even some distributions calculated from the kinematics of the final state top-pair, an implementation in a SMC code, by virtue of parton shower, hadronization and automatic decay of unstable particles, offers a description of the electroweak top-pair production and its NLO QCD corrections much closer to what is observed in detectors.

[17] Excluding the simulation of detector effects that can be performed using detector simulation tools such as DELPHES [125].

At next-to-leading order, the usual formulation of the parton shower algorithm suffers from a conceptual problem. In a parton shower, the first and consequent initial and final state radiation is automatically generated in the collinear approximation. Next-to-leading order matrix elements include the description of the first radiation valid also away from this limit. If one would interface events, generated using a NLO Monte Carlo event generator, with the parton shower algorithm, the first radiation would be included "twice". This problem is known under the name of overcounting and can be overcome by consistently matching the NLO matrix elements with the parton shower.

In this section we describe the implementation of the electroweak top-pair production including its NLO QCD corrections in the `POWHEG BOX` framework compatible with the parton shower algorithm. The events generated using `POWHEG BOX` can be passed to any generic SMC code capable of performing parton showers on events generated in an external event generator. We start by reviewing the basics of the parton shower algorithm. We then briefly discuss the POWHEG method and its implementation in the `POWHEG BOX` framework. Finally, we present the implementation of the top-pair production up to order $\mathcal{O}(\alpha_S\alpha_W^2)$, calculated in the previous sections, in `POWHEG BOX`. In the last section we show numerical results for NLO QCD corrections to the electroweak top-pair production generated using `POWHEG BOX` and showered with `Pythia`.

2.4.1 Basics of QCD parton showers

Let us start by looking at matrix elements in regions of the phase space close to collinear configurations. It can be shown that the squared amplitudes near the collinear limit factorize. Moreover, this factorization is of the form of amplitudes for the production of the parent parton times a splitting factor that only depends on the particular splitting involved and on its kinematics. Furthermore, in as much as the phase space can always be written in factorized form the aforementioned factorization applies to the whole cross section. Given a tree-level amplitude with $n+1$ final state particles and assuming that a final state quark goes collinear to a final state gluon, one can write

$$|\mathcal{M}_{n+1}|^2 \to |\mathcal{M}_n|^2 d\Phi_n \times \frac{\alpha_S}{2\pi}\frac{dt}{t}\hat{P}_{q,qg}(z)dz\frac{d\phi}{2\pi} \ , \tag{2.117}$$

where $\mathcal{M}_{n+1}$ and $\mathcal{M}_n$ are the amplitudes for the $n+1$ and n particle processes respectively, $\hat{P}_{q,qg}$ is the Altarelli-Parisi splitting function for the $q \to qg$ splitting and variables t, ϕ and z describe the kinematics of the splitting. The n-particle phase space is defined as

$$d\Phi_n = (2\pi)^4\delta^4\left(q - \sum_{i=1}^{n} p_i\right)\prod_{i=1}^{n}\frac{d^3p_i}{(2\pi^3)2p_i^0} \ . \tag{2.118}$$

This factorization can be pictorially represented as

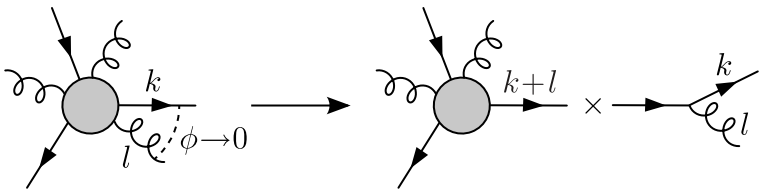

where the amplitudes are represented by gray blobs. Similar factorization formulae hold also for the g → gg and g → $q\overline{q}$ collinear splittings where the appropriate splitting function has to be used.

In eq. (2.117), the variable t vanishes in the collinear limit, z yields the momentum fraction of the outgoing quark relative to the momentum of the quark that has split in the collinear limit

$$k \to z(k+l) \text{ for } t \to 0, \tag{2.119}$$

and ϕ is the azimuthal angle of the plane spanned by $\overrightarrow{k}$, $\overrightarrow{l}$ with respect to the $\overrightarrow{k+l}$ direction. There is an ambiguity in the definition of t and the usual candidates are the virtuality, $t = (k+l)^2$, the transverse momentum, $t = k_\perp^2$, or the angular variable, $t = E^2\phi^2$ where E is the energy of the parton before splitting. The factorization of eq. (2.117) is valid as long as the value of t between the two collinear partons is the smallest of the whole amplitude.

In order to describe an exclusive final state, one would like to sum the perturbative expansion to all orders in α_S. This is, clearly, an impossible task. However, if we limit ourselves to an ordered sequence of the most singular terms in the perturbative expansion, in this case to all terms that carry the collinear singularities dt/t, we can apply the factorization of eq. (2.117) recursively

$$|\mathcal{M}_{n+2}|^2 \to |\mathcal{M}_n| d\Phi_n \times \frac{\alpha_S}{2\pi}\frac{dt'}{t'}\hat{P}_{q,qg}(z')dz'\frac{d\phi'}{2\pi} \times \frac{\alpha_S}{2\pi}\frac{dt}{t}\hat{P}_{q,qg}(z)dz\frac{d\phi}{2\pi} \times \theta(t'-t) \ , \tag{2.120}$$

where θ is the usual Heaviside function. The recursive collinear factorization is sometimes also called the leading-log approximation[18]. Take for example the qg splitting, a real emission cross section for n splittings can be written as

$$\sigma^{\text{LO}}\alpha_S^n \int \frac{dt_1}{t_1}\cdots\frac{dt_n}{t_n}\theta(Q^2 > t_1 > \cdots > t_n > \lambda^2) = \sigma^{\text{LO}}\frac{1}{n!}\alpha_S^n \log^n\frac{Q^2}{\lambda^2} \ , \tag{2.121}$$

where σ^{LO} is the LO cross section, Q its hard scale, λ an infrared cut-off and the function θ is equal to 1 if its argument is true and zero otherwise.

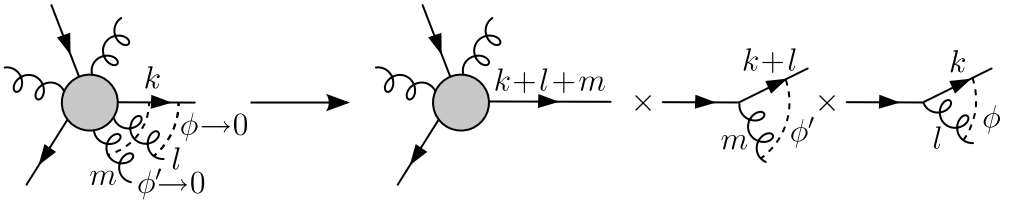

Figure 2.12: Pictorial representation of the recursive application of the collinear factorization formula in eq. (2.120).

On can easily see that when the gluon becomes collinear to the quark, eq. (2.121) will have a divergence as $t \to 0$. Even though, the integration is limited by a physical cut-off, e.g. Λ_{QCD}, the presence of the divergence implies that the real cross section is sensitive to low energy phenomena, which cannot be described by perturbative QCD. Fortunately, the infrared safety of the total cross section is guaranteed if virtual corrections are included, as the IR divergences cancel in the sum of real and virtual contributions. Therefore, for the reasons of consistency, one also has to include virtual contributions.

The virtual contributions are implemented in the parton shower algorithm via Sudakov form factors. If we interpret the integral of the splitting factor

$$dP = \frac{\alpha_S}{2\pi}\frac{dt}{t}\int\frac{d\phi}{2\pi}\int \hat{P}_{i,jl}(z)dz \tag{2.122}$$

[18]Leading-log refers to a single power of logarithmic enhancement for every power of α_S.

as the probability of a branching $i \to jl$ in the phase space element $[t, t+dt]$, $1-dP$ represents the probability of no branching in the same interval. Diagrammatically, the probability of no branching must correspond to the amplitude squared of the sum of all diagrams with no real contribution, i.e. the amplitude squared of the virtual contributions to all orders in the leading-log approximation.

Provided an event has been generated according to the LO matrix elements, the parton shower algorithm proceeds as follows:

- For each external coloured parton in the hard interaction, all possible tree-level graphs that can arise from it, obtained by letting the quark split into a qg pair, the gluon split into a gg or a $q\overline{q}$ pair for any quark flavour, are considered. To each splitting occurred, one associates a t, z and ϕ value, which are defined by the splitting kinematics.

- The previous step is iterated as many times as desired, for each possible coloured leg present at any stage. One imposes that the value of t for splitting near the hard process must be less than the hard process scale Q^2, and all subsequent values of t are in decreasing order as proceeding towards the branches of the tree graph. Then:

  - Each vertex obtained in this way has the weight

$$\theta(t-t_0)\frac{\alpha_S(t)}{2\pi}\frac{dt}{t}\hat{P}_{i,jl}(z)dz\frac{d\phi}{2\pi}, \tag{2.123}$$

    where $\alpha_S(t)$ is the QCD running coupling evaluated at the scale t.

  - Each line in the graph has weight $\Delta_i(t', t'')$, where t' is the t value associated with the upstream vertex, t'' with the downstream vertex, and

$$\Delta_i(t', t'') = \exp\left[-\sum_{(jl)}\int_{t''}^{t'}\frac{dt}{t}\int_0^1 dz\frac{\alpha_S(t)}{2\pi}\hat{P}_{i,jl}(z)\right]. \tag{2.124}$$

    In the case of last line, t'' is replaced by the infrared cutoff t_0. The weights $\Delta_i(t', t'')$ are called Sudakov form factors and represent all the dominant virtual corrections.

- Given the initial hard parton momenta, and the values of the t, z and ϕ variables at each splitting vertex, one reconstructs all the momenta in the tree graph. Since a parton line followed by a splitting process acquires a positive virtuality larger than its mass, the momenta of the partons must be adjusted so that the momentum is conserved.

The result of the parton shower algorithm applied to a tree process can be pictorially represented as a tree of splittings with decreasing angles, such that at a given splitting vertex, the splitting angle is by a factor α_S smaller than the previous one. At the point when t reaches the Λ_{QCD} scale, the hadronization algorithm is invoked.

Up until now, we have ignored the issue of soft IR singularities in the parton shower. In fact, besides having collinear singularities, QCD amplitudes manifest soft singularities associated to soft gluon emissions at any angle and are associated with phase space regions in which $z \to 0$ or $z \to 1$. The proper treatment of soft singularities is implemented in publicly available SMC tools; for brevity we do not discuss it here and refer the reader to [126] for a detailed discussion.

We have discussed that additional low angle QCD emissions can be generated automatically using the parton shower algorithm. A parton shower, thus, besides allowing the simulation of hadronization effects, effectively resums the contribution in the near collinear regions to all orders

of the perturbation theory. The parton shower in its usual formulation cannot be applied to events generated using NLO QCD Monte Carlo event generators. However, novel methods have been developed in the past decade allowing for its consistent matching with NLO QCD corrections, as we will see below.

2.4.2 Matching next-to-leading order QCD corrections with Shower Monte Carlos

Next-to-leading order QCD computations have become standard tools for phenomenological studies at hadron colliders. While leading order calculations, implemented in the context of general purpose SMC programs, have been the main tools used in experimental analyses, SMCs include dominant QCD effects at the leading logarithmic level, but do not provide NLO accuracy. For the purpose of precision measurements, a LO SMC approach used to simulate hadronic collisions down to the detector level, is lacking accuracy. When using the SMC output to correct the measurement for detector effects the comparison with NLO calculations has limitations leading to larger uncertainties. For this reason, it is clear that SMC programs should be improved by including next-to-leading logarithmic accuracy.

The problem of merging NLO calculations with parton shower simulations is basically that of avoiding overcounting, because the SMC programs do implement approximate NLO corrections already. Recently, two acceptable solutions were proposed. First, the MC@NLO [127] method relying on the subtraction from the exact NLO cross section its approximation as implemented in the SMC program. This method is SMC dependent and can lead to events with negative weights because, in general, the exact NLO cross section minus the SMC subtraction terms does not need to be positive. Infrared safe cross sections, however, are always positive. Second, a way to overcome the problem of negative weighted events was proposed, namely the POWHEG (Positive Weight Hardest Emission Generator) method [71]. Moreover, the POWHEG method does not depend on the details of the implementation of the parton shower algorithm, in contrast with MC@NLO, and thus is not SMC specific. In the POWHEG method the hardest emission is generated first and its output can be interfaced to any SMC program that is either p_T-ordered or allows the implementation of a p_T veto.

In the next two sections we review the basic building blocks of the POWHEG method. We will introduce all the concepts required for the understanding of the `POWHEG BOX` framework and show how soft and collinear singularities are dealt with in the POWHEG method. Then, we briefly discuss the implementation of the POWHEG method within the `POWHEG BOX` framework.

POWHEG method: Notations

We recall that the total cross section of a $2 \to n$ hadronic collision can be written at NLO as:

$$\sigma_{\rm NLO} = \int d\mathbf{\Phi}_n \mathcal{L}\left[\mathcal{B}(\mathbf{\Phi}_n) + \mathcal{V}_{\rm ren}(\mathbf{\Phi}_n)\right] + \int d\mathbf{\Phi}_{n+1}\mathcal{L}\mathcal{R}(\mathbf{\Phi}_{n+1}) + \int d\mathbf{\Phi}_{n,1}\mathcal{L}\mathcal{G}_1(\mathbf{\Phi}_{n,1}) + \int d\mathbf{\Phi}_{n,2}\mathcal{L}\mathcal{G}_2(\mathbf{\Phi}_{n,2}), \quad (2.125)$$

where $\mathcal{B}$, $\mathcal{V}_{\rm ren}$ and $\mathcal{R}$ respectively denote the squared Born matrix element, the renormalized virtual contribution and the real contribution, and $\mathcal{L}$ is the product of parton distribution functions. The collinear counterterms for each of the incoming partons labeled 1 and 2, cancelling the initial state collinear singularities, are contained in the terms $\mathcal{G}_1$ and $\mathcal{G}_2$. The n-body final state phase space

can be described by a set of variables

$$\mathbf{\Phi}_n = \{x_1, x_2; p_1, \ldots, p_n\}, \tag{2.126}$$

with its differential defined as

$$d\mathbf{\Phi}_n = dx_1 dx_2 d\Phi_n(x_1 K_1 + x_2 K_2; p_1, \ldots p_n) \ , \tag{2.127}$$

where $d\Phi_n$ is the usual n-particle phase space, K_i and x_i are the momenta of the incoming hadrons and the momentum fractions of the incoming partons respectively, while p_i are the momenta of final state particles. The phase spaces in the integrals of the collinear counterterms, $\mathbf{\Phi}_{n,1(2)}$, effectively correspond to n-body final state configurations, except for the energy degree of freedom of the parton collinear to the beam

$$\mathbf{\Phi}_{n,1} = \{x_1, x_2, z; p_1, \ldots, p_n\}, \quad z x_1 K_1 + x_2 K_2 = \sum_i p_i, \tag{2.128}$$

$$\mathbf{\Phi}_{n,2} = \{x_1, x_2, z; p_1, \ldots, p_n\}, \quad x_1 K_1 + z x_2 K_2 = \sum_i p_i, \tag{2.129}$$

where z is the fraction of momentum of the incoming parton after radiation.

Let us consider a generic observable O, a function of the final state momenta. Its expectation value is given by

$$\begin{aligned}\langle O \rangle = \int d\mathbf{\Phi}_n \mathcal{L} O_n(\mathbf{\Phi}_n) \left[\mathcal{B}(\mathbf{\Phi}_n) + \mathcal{V}_{\rm ren}(\mathbf{\Phi}_n)\right] + \int d\mathbf{\Phi}_{n+1} \mathcal{L} O_{n+1}(\mathbf{\Phi}_{n+1}) \mathcal{R}(\mathbf{\Phi}_{n+1}) \\ + \int d\mathbf{\Phi}_{n,1} \mathcal{L} O_n(\overline{\mathbf{\Phi}}_{n,1}) \mathcal{G}_1(\mathbf{\Phi}_{n,1}) + \int d\mathbf{\Phi}_{n,2} \mathcal{L} O_n(\overline{\mathbf{\Phi}}_{n,2}) \mathcal{G}_2(\mathbf{\Phi}_{n,2}),\end{aligned} \tag{2.130}$$

where O_n and O_{n+1} are the expressions of the observable O in terms of n and $(n+1)$ final state particle momenta. O is required to be an infrared-safe observable. Note that thanks to the infrared safety, the observable O in the integrals over the collinear counterterms depends on the underlying n-body configuration $\overline{\mathbf{\Phi}}_{n,1(2)}$ of the $(n+1)$-body collinear configuration of the real radiation $\mathbf{\Phi}_{n,1(2)}$, where

$$\overline{\mathbf{\Phi}}_{n,1(2)} = \{\bar{x}_1, \bar{x}_2; p_1, \ldots, p_n\}, \quad \bar{x}_{1(2)} = z x_{1(2)}, \bar{x}_{2(1)} = x_{2(1)}. \tag{2.131}$$

Furthermore, the Born contribution is required to be infrared finite. Under these assumptions, the real matrix elements are finite in the whole phase space $d\Phi_{n+1}$, except for regions that correspond to soft and collinear emissions. Moreover, the divergences of each term on the r.h.s. of eq. (2.130) cancel in the sum, such that the total cross section is finite. The integrals in eq. (2.130), however, are separately divergent and thus not suitable for numerical evaluation. In the following, we will show how one can overcome this problem and turn the expression for the expectation value into a sum of integrals that are separately finite and numerically integrable.

POWHEG method: Dipole subtraction

The real $(n+1)$-body final state configuration, $\mathbf{\Phi}_{n+1}$, in general contains multiple collinear and soft configurations. Let us now assume that $\mathbf{\Phi}_{n+1}$ can be decomposed into α singular regions, each of them containing at most one singular configuration, via a mapping $M^{(\alpha)}$

$$\tilde{\mathbf{\Phi}}^{(\alpha)}_{n+1} = M^{(\alpha)}(\mathbf{\Phi}_{n+1}), \tilde{\mathbf{\Phi}}^{(\alpha)}_{n+1} = [\{\tilde{x}_1, \tilde{x}_2; \tilde{p}_1, \ldots, \tilde{p}_{n+1}\}]_\alpha = \{\tilde{x}_1^{(\alpha)}, \tilde{x}_2^{(\alpha)}; \tilde{p}_1^{(\alpha)}, \ldots, \tilde{p}_{n+1}^{(\alpha)}\}, \tag{2.132}$$

where $[\dots]_\alpha$ means "in the context of a singular region α". As we have seen in Section 2.3.3, the infrared singularities can be treated within a dipole subtraction formalism. Let $\mathcal{C}^{(\alpha)}$ be a function containing the real counterterms for a singular region α. The real counterterms have the property that for any infrared-safe observable $O_{n+1}(\mathbf{\Phi}_{n+1})$, vanishing fast enough if $\mathbf{\Phi}_{n+1}$ approaches two singular regions at the same time, the function

$$\mathcal{R}(\mathbf{\Phi}_{n+1})O_{n+1}(\mathbf{\Phi}_{n+1}) - \sum_\alpha \mathcal{C}^{(\alpha)}(\mathbf{\Phi}_{n+1})O_{n+1}\left(M^{(\alpha)}(\mathbf{\Phi}_{n+1})\right) \tag{2.133}$$

has at most integrable singularities in the $\mathbf{\Phi}_{n+1}$ space.

The contribution to any observable O coming from the real radiation can be rewritten using the real counterterms in the following way

$$\begin{aligned}\int d\mathbf{\Phi}_{n+1}\mathcal{L}O_{n+1}(\mathbf{\Phi}_{n+1})\mathcal{R}(\mathbf{\Phi}_{n+1}) = \sum_\alpha \int d\mathbf{\Phi}_{n+1}\left[\tilde{\mathcal{L}}O_n(\overline{\mathbf{\Phi}}_n)\mathcal{C}(\mathbf{\Phi}_{n+1})\right]_\alpha \\ + \int d\mathbf{\Phi}_{n+1}\left\{\mathcal{L}O_{n+1}(\mathbf{\Phi}_{n+1})\mathcal{R}(\mathbf{\Phi}_{n+1}) - \sum_\alpha \left[\tilde{\mathcal{L}}O_n(\overline{\mathbf{\Phi}}_n)\mathcal{C}(\mathbf{\Phi}_{n+1})\right]_\alpha\right\},\end{aligned} \tag{2.134}$$

where $\tilde{\mathcal{L}} = \mathcal{L}(\tilde{x}_1, \tilde{x}_2)$. The second term in the r.h.s. of eq. (2.134) is integrable in $D = 4$ dimensions while the first term is divergent. In order to deal with it, we introduce, for each α, the $(n+1)$-body phase space parametrization

$$\mathbf{\Phi}_{n+1} \overset{(\alpha)}{\Longleftrightarrow} \left\{\overline{\mathbf{\Phi}}_n^{(\alpha)}, \Phi_{\text{rad}}^{(\alpha)}\right\}, \quad d\mathbf{\Phi}_{n+1} \overset{(\alpha)}{\Longleftrightarrow} d\mathbf{\Phi}_n^{(\alpha)} d\Phi_{\text{rad}}^{(\alpha)} \tag{2.135}$$

where $\overline{\mathbf{\Phi}}_n^{(\alpha)}$ is the n-body underlying configuration of the $(n+1)$-body real configuration and $\Phi_{\text{rad}}^{(\alpha)}$ describes the radiation process. The phase space is, thus, in each singular region decomposed into the phase space of the underlying Born configuration and the phase space of the additional emission.

The underlying configuration of a region α containing one singular configuration, described by $\tilde{\mathbf{\Phi}}_{n+1}^{(\alpha)}$, can be obtained as follows:

- If $\alpha \in$ S (i.e. it is a soft region), $\overline{\mathbf{\Phi}}_n^{(\alpha)}$ is obtained by deleting the zero momentum parton.
- If $\alpha \in$ FSC (i.e. it is a final state collinear region), $\overline{\mathbf{\Phi}}_n^{(\alpha)}$ is obtained by replacing the momenta of the two collinear partons with their sum.
- If $\alpha \in$ ISC (i.e. it is a initial state collinear region), $\overline{\mathbf{\Phi}}_n^{(\alpha)}$ is obtained by deleting the radiated collinear parton, and by replacing the momentum fraction of the initial state radiating parton with its momentum fraction after radiation.

The underlying configurations $\overline{\mathbf{\Phi}}_{n,1(2)}$, in eq. (2.130), are of the ISC type. Note that the procedure, outlined above, implies that the momentum fractions $\overline{x}_1$, $\overline{x}_2$ of the underlying n-body configuration are identical to the original momentum fractions $\tilde{x}_1$, $\tilde{x}_2$ of the $(n+1)$-body configuration in S and FSC regions, while they differ in ISC regions.

The first term in the r.h.s. of eq. (2.134) can then be, depending on the type of the singular region, written as

$$\left[\int d\mathbf{\Phi}_{n+1}\tilde{\mathcal{L}}O_n(\mathbf{\Phi}_n)\mathcal{C}(\mathbf{\Phi}_{n+1}) = \int d\mathbf{\Phi}_n \tilde{\mathcal{L}}O_n(\mathbf{\Phi}_n)\overline{\mathcal{C}}(\overline{\mathbf{\Phi}}_n)\right]_{\alpha\in\{\text{FSC,S}\}}, \tag{2.136}$$

$$\left[\int d\mathbf{\Phi}_{n+1}\tilde{\mathcal{L}}O_n(\mathbf{\Phi}_n)\mathcal{C}(\mathbf{\Phi}_{n+1}) = \int d\mathbf{\Phi}_n \frac{dz}{z}\tilde{\mathcal{L}}O_n(\mathbf{\Phi}_n)\overline{\mathcal{C}}(\overline{\mathbf{\Phi}}_n, z)\right]_{\alpha\in\{\text{ISC}\}}, \tag{2.137}$$

where $\overline{\mathcal{C}}$ are the integrated dipoles

$$\left[\overline{\mathcal{C}}(\overline{\mathbf{\Phi}}_n) = \int d\Phi_{\rm rad}\mathcal{C}(\mathbf{\Phi}_{n+1})\right]_{\alpha\in\{\rm FSC,S\}}, \tag{2.138}$$

$$\left[\overline{\mathcal{C}}(\overline{\mathbf{\Phi}}_n, z) = \int d\Phi_{\rm rad}\mathcal{C}(\mathbf{\Phi}_{n+1})z\delta(z - \frac{\overline{x}_{1(2)}}{\tilde{x}_{1(2)}})\right]_{\alpha\in\{\rm ISC_{1(2)}\}}, \tag{2.139}$$

and where the parton distribution functions for the underlying configurations of singular regions can be defined as

$$\tilde{\mathcal{L}} = \mathcal{L}(\tilde{x}_1, \tilde{x}_2) = \begin{cases} \mathcal{L}(\overline{x}_1, \overline{x}_2) \text{ for } \alpha \in \{\rm FSC, S\} \\ \mathcal{L}(\overline{x}_1/z, \overline{x}_2) \text{ for } \alpha \in \{\rm ISC_1\} \\ \mathcal{L}(\overline{x}_1, \overline{x}_2/z) \text{ for } \alpha \in \{\rm ISC_2\} \end{cases} \tag{2.140}$$

thanks to the way the S and FSC regions are constructed and thanks to the delta function in eq. (2.139) in the case of ISC regions.

The choice of the mapping $M^{(\alpha)}$ and the counterterms $C^{(\alpha)}$ should be such that the integrals in eqs. (2.138) and (2.139) are easily performed analytically in D dimensions so that the divergences appear as $1/(D-4)$ poles, similarly to the singularities in virtual corrections.

After the dipole subtraction the expectation value for the observable O in eq. (2.130) becomes

$$\begin{aligned}\langle O\rangle = &\int d\mathbf{\Phi}_n \mathcal{L}O_n(\mathbf{\Phi}_n)\left[\mathcal{B}(\mathbf{\Phi}_n) + \mathcal{V}(\mathbf{\Phi}_n)\right] \\ &+ \int d\mathbf{\Phi}_{n+1}\left\{\mathcal{L}O_{n+1}(\mathbf{\Phi}_{n+1})\mathcal{R}(\mathbf{\Phi}_{n+1}) - \sum_\alpha\left[\tilde{\mathcal{L}}O_n(\overline{\mathbf{\Phi}}_n)\mathcal{C}(\mathbf{\Phi}_{n+1})\right]_\alpha\right\} \\ &+ \int d\mathbf{\Phi}_{n,1}\tilde{\mathcal{L}}O_n(\overline{\mathbf{\Phi}}_n)\mathcal{G}_1^{\rm fin}(\mathbf{\Phi}_{n,1}) + \int d\mathbf{\Phi}_{n,2}\tilde{\mathcal{L}}O_n(\overline{\mathbf{\Phi}}_n)\mathcal{G}_2^{\rm fin}(\mathbf{\Phi}_{n,2}),\end{aligned} \tag{2.141}$$

where we have used the fact that it is always possible to write

$$\mathcal{G}_{1(2)}(\mathbf{\Phi}_{n,1(2)}) + \sum_{\alpha\in\{\rm ISC_{1(2)}\}}\overline{\mathcal{C}}^{(\alpha)}(\mathbf{\Phi}_{n,1(2)}) = \mathcal{G}_{1(2)}^{\rm fin}(\mathbf{\Phi}_{n,1(2)}) + \delta(1-z)\mathcal{G}_{1(2)}^{\rm div}(\overline{\mathbf{\Phi}}_n) \tag{2.142}$$

where the $\mathcal{G}_{1(2)}^{\rm fin}(\mathbf{\Phi}_{n,1(2)})$, often referred to as collinear remnants, are finite and

$$\mathcal{V} = \mathcal{V}_{\rm ren} + \sum_{\alpha\in\{\rm FSC,ISC\}}\overline{\mathcal{C}}^{(\alpha)}(\mathbf{\Phi}_n) + \sum_{i=1}^{2}\mathcal{G}_i^{\rm div}(\mathbf{\Phi}_n), \tag{2.143}$$

in which the $1/(D-4)$ poles cancel. Note that in eq. (2.143) the n-body underlying configuration $\overline{\mathbf{\Phi}}_n$ was identified with the n-body Born configuration $\mathbf{\Phi}_n$. All the integrals in eq. (2.141) are now finite in 4 dimensions and can be integrated numerically.

POWHEG method: Real counterterms

Before proceeding, let us also briefly outline how real counterterms can be generated from real matrix elements automatically. The second term in eq. (2.141), corresponding to the sum of real contribution and real counterterms, can be simplified in the following way. Let us for simplicity assume that there is just one singular region. In 4 dimensions, we describe the kinematics of the

emitted parton (with momentum q) in the center of mass (CM) frame of the incoming partons with the following variables

$$\xi = 2q^0/\sqrt{\hat{s}}, \quad y = \cos\theta, \quad \phi, \tag{2.144}$$

where $\hat{s}$ is the partonic CM energy, θ is the polar angle of the emitted parton relative to a reference direction (typically another parton), and ϕ is an azimuthal angle around the same reference direction. The soft and collinear singular regions are associated with $\xi \to 0$ and $y \to 1$ respectively. In, $D = 4 - 2\epsilon$ dimensions, we can write

$$\frac{d^{D-1}q}{2q^0(2\pi)^{D-1}} = \frac{\hat{s}^{1-\epsilon}}{(4\pi)^{D-1}}\xi^{1-2\epsilon}(1-y)^{-\epsilon}d\xi dy d\Omega^{D-2}, \tag{2.145}$$

where

$$d\Omega^{D-2} = (\sin\phi)^{-2\epsilon}d\phi d\Omega^{D-3}, \quad \int d\Omega^{D-3} = \frac{2\pi^{\frac{D-3}{2}}}{\Gamma\left(\frac{D-3}{2}\right)}. \tag{2.146}$$

If we write the real contribution as

$$\mathcal{R} = \frac{1}{\xi^2}\frac{1}{1-y}[\xi^2(1-y)\mathcal{R}], \tag{2.147}$$

then $[\xi^2(1-y)\mathcal{R}]$ is regular for $\xi \to 0$ and $y \to 1$. The phase space integral of $\mathcal{R}$ is infrared divergent and the singular part of the integration is proportional to [71]

$$\begin{aligned}\int_{-1}^{1} dy(1-y)^{-1-\epsilon}\int_0^1 d\xi\xi^{-1-2\epsilon}g(\xi,y) = &-\frac{1}{2\epsilon}\int_{-1}^{1}dy(1-y)^{-1-\epsilon}g(0,y)\\ &-\int_0^1 d\xi\left[\frac{2^{-\epsilon}}{\epsilon}\left(\frac{1}{\xi}\right)_+ - 2\left(\frac{\log\xi}{\xi}\right)_+\right]g(\xi,1)\\ &+\int_{-1}^{1}dy\int_0^1 d\xi\left(\frac{1}{\xi}\right)_+\left(\frac{1}{1-y}\right)_+ g(\xi,y) + \mathcal{O}(\epsilon),\end{aligned} \tag{2.148}$$

where $g(\xi,y) = \xi^2(1-y)\mathcal{R}$ and we have defined the + distributions in the usual way

$$\int_0^1 d\xi F(\xi)_+ f(\xi) = \int_0^1 d\xi F(\xi)(f(\xi) - f(0)), \text{ where } F \in \left\{\frac{1}{\xi}, \frac{\log\xi}{\xi}\right\}, \tag{2.149}$$

$$\int_{-1}^{1} dy\left(\frac{1}{1-y}\right)_+ f(y) = \int_{-1}^{1} dy\frac{f(y)-f(1)}{1-y}. \tag{2.150}$$

The first and second terms in eq. (2.148), after integration in y and ϕ, give a contribution with the same structure as the virtual term, with which they are combined. That is, the first and second terms correspond to the integrated dipoles. It is found that the last term, of the form

$$\int_{-1}^{1}dy\int_0^1 d\xi\left(\frac{1}{\xi}\right)_+\left(\frac{1}{1-y}\right)_+ g(\xi,y) = \int_{-1}^{1}dy\int_0^1 d\xi\xi\hat{\mathcal{R}}, \tag{2.151}$$

where

$$\hat{\mathcal{R}} = \frac{1}{\xi}\left\{\left(\frac{1}{\xi}\right)_+\left(\frac{1}{1-y}\right)_+[\xi^2(1-y)\mathcal{R}]\right\} \tag{2.152}$$

corresponds to the sum of the real contribution and the real counterterms. The expectation value of the observable O, thus, can be written as:

$$\langle O\rangle = \int d\mathbf{\Phi}_n \mathcal{L}O_n(\mathbf{\Phi}_n)\left[\mathcal{B}(\mathbf{\Phi}_n)+\mathcal{V}_{\rm fin}(\mathbf{\Phi}_n)\right] + \int d\mathbf{\Phi}_{n+1}\mathcal{L}O_{n+1}(\mathbf{\Phi}_{n+1})\hat{\mathcal{R}}(\mathbf{\Phi}_{n+1}) + \int d\mathbf{\Phi}_{n,1}\tilde{\mathcal{L}}O_n(\overline{\mathbf{\Phi}}_n)\mathcal{G}_1^{\rm fin}(\mathbf{\Phi}_{n,1}) + \int d\mathbf{\Phi}_{n,2}\tilde{\mathcal{L}}O_n(\overline{\mathbf{\Phi}}_n)\mathcal{G}_2^{\rm fin}(\mathbf{\Phi}_{n,2}). \quad (2.153)$$

By handling the + distributions in $\hat{\mathcal{R}}$ according to the prescriptions (2.149) and (2.150) one automatically generates the real counterterms, provided the variables ξ and y appear in the phase space parametrization. If more than one singular region is present, the real cross section is decomposed into a sum of terms, each of them having singularities in no more than one singular region. For each term, the phase space is parametrized in such a way that the variables ξ and y, appropriate to that particular singular region, are present. Note that, in this procedure, the expression for $\mathcal{R}$ in 4-dimensions is sufficient, since one can use the collinear approximation in the $y \to 1$ limit in order to obtain the singular parts of $\mathcal{R}$ in D-dimensions.

POWHEG method: Generation of hardest emission

The embedding of a NLO computation into a Monte Carlo framework aims at reaching NLO accuracy for inclusive observables, maintaining the leading logarithmic accuracy of the shower approach. This requires the hardest emission to be generated according to a distribution correct also away from the collinear direction and that the integrated quantities around the soft and collinear directions have the NLO accuracy. Within the POWHEG method, the generation of the hardest emission is performed first, using the full NLO accuracy[19], and using the SMC to generate the subsequent radiation.

In a SMC, the event generation starts from a kinematic configuration which is generated according to an exact LO computation. The final state multiplicity is subsequently iteratively increased by letting each initial and final state parton branch into a couple of partons with a probability related to a Sudakov form factor. Thus, at a given stage of the shower, the scattering process is described by m partons. During the following splitting into a pairs of partons, generating an $(m+1)$-body final state, the algorithm defines a mapping

$$\mathbf{\Phi}_{n+1} \overset{(\alpha)}{\Longleftrightarrow} \left\{\overline{\mathbf{\Phi}}_n^{(\alpha)}, \Phi_{\rm rad}^{(\alpha)}\right\}, \quad (2.154)$$

fully analogous to the mapping in eq. (2.135). Also in this case, there is one mapping for each singular region, where the singular region is associated with the parton undergoing the splitting. Note that, the mapping in eq. (2.154) acts non-trivially also on the momenta of the partons that do not undergo any splitting and the momentum conservation must be restored.

The Sudakov form factor within the POWHEG method can be written as

$$\Delta(\mathbf{\Phi}_n, p_T^{\rm min}) = \exp\left\{-\int \frac{[d\Phi_{\rm rad}\mathcal{R}(\mathbf{\Phi}_{n+1})\theta(k_T(\mathbf{\Phi}_{n+1})-p_T^{\rm min})]_{\overline{\mathbf{\Phi}}_n=\mathbf{\Phi}_n}}{\mathcal{B}(\mathbf{\Phi}_n)}\right\}. \quad (2.155)$$

The function $k_T(\mathbf{\Phi}_{n+1})$ should be equal, near the singular limit, to the transverse momentum of the emitted parton relative to the emitting one. The POWHEG cross section for the generation of

[19]Note that the accuracy of the generation of the hardest emission within the POWHEG method is not exactly NLO, but rather NLO up to the terms originating from higher order corrections.

the hardest event is then

$$d\sigma = \overline{\mathcal{B}}(\mathbf{\Phi}_n) d\mathbf{\Phi}_n \left\{ \Delta(\mathbf{\Phi}_n, p_T^{\min}) + \Delta(\mathbf{\Phi}_n, k_T(\mathbf{\Phi}_{n+1})) \frac{\mathcal{R}(\mathbf{\Phi}_{n+1})}{\mathcal{B}(\mathbf{\Phi}_n)} d\Phi_{\text{rad}} \right\}_{\overline{\mathbf{\Phi}}_n = \mathbf{\Phi}_n}, \tag{2.156}$$

where

$$\overline{\mathcal{B}}(\mathbf{\Phi}_n) = \mathcal{L}[\mathcal{B}(\mathbf{\Phi}_n) + \mathcal{V}(\mathbf{\Phi}_n)] + \left[\int d\Phi_{rad} \mathcal{L}[\mathcal{R}(\mathbf{\Phi}_{n+1}) - C(\mathbf{\Phi}_{n+1})] + \int \frac{dz}{z} \mathcal{L}[\mathcal{G}_1^{\text{fin}}(\mathbf{\Phi}_{n,1}) + \mathcal{G}_2^{\text{fin}}(\mathbf{\Phi}_{n,2})] \right]_{\overline{\mathbf{\Phi}}_n = \mathbf{\Phi}_n}. \tag{2.157}$$

Furthermore, it was assumed that $\mathbf{\Phi}_{n+1}$ is parametrized in terms of Φ_{rad} and $\mathbf{\Phi}_n$. The $p_T^{\min}$ value was introduced as a lower cut-off on the transverse momentum, that is needed in order to avoid to reach unphysical values of the strong coupling constant and of the parton density functions. θ is the usual step function rendering values $k_T(\mathbf{\Phi}_{n+1}) < p_T^{\min}$ prohibited.

The POWHEG formula in eq. (2.156) can be used to feed a SMC program, that will perform all subsequent showers and hadronization. In the following section we will show how the POWHEG method is embedded in the `POWHEG BOX` framework.

`POWHEG BOX` framework

The theoretical construction, described in the previous section, is in practice implemented in a computer framework called `POWHEG BOX` [72]. The aim of this framework is to construct a POWHEG implementation of a QCD NLO process automatically, given the following ingredients

- The list of all flavour structures of the Born process.
- The list of all flavour structures of the real process.
- The Born phase space.
- The Born squared amplitudes $\mathcal{B}$, the colour correlated ones $\mathcal{B}_{ij}$ and spin correlated ones $\mathcal{B}_{\mu\nu}$, calculated in 4-dimensions.
- The real matrix elements for all relevant partonic processes, calculated in 4-dimensions.
- The finite part of the renormalized virtual corrections, calculated in D-dimensions.
- The Born colour structures in the limit of a large number of colours.

If all these ingredients are provided, the `POWHEG BOX` does all the rest. It automatically finds all the singular regions, builds the soft and collinear remnants, generates the scattering with Born underlying configuration using the full NLO formula and then generates the hardest additional radiation according to the POWHEG Sudakov form factor.

The `POWHEG BOX` has been successfully used for many SM processes such as single W and Z production [128], Higgs boson production [129, 130], single top-quark and heavy-quark pair production [131, 132], or recently for beyond SM processes like charged Higgs bosons production or slepton pair production [133, 134]. Note that the heavy-quark pair production implementation contains the QCD corrections to the top-pair production at order $\mathcal{O}(\alpha_S^2)$. In this section, we briefly review the internal workings of `POWHEG BOX`, while the implementation of the electroweak top-pair production and its corrections at order $\mathcal{O}(\alpha_S \alpha_W^2)$ will be discussed in Section 2.4.3.

The POWHEG BOX framework consists of algorithms and formulae relevant for the POWHEG method implemented in Fortran 77. In order to implement a new process into POWHEG BOX, the user has to provide routines initializing the appropriate input parameters and numerical routines calculating the amplitudes squared of the Born contribution and its virtual and real corrections. In the following paragraphs, we briefly outline the structure of the code, the procedure for event generation and some of the related setting requiring user input. Remaining aspects of the procedure of implementing a new process into POWHEG BOX will be discussed and illustrated with the implementation of electroweak top-pair production in Section 2.4.3. For more details, the reader is referred to the POWHEG BOX manual in [72].

The flavour structure of the process to be implemented in POWHEG BOX is specified by a list of flavour configurations stored in the arrays flst_born and flst_real. Each of the elements of these arrays contains a list of initial and final state particles of the Born and real process represented by their PDG codes [44] with the exception of the gluon, which is assigned the code 0. Virtual contributions have the same flavour structure as the corresponding Born process. The flst_born and flst_real arrays are declared in the header file pwhg_flst.h and the length of their entries nlegborn and nlegreal[20] in the header file nlegborn.h.

The event generation starts with the phase space. Given a vector of random variables X_{born}, with length equal to the number of independent variables describing the phase space, the Born momenta are calculated in a routine provided by the user. The number of independent variables describing the phase space is $3n-2$, where n is the number of final state particles, if there is no final state resonance in the process. Each final state resonance requires an additional random variable to describe its virtuality. The number of final state particles is calculated from the length of the flst_born array elements, which is specified by the user.

From the vector of random variables, the user-provided routine born_phsp calculates the arrays kn_pborn and kn_cmpborn containing the lists of Born momenta $k_1, k_2, p_1, \ldots$ in the laboratory frame and CM frame, respectively. The values of kn_xb1 and kn_xb2 are respectively set to the parton momentum fractions x_1 and x_2, and the value kn_sborn is set to the squared CM energy of the Born process. Furthermore, the masses of the Born process initial and final state particles are filled in the array kn_masses, and kn_minmass is set to a fixed lower bound on the mass of the final state (in the case of top-pair production this is equal to $2m_t$). Finally, the variable kn_jacborn is filled with the Jacobian of the random variable to phase space transformation

$$J_{\text{born}} = \left| \frac{\partial \mathbf{\Phi}_n}{\partial X_{\text{born}}} \right| . \tag{2.158}$$

Note that variables with a prefix kn_ are declared in the header file pwhg_kn.h.

Once the Born momenta are known the amplitudes squared of the Born and virtual contributions can be calculated. The Born matrix element, the colour correlated Born amplitudes, defined in eq. (2.108), and the spin correlated Born amplitudes, defined below, are calculated in the user-provided routine setborn in 4-dimensions. The spin correlated Born amplitude is defined to be non-zero if the j^{th} Born leg is a gluon and is basically the Born cross section obtained by leaving the gluon indices of the j^{th} leg uncontracted. More precisely

$$\mathcal{B}_j^{\mu\nu} = N \sum_{\{i\},s_j,s'_j} \mathcal{M}(\{i\},s_j)\mathcal{M}^\dagger(\{i\},s'_j)(\epsilon^\mu_{s_j})^* \epsilon^\nu_{s'_j} \tag{2.159}$$

where $\mathcal{M}(\{i\},s_j)$ is the Born amplitude, $\{i\}$ represent collectively all remaining spins and colours of the incoming and outgoing particles, s_j represents the spin of the j^{th} particle of the process,

[20] Note that in POWHEG BOX, nlegreal is set automatically to nlegborn + 1.

$\epsilon^{\mu}_{s_j}$ are the polarization vectors and the factor N is the appropriate normalization factor including averages over initial spin and colour and symmetry factors. The user-provided routine `setvirtual` returns the finite part of the renormalized virtual contribution $\mathcal{V}_{\rm fin}$ calculated in D-dimensions and regularized using dimensional regularization. $\mathcal{V}_{\rm fin}$ can be related to the renormalized virtual contribution $\mathcal{V}_{\rm ren}$, in $D = 4 - 2\epsilon$ dimensional space, as follows

$$\mathcal{V}_{\rm ren} = \frac{(4\pi)^{\epsilon}}{\Gamma(1-\epsilon)} \left(\frac{\mu_r^2}{Q^2}\right)^{\epsilon} \frac{\alpha_S}{2\pi} \left[\frac{1}{\epsilon^2} a\mathcal{B} + \frac{1}{\epsilon} \sum_{i,j} c_{ij}\mathcal{B}_{ij} + \mathcal{V}_{fin}\right], \tag{2.160}$$

where the coefficients a and c_{ij} do not depend upon ϵ and the scale Q is in `POWHEG BOX` set to the renormalization scale μ_r. $\mathcal{V}_{fin}$ is literally the renormalized virtual contribution stripped off the $1/\epsilon^2$ and $1/\epsilon$ poles and is up to the normalization equal to the renormalized virtual matrix elements in eq. (2.116), in which we have subtracted the IR singularities using the CS dipole subtraction formalism.

One of the basic ingredients of the POWHEG method is the decomposition of the real phase space into singular regions, containing only one singular configuration, and the dipole subtraction. The dipole subtraction method implemented in `POWHEG BOX`, is the FKS dipole subtraction [121] in which the decomposition into singular regions is easier than in the CS formalism[21]. We recall that the singularities in virtual corrections are cancelled by the singularities in integrated dipoles containing the 1-body phase space integrals of real and collinear counterterms. Also, the singularities in real corrections are cancelled using the real counterterms which can be obtained by regularizing the real contribution using the + distributions assuming that the real phase space was decomposed into singular regions. Finally, the collinear remnants of the collinear renormalization are added to the total cross section. `POWHEG BOX` automatically generates the finite parts of the integrated dipoles, decomposes the real phase space, handles the real contribution using the + distributions and generates the collinear remnants automatically within the FKS dipole subtraction framework.

As already mentioned, the decomposition of the real phase space into singular regions is performed automatically. Given the list of flavours of the real graphs, in `flst_real`, one is faced with the combinatoric problem of finding all singular regions grouped according to their underlying Born configurations. This can be achieved for final state soft collinear regions[22] by the following procedure. First, one loops over all massless parton pairs `i` and `j`. If `i` and `j` can come from the splitting of the same parton, a new list is built from the original one by deleting partons `i, j` and adding a parton with the appropriate flavour, i.e. if `i, j` have opposite flavour, or are both gluons, a gluon is added. Then one tests whether the newly built flavour list, which now has one particle less, is an admissible flavour structure for the Born cross section. This is done by checking whether this list is up to a permutation of the final state partons equal to one of the elements of the Born flavour structure list. Initial state singular regions[23] can be obtained in a similar fashion. This procedure will lead to a list of all the possible singular configurations in which only one pair of partons can be collinear or one parton soft (or both).

[21] It turns out that, within the CS dipole subtraction framework, it is impossible to simple weight the real cross sections with factors that vanish in all but one singular regions, in contrast with the FKS framework [72].

[22] A final state collinear region is defined as a region in which a final state parton i is becoming collinear to a final state parton j, or soft.

[23] An initial state collinear region is defined as a region in which a final state parton i is becoming collinear to either initial state partons $j = 1, 2$, or soft.

In order to generate an event, POWHEG BOX first generates a Born kinematic and flavour configuration, with a probability proportional to

$$\overline{B}(\mathbf{\Phi}_n) = \left[\sum_{f_b} \overline{B}^{f_b}(\mathbf{\Phi}_n)\right] d\mathbf{\Phi}_n \tag{2.161}$$

where

$$\overline{B}^{f_b}(\mathbf{\Phi}_n) = \int_0^1 dX_{\rm rad}^{(1)} \int_0^1 dX_{\rm rad}^{(2)} \int_0^1 dX_{\rm rad}^{(3)} \tilde{B}^{f_b}(\mathbf{\Phi}_n, X_{\rm rad}) \tag{2.162}$$

and the function $\tilde{B}^{f_b}$ is defined as

$$\begin{aligned}\tilde{B}^{f_b}(\mathbf{\Phi}_n, X_{\rm rad}) = [\mathcal{L}(\mathcal{B}(\mathbf{\Phi}_n) + \mathcal{V}(\mathbf{\Phi}_n))]_{f_b} + \sum_{\alpha_r \in \{\alpha_r | f_b\}} \left[\left|\frac{\partial \Phi_{\rm rad}}{\partial X_{\rm rad}}\right| \mathcal{L}\hat{\mathcal{R}}(\mathbf{\Phi}_n)\right]_{\alpha_r}^{\overline{\mathbf{\Phi}}_n^{\alpha_r}=\mathbf{\Phi}_n} \\ + \sum_{\alpha_1 \in \{\alpha_1 | f_b\}} \frac{1}{z}\left|\frac{\partial z}{\partial X_{\rm rad}^{(1)}}\right| \tilde{\mathcal{L}}(\mathcal{G}_1^{\rm fin})^{\alpha_1}(\phi_{n,1}) + \sum_{\alpha_2 \in \{\alpha_2 | f_b\}} \frac{1}{z}\left|\frac{\partial z}{\partial X_{\rm rad}^{(1)}}\right| \tilde{\mathcal{L}}(\mathcal{G}_2^{\rm fin})^{\alpha_2}(\phi_{n,2})\end{aligned} \tag{2.163}$$

In eqs. (2.161) - (2.163), f_b is an element of the flst_born array and $\alpha_r | f_b$ selects a singular regions α_r that has f_b as the underlying Born configuration. Furthermore the radiation variables $\Phi_{\rm rad}$ were in each singular region parametrized by three variables in the unit cube $X_{\rm rad} = \{X_{\rm rad}^{(1)}, X_{\rm rad}^{(2)}, X_{\rm rad}^{(3)}\}$ and the real contribution $\hat{\mathcal{R}}$ has been properly regularized in each singular region using the + distributions, see eq. (2.152). The radiation is then generated using the POWHEG Sudakov form factor

$$\Delta^{f_b}(\mathbf{\Phi}_n, p_T^{\rm min}) = \prod_{\alpha_r \in \{\alpha_r | f_b\}} \Delta_{\alpha_r}^{f_b}(\mathbf{\Phi}_n, p_T^{\rm min}), \tag{2.164}$$

where

$$\Delta_{\alpha_r}^{f_b}(\mathbf{\Phi}_n, p_T^{\rm min}) = \exp\left\{-\left[\int d\Phi_{\rm rad} \frac{\mathcal{R}(\mathbf{\Phi}_{n+1})}{\mathcal{B}^{f_b}(\mathbf{\Phi}_n)} \theta(k_T(\mathbf{\Phi}_{n+1}) - p_T^{\rm min})\right]_{\alpha_r}^{\overline{\mathbf{\Phi}}_n^{\alpha_r}=\mathbf{\Phi}_n}\right\}. \tag{2.165}$$

In conclusion, the construction of a POWHEG implementation is in POWHEG BOX automatic provided that the user furnishes the lists of flavour structures flst_born and flst_real, a routine calculating the phase space born_phsp, and routines calculating the Born matrix element, virtual and real contributions in routines setborn, setvirtual, setreal respectively. The Born and real contributions should be provided in 4-dimensions, the virtual contribution calculated in D-dimensions using dimensional regularization, renormalized and stripped off the $1/(D-4)$ poles.

2.4.3 Electroweak top-pair production in POWHEG BOX

The electroweak top-pair production and its corrections at order $\mathcal{O}(\alpha_S \alpha_W^2)$ have been implemented in the NLO Monte Carlo event generator POWHEG BOX and in this section we discuss the details of this implementation. The most recent version of the POWHEG BOX package, at the time of checkout at revision 2220, was obtained from the svn repository at svn://powhegbox.mib.infn.it/trunk/POWHEG-BOX. As per author's recommendations we have implemented the electroweak top-pair production in a new directory Zprime. At the time of writing of this manuscript, this implementation has not been committed to the repository and thus is not publicly available.

In the following, we discuss how to specify the process which is being implemented in the subroutine `init_processes` and the implementation of the subroutines `born_phsp`, `setborn`, `setvirtual` and `setreal`, the role of which has been explained in the previous section. Furthermore, we discuss the subroutine `init_couplings` used for the initialization of various input parameters such as couplings and masses.

It is important to note that in this implementation we assume that final state top-quarks are produced on-shell. Their decay can be automatically taken into account at leading order accuracy by Shower Monte Carlo tools such as `Pythia`.

Process specification: `init_processes`, `nlegborn.h`

The process under consideration is specified via the lists of Born and real flavour configurations in the arrays `flst_born` and `flst_real`. Each entry of these arrays contains a list of PDG codes corresponding to the particles on the external lines of the process. For example, the entry `[-1,1,6,-6]` specifies a flavour configuration of the tree-level scattering of $d\bar{d}$ with a top-pair in the final state. Every possible flavour configuration, in general, leads to a different event and so each one has to be specified. Note that the flavour configurations identical up to a permutation of the final state particles are considered equivalent.

Because we rely on SMCs to handle the top quark decay, the Born contribution to the top-pair production can be in the context of its `POWHEG BOX` implementation considered a $2 \to 2$ process. Therefore, we set `nlegborn = 4` and the respective lengths of Born and real flavour configuration entries are equal to 4 and 5. The Born flavour configuration array `flst_born` contains the following 10 entries

```
flst_born = [[-5,5,6,-6], ..., [-1,1,6,-6], [1,-1,6,-6], ..., [5,-5,6,-6]]
```

since we work in the 5 light flavour scheme and both initial state configurations $q\bar{q}$ and $\bar{q}q$ have to be considered. The number of light flavours also has to be specified in the variable `st_nlight`, which is passed to the subroutine implementing the running of α_S. The variable `maxprocborn`, specifying the number of inequivalent Born flavour configurations, was correspondingly set to 10. Note that the code snippets, as the one above, are written throughout this section in a pseudo language.

The real contribution can proceed via the channels $q\bar{q}$, $\bar{q}q$, gq and $g\bar{q}$. The array `flst_real` of real flavour configurations, thus, was initialized with the following 30 flavour configurations

```
flst_real =
  [[-5,5,6,-6,0], ..., [-1,1,6,-6], [1,-1,6,-6], ..., [5,-5,6,-6,0],
   [0,-5,6,-6,-5], ..., [0,-1,6,-6,-1], [0,1,6,-6,1], ..., [0,5,6,-6,5],
   [-5,0,6,-6,-5], ..., [-1,0,6,-6,-1], [1,0,6,-6,1], ..., [5,0,6,-6,5]]
```

and the variable `maxprocreal` was correspondingly set to 30.

It is important to note that the variables `nlegborn`, `maxprocborn` and `maxprocreal` have to be initialized in the header file `nlegborn.h` which is included in all the `POWHEG BOX` source files.

`POWHEG BOX` requires the final state particles, in the lists of flavour configurations, to be ordered in the following way: colourless particles, massive coloured particles and massless coloured particles. The index of the first light parton in those arrays must be specified in the variable `flst_lightpart` which we set to 5.

In the subroutine `init_processes`, we also implement the initialization of the array `kn_masses` and the variable `kn_minmass`:

```
kn_masses = [0,0,mt,mt,0]
kn_minmass = 2*mt
```

where `mt` is set equal to the top quark mass and can be modified in the `POWHEG BOX` input file `powheg.input`. More detailed discussion regarding the input file, corresponding to our implementation, can be found in one of the following subsections.

Phase space: `born_phsp`

We recall that the phase space for contributions with Born-like flavour structures, the Born and virtual contributions, are calculated in the `POWHEG BOX` in the subroutine `born_phsp` which has to be provided by the user. Given a vector of random variables $X_{\rm born}$ generated within `POWHEG BOX`, the code in `born_phsp` should calculate the Born momenta k_1, k_2, p_1 and p_2 in the CM and laboratory frame, the incoming parton momentum fractions x_1 and x_2, the partonic CM energy $\hat{s}$ and the Jacobian of the random variable to phase space transformation J.

The event generation is conveniently performed in terms of the invariant mass M, the rapidity Y of the top-pair in the laboratory frame and the angle θ_1 between $\vec{k}_1$ and $\vec{p}_1$ in the partonic CM frame [132]. The invariant mass and the rapidity are given by

$$M^2 = (p_1 + p_2)^2 = x_1 x_2 s_{\rm had}, \quad Y = \frac{1}{2}\log\frac{x_1}{x_2}, \tag{2.166}$$

where $s_{\rm had}$ is the hadronic squared CM energy. The momentum fractions can be expressed in terms of the invariant mass M and rapidity Y as follows,

$$x_1 = \sqrt{\frac{M^2}{s_{\rm had}}}e^{Y}, \quad x_2 = \sqrt{\frac{M^2}{s_{\rm had}}}e^{-Y}, \text{ and } dx_1 dx_2 = \frac{1}{s_{\rm had}} dY dM^2, \tag{2.167}$$

and for the integration measure of integrals over Born-like configurations one finds

$$d\mathbf{\Phi}_2 = d\Phi_2 dx_1 dx_2 = \frac{\beta}{16\pi s_{\rm had}} d\cos\theta_1 dM^2 dY, \tag{2.168}$$

where

$$\beta = \sqrt{1 - \frac{4m_{\rm t}^2}{M^2}}. \tag{2.169}$$

The appropriate integration region is then

$$4m_{\rm t}^2 \le M^2 \le s_{\rm had}, \quad \frac{1}{2}\log\frac{M^2}{S} \le Y \le -\frac{1}{2}\log\frac{M^2}{S}, \quad -1 \le \cos\theta_1 \le 1. \tag{2.170}$$

Born, virtual and real contributions: `setborn`, `setvirtual` **and** `setreal`

The expressions for the Born contribution, and the colour and spin correlated Born are implemented in the subroutine `setborn`. Note that the Born contribution in eq. (2.20) includes a sum over all the possible initial state quarks and the flux factor. Since `POWHEG BOX` requires the amplitudes to be implemented for each flavour structure separately and without the flux factor, we have implemented the following expression in `setborn`:

$$\texttt{born(qi)} = 2\hat{s}\left(\mathcal{B}_q(\gamma,\gamma) + \mathcal{B}_q(\mathrm{Z},\mathrm{Z}) + \mathcal{B}_q(\mathrm{Z}',\mathrm{Z}') + \sum_{B\neq B'}\mathcal{B}_q(B,B')\right), \tag{2.171}$$

where the PDG code `qi` $\in 1,2,3,4,5$ of the quark q, labeling the initial state quark in the r.h.s. of eq. (2.171), denotes the corresponding flavour structure `[qi,-qi,6,-6]`. The expressions for the general interference term $\mathcal{B}_q(B,B')$ can be found in eq. (2.18).

The colour correlated Born `bornjk(j,k,qi)` $= (\mathcal{B}_q)^{j,k}$, defined in eq. (2.108), is used to calculate the scalar products of colour charges $\mathbf{T}_j \cdot \mathbf{T}_k$ employed in the dipole subtraction formalism, see Section 2.3.3. Note that $(\mathcal{B}_q)^{j,k}$ is a symmetric matrix and moreover it is sufficient to know its off-diagonal entries $j \neq k$. The calculation of its elements amounts to attaching an additional colour charge matrix, $t^l_{\alpha\beta}$ for quarks and $-t^l_{\beta\alpha}$ for anti-quarks, between the external lines $j,k \in \{1,2,3,4\}$, where the 1, 2, 3 and 4 label respectively the external lines with momenta k_1, k_2, p_1, p_2. It is easy to see, that in the case of EW top-pair production this leads to 0 if j is an initial state and k a final state external line or vice versa[24]. If j and k are both initial or both final state external lines we have:

$$\texttt{bornjk(j,k,qi)} = C_F \texttt{born(qi)}, \tag{2.172}$$

where $C_F = 4/3$.

Since there are no tree-level diagrams with external gluons contributing to the EW top-pair production, the spin correlated Born `bornmunu(mu,nu,j,qi)` $= (\mathcal{B}_q)^{\mu\nu}_j$, defined in eq. (2.159), is equal to zero

$$\texttt{bornmunu(mu,nu,j,qi)} = 0. \tag{2.173}$$

The virtual contribution is implemented in the subroutine `setvirtual`. Similarly as in the case of Born matrix element, we have implemented the expressions for the virtual corrections for each flavour configuration separately, labeled by the light quark in the initial state q:

$$\texttt{virtual(qi)} = 2\hat{s}\frac{2\pi}{\alpha_S}\frac{\Gamma(1+\epsilon)}{\Gamma(1-\epsilon)}(m_t)^\epsilon \int d\mathbf{\Phi}_2 \mathcal{L}\left\{\sum_q \sum_{B,B'}\left[\mathcal{V}^{\mathrm{i}}_q(B,B') + \mathcal{V}^{\mathrm{f}}_q(B,B')\right] + \text{c.c.}\right\}. \tag{2.174}$$

The expressions for the general interference terms $\mathcal{V}^{\mathrm{i(f)}}(B,B')$ before the insertion of master integrals can be found in eqs. (2.44), (2.45) and the expressions for the master integrals in eqs. (2.65), (2.66) and (2.67). The HPLs are numerically evaluated as described in [135].

The real contribution is expected to be implemented in the subroutine `setreal`. We implement the formulae calculated in Section 2.3.2 stripped off the flux factor and a factor $\alpha_S/(2\pi)$, similarly to the virtual contributions. For convenience, `POWHEG BOX` provides a mechanism for checking the consistency of the Born matrix element and real contribution. During the initialization, it calculates for each singular region the ratios of soft and collinear approximations of the real part and their limiting behaviours constructed from the colour correlated and spin correlated Born amplitudes, and writes them out into the file `pwhg_checklimits`. The double soft-collinear and collinear-soft limits are also tested, however, they do not depend on the real amplitudes, but only on the Born contribution.

The soft and collinear singularities of the real contribution originating from the soft gluon emission, or initial and final state collinear $q \to \mathrm{g}q$ splitting in the channel $q\bar{q}$ are treated automatically within `POWHEG BOX`, as explained in the previous sections. The collinear singularities in the channels $\mathrm{g}q$ and $\mathrm{g}\bar{q}$, however, are left untreated. In principle, it would be possible to perform the appropriate mass factorization, include the photon in the definition of PDFs and generate the corresponding real counterterms. Due to lack of time, however, we temporarily opt to regulate the collinear singularities in the quark-gluon channels with a non-zero photon mass. For an example of mass factorization in the case of QED corrections to the SM top-pair production, in which the regulation of IR singularities is obtained by phase-space slicing, see Ref. [90].

[24] This leads to a trace over an odd number of traceless colour matrices.

Input parameters: `init_couplings`, `powheg.input`

The handling of input parameters which can be specified in the file `powheg.input` is implemented in the subroutine `init_couplings`. In this subsection we discuss the settings relevant to the `Zprime` implementation handled by `init_couplings`, a more complete description of `powheg.input` is contained in the following subsection.

As described in the previous sections, we keep beyond the SM neutral currents general, parameterized by the Z′ mass and its couplings to the SM fermions: $m_{\mathrm{Z}'}$ (`mzp`), $a^q_{\mathrm{Z}'}$ (`azpu`, `azpd`, ...), $b^q_{\mathrm{Z}'}$ (`bzpu`, ...). The width of Z′ is also considered as a free parameter and can be specified in `gzp`. Furthermore, we allow users to modify the SM parameters entering the formulae for EW top-pair production such as $\mathrm{s}^2_{\theta_W}$ (`sthw2`), m_{t} (`mt`), the Z mass and width (`mz` and `gz`) and finally the inverse of α_{EM} (`alphaem_inv`) which fixes the value of $\alpha_W = \alpha_{\mathrm{EM}}/\mathrm{s}^2_{\theta_W}$.

The factorization and renormalization scales, μ_f and μ_r, are fixed to the partonic CM energy $\hat{s}$ and can be varied by setting the appropriate variables `renscfact` and `factscfact`.

The value of the photon mass, which we use in the expressions for the real contribution in the quark-gluon channels to regulate the corresponding collinear divergences can be modified by setting the value of `mg`.

Finally, we allow the user to switch on and off the contributions corresponding to the photon, Z and Z′ exchange. To generate the top-pair production mediated only by photon, only by Z or only by Z′ exchange, the `channel` should be set to 1, 2 or 3 respectively. The settings `channel = 4, 5, 6`, respectively, correspond to the contributions mediated by photon/Z, photon/Z′, Z/Z′, where the slash signifies the sum of the individual contributions including their interference. Finally the full matrix element containing the contributions from photon, Z and Z′, and all their interferences are selected by setting `channel = 7`.

Compiling and running `POWHEG BOX: Zprime`

Our implementation of EW top-pair production can be compiled using a provided `Makefile`. Executing

```
$ make
```

should build the binary `pwhg_main`. If the use of LHAPDF [136] interface to parton distribution functions is required by the user, the executable `lhapdf-config` has to be in the system path.

A typical run would then be executed in a new directory containing the input file `powheg.input`. In the input file, the hadronic CM energy can be set for each beam separately in variables `ebeam1` and `ebeam2` and the PDFs for the two beams can be specified in the variables `lhans1` and `lhans2`. Events will be generated if the variable `numevts` specifying the number of events to generate is set to a value larger than 0. Note that it is also possible to simulate only the Born contribution and this is achieved by setting the variable `bornonly = 1`. For more settings, the reader is encouraged to consult the `POWHEG BOX` manual [72] or the comments in the `powheg.input` file.

During the initialization, the consistency between the real and the Born contribution is checked and the result is stored in `pwhg_checklimits`. This is followed by the integration and event generation. The result of the integration is printed on screen as well as saved in the file `pwgstat.dat` and the events in the Les Houches Event file [137] are stored in the file `pwgevents.lhe`.

2.4.4 Final remarks

As discussed in this section, the NLO calculations and the parton shower algorithm are not compatible due to the fact that the parton shower includes approximate NLO corrections already. There

exist, however, methods allowing for a consistent matching of fixed NLO calculations with parton showers. One of these methods is the POWHEG method, which generates only positive weighted events and is independent of the details of the implementation of the parton shower as long as it is p_T ordered or allows for the implementation of a p_T veto. We have explained some of the basic features of the method, relying on the dipole subtraction formalism to treat IR singularities. Moreover, a fairly automated implementation of this method exists in the `POWHEG BOX` package, which we have used for the implementation of the EW top-pair production and its QCD corrections. The details of the implementation were given in Section 2.4.3.

2.5 Automation

Calculating 1-loop corrections to a given process beyond the SM (BSM) is not an easy task. Therefore, we have tried to do as much of the calculation described in the previous sections as possible automatically. At the time we have started the calculation, no publicly available tool, able to perform 1-loop calculations without significant user input, existed. Perhaps, with the exception of the FeynArts/FormCalc/LoopTools [138] framework. On the other hand, tools capable of accomplishing some parts of loop calculations such as QGRAF [94] and FORM [96] were made publicly available a long time ago.

With the technological progress, the automation became a popular subject of interest and many new tools capable to calculate 1-loop QCD corrections to any SM process appeared. To list a few, there is MadLoop [139], GoSam [140] and MadGolem [141]. Many of the groups developing these tools are now working on automating the calculation of BSM amplitudes at 1-loop.

In a typical 1-loop calculation one needs to calculate Born matrix elements, virtual corrections in D-dimensions and contributions originating from real diagrams with an additional external line. In order to obtain a finite result, virtual contributions have to be renormalized and one needs to find a suitable procedure to cancel the IR divergences between virtual and real contributions. Eventually one also has to treat the initial state collinear singularities which do not cancel in the sum of real and virtual contributions.

In Feynman diagram based methods, the calculation of BSM Born, virtual and real contributions can be split into the following tasks:

- model specification, derivation of Feynman rules: FeynRules [142, 143], LanHEP [144]
- generation of Feynman diagrams: QGRAF, DIANA [95], FeynArts
- translation of Feynman diagrams in to corresponding formulae: DIANA
- Feynman diagram substitution, calculation of traces and further algebraic manipulations: FORM
- renormalization of virtual corrections: QGRAF, DIANA, FORM
- evaluation of loop integrals: Golem [145], LoopTools, Reduze [101, 109]
- treatment of QCD IR singularities: `POWHEG BOX`
- numerics: `POWHEG BOX`

In the list above, we also mention the tools which could be in principle employed for a given task. However, this does not necessarily mean that this task has been fully automated. In particular,

the renormalization of virtual contributions could be achieved using the same tools that have been used for its calculation.

The particle content of BSM theories can be very large and the derivation of the corresponding Feynman rules can thus be a complex task. Therefore it is desirable to automate it, which can be done using FeynRules or LanHEP. The authors of FeynRules have recently developed the Universal FeynRules output (UFO) standard [143] allowing for convenient interfacing of FeynRules results.

The generation of Feynman diagrams has also been automated and QGRAF can generate Feynman diagrams with a general number of legs and loops. The output of QGRAF is not immediately suitable for the calculation of amplitudes and further work is needed. For this purpose, DIANA has been developed. In DIANA, a script written in its native language is launched for every diagram generated by QGRAF, which DIANA embeds. In particular, DIANA can distribute the Lorentz and colour indices and momenta automatically and generate the input for any computer algebra system (CAS).

After the generation of diagrams and its translation to amplitudes, the calculation of Dirac traces and further symbolic manipulation can be achieved e.g. with FORM. FORM is a CAS which is particularly suitable for efficient symbolic computations one encounters in higher-order calculations.

The renormalization of virtual corrections could be in principle achieved with the combination of QGRAF, DIANA and FORM as it has been demonstrated for SM processes in [146].

For the evaluation of loop integrals, various approaches exist. One can reduce the loop integrals with tensorial structure in its numerators into a set of scalar loop integrals using the Passarino-Veltman decomposition [147]. These scalar integrals, however, are not all independent and the coefficients of the decomposition can become singular in some points of the phase space, which is known as the inverse Gram determinant problem. The scalar loop integrals can then be evaluated numerically using packages such as LoopTools. There exist also a mixed approach of Passarino-Veltman decomposition and numerical evaluation in the Golem package, which overcomes the problem of inverse determinant. Alternatively, one can use IBP identities to reduce tensor as well as scalar loop integrals into a set of independent master integrals avoiding the issue of inverse Gram determinant. The master scalar integrals can then be calculated analytically using the differential equation method or numerically using LoopTools.

Finally, the expressions/codes obtained in the previous steps can be implemented in NLO Monte Carlo tools allowing for consistent matching with the parton shower algorithm such as `POWHEG BOX`.

Even though each step in the procedure described above is well defined and can be accomplished for any BSM process, some steps even fully automatically, the user input required between each step is considerable rendering 1-loop calculation a very time consuming task. Therefore, we have decided to interface the individual tools in order to minimize the user input and make the calculation of 1-loop corrections as comfortable as possible. Our effort resulted in a collection of Python scripts, which we refer to as `bsmLoops`. In the following section we describe some features of `bsmLoops`. We avoid getting into technical details since some steps of the automation of the full calculation have not yet been implemented and we do not plan to publish this tool in the near future.

Loop calculations in `bsmLoops`

The calculation of amplitudes is based on the Feynman diagram approach. Let us denote D and I two processes associated with their respective sets of Feynman diagram. In the calculation of the amplitude $\mathcal{M}(d_1)\mathcal{M}(d_2)^*$ of the interference of two diagrams d_1 and d_2 from their respective sets $d_1 \in D$ and $d_2 \in I$, we avoid performing the charge conjugation by inverting the second diagram.

For the inverted diagram we use the so-called Feynman rules for the shadowed region[25]. In the following we will refer to the sets D and I as the regular or direct and shadowed or inverse process respectively. These sets are equal in the case of Born or real contribution, but they are different in the case of virtual contributions in which the amplitude is calculated by interfering 1-loop and tree-level diagrams. The calculation of the amplitude squared of $q\overline{q} \to t\bar{t}$ is thus obtained as the product of $\mathcal{M}_{q\bar{q}\to t\bar{t}}\mathcal{M}_{t\bar{t}\to q\bar{q}}$.

The input of `bsmLoops` is the model file, at the moment in the format compatible with DIANA, and the process specification. The process is specified by listing the external particles and number of loops. The virtual corrections to $d\bar{d} \to t\bar{t}$ at order $\mathcal{O}(\alpha_S\alpha_W)$ in the SM with an additional Z′-boson would be in the `bsmLoops` input file specified as follows:

```
processes:
  - uu_ttNLO: # optional name
      ingoing:
        - d: {}
        - D: {}
      outgoing:
        - t: {mass: mt}
        - T: {mass: mt}
      loops: 1
  - tt_uuLOI: # optional name
      inverse: True
      ingoing:
        - t: {mass: mt}
        - T: {mass: mt}
      outgoing:
        - d: {}
        - D: {}
      loops: 0
modelFile: ../inc/model.SMwZp
```

where the file `model.SMwZp` is a DIANA model file listing all propagators and vertices. The Born, real and virtual contributions have to be specified separately but can be calculated in a single run. Also, at the moment we do not implement any collective particle tags and for pp scattering, each combination of the initial state has to be specified separately.

Given the model file and the process, the Feynman diagrams, including the Lorentz and colour indices and momenta on lines, are generated fully automatically and stored in a SQL database. At this stage, the user can calculate the traces or request the generation of interference terms which are obtained by a Cartesian product of the SQL tables storing all the diagrams, matching the direct and inverse process appropriately.

Note that in the near future, we plan to implement the interface to the UFO. Also, at the moment we support only MySQL databases, which require the installation of a database server. This task is non-trivial, but many scientific institutes may already provide a fully functional installation of a MySQL database server. Since the SQL language, which is used for the specification of data structures and communication with the server is highly standardized, the transition towards an implementation which does not require a database server, but rather stores the data on a local hard drive, such as SQLite, should not pose considerable effort.

[25]The notion of shadowed regions was introduced in [93].

The calculation of traces in the language of `bsmLoops` refers to the execution of FORM on a source file generated according to a pre-programmed template. `bsmLoops` contains a collection of such templates suitable for various purposes, such as the calculation of Born, virtual and real contributions. Besides, our FORM code base contains a set of functions, usable in these templates, which are completely process independent. For example, the spin sums, the translation from the scalar products into Mandelstam variables or translation of loop momenta suitable for further processing are written to be valid for any $2 \to n$ process. The result of each trace is stored in a separate FORM log file and subsequently extracted and stored in the SQL database.

For the Born and real contributions the final step of the calculation is to sum all the traces which can be done automatically on user request. This task is similar to the calculation of traces. Again, `bsmLoops` executes FORM code on a source file generated from a pre-programmed template. This time however, only one FORM file is generated figuring the sum of all the traces calculated in the previous step.

For the calculation of virtual contributions `bsmLoops` offers one more step which is the reduction of loop integrals using Reduze. Loop integrals are from the traces extracted automatically. Subsequently, we build the auxiliary topologies (including eventual completion as described in Section 2.3.1), pass them to Reduze, extract the expressions for the reduction and use FORM to apply them and store the results in the database. These results can be summed automatically as described in the previous paragraph.

The procedure outlined in the paragraphs above requires no user input whatsoever, except for eventual filtering of diagrams specified in the process description. For example, if one requests the diagrams for scattering of $\mathrm{d\bar{d}} \to \mathrm{t\bar{t}}$ at 1-loop, all the loop diagrams at orders $\mathcal{O}(\alpha_S^3)$, $\mathcal{O}(\alpha_S^2\alpha_W)$, $\mathcal{O}(\alpha_S\alpha_W^2)$ and $\mathcal{O}(\alpha_W^3)$ are generated. The filtering is implemented as filtering on SQL data and the diagrams can be filtered based on the power of g_W and g_S in the diagrams and also on the external particles and so on.

At this stage one would renormalise the virtual contributions. We have not yet implemented this step, although, `bsmLoops` can be used for the calculation of self energies and vacuum polarizations as well as for the generation of "counter term diagrams". To finalize the step of the renormalization one would have to automate the calculation of n-point functions and the extraction of renormalization constants.

In the calculation of QCD corrections to EW top-production we have calculated the master integrals analytically. The summing capabilities of `bsmLoops`, however, can be used to generate a Fortran code which could subsequently be linked to numerical codes able to evaluate the expansion of scalar loop integrals around $D \to 4$ up to a required order.

From the description of the `POWHEG BOX` framework it is clear that there are no steps which could not be easily automated (except for the treatment of non-QCD IR singularities) and such an automation has been very recently achieved within the framework of GoSam [148].

In order to make `bsmLoops` competitive in the present environment, further work is necessary. As mentioned, we plan to implement the interface to the UFO, the automatic generation of the `POWHEG BOX` implementation is feasible, but the automation of renormalization presents a significant task. Also, a considerable amount of work is required for validation, since at the moment bsmLoops has been fully used only for one process.

The formulation of `bsmLoops` is very robust and modular. For a skilled FORM user it can be used to perform many sorts of higher-order calculations. In addition to top pair production discussed in this thesis, it has been used for the calculation of NLO virtual correction to single-top production beyond the SM, which we also plan to implement in `POWHEG BOX` [149]. Note that we have also calculated 1-loop corrections to top-pair production at order $O(\alpha_S^2\alpha_W)$ using `bsmLoops`,

but due to the lack of time and the complexity of UV renormalization this calculation has not yet been finished. Moreover, `bsmLoops` does not in principle have any limits on the number of loops and has been tested for the calculation of virtual corrections to Moeller scattering at NNLO QED. Currently, its limits are being tested in the calculation of semi-inclusive electron-positron scattering at NNNLO by employing the method in [150].

In conclusion, we have developed a set of scripts, collectively referred to as `bsmLoops`, interfacing various tools often used in higher-order calculations which have aided the calculation of QCD corrections to the EW top-pair production. More specifically, `bsmLoops` embeds QGRAF/DIANA, FORM and Reduze interfaced in Python. It minimizes the user input in the calculation of Born, virtual and real amplitudes, but so far it does not automate the renormalization. In the near future we plan to extend it starting with an interface to the UFO and an interface to `POWHEG BOX`.

2.6 Electroweak top-pair production at next-to-leading order QCD accuracy at the Large Hadron Collider

We have calculated the QCD corrections to the EW top-pair production in theories with an additional Z′ boson and implemented the formulae derived in the previous sections in the `POWHEG BOX` Monte Carlo event generator. Here we refer to this implementation as `POWHEG BOX: Zprime` (`PBZp`). In this section we present the numerical results obtained using `PBZp`. Due to the lack of time, we have studied the electroweak top-pair production only in the SSM, in which the Z′-boson has SM-like couplings. A more complete study including the other G(221) models is planned as part of a future study.

We begin by discussing the validation of the `PBZp` code. This includes the comparison of the LO EW top-pair production cross section obtained using `PBZp` against the cross sections calculated in general purpose Monte Carlo event generators `Pythia 6.4` and MadGraph5 (MG5) [151]. Furthermore we report on the consistency cross-check of the real contribution in the $q\overline{q}$ channel implemented in the `POWHEG BOX` framework, and compare the `PBZp` predictions for the $gq(\overline{q})$ real contribution against the predictions of MG5. The consistency of the remaining piece, the virtual contribution, was verified by subtracting the CS dipoles from the renormalized virtual contribution resulting in a finite expression, as explained in Section 2.3.3. We did not compare our results against the calculation presented in [75], because Melnikov et al. do not consider the same set of NLO corrections. In the remaining parts of this section we show the impact of the QCD corrections on the resonant production of an SSM Z′ with a mass of 4 TeV and its subsequent decay to the pair of top quarks at the LHC.

2.6.1 Validation

Leading order

In the first step we compare the dependence of the sum of the total cross sections of a single resonant γ, Z- and Z′-boson production and its decay into a top-pair at a pp collider on the CM energy $\sqrt{s_{\text{had}}}$ including all the interferences. We set the Z′ boson mass equal to $M_{Z'} = 0.8$ TeV[26], and the Z- and Z′-boson widths to their respective values as calculated in `Pythia`[27]. The remaining input

[26]Note that such a light SSM Z′-boson is excluded and the numerical results shown in Figure 2.13 serve only for the purpose of comparison of our results with those of the general purpose Monte Carlo generators.

[27]The resonance widths in `Pythia` are calculated automatically and do not necessarily correspond to the values obtained from the experiment.

parameters, listed in Section 2.4.3, are set to their respective values extracted from experiment, and the value of α_{EM} to its value at the scale of the Z pole mass [44]. The input parameters of `Pythia` and MG5 are set to match the input parameters of `PBZp` as closely as possible.

In the upper part of Figure 2.13, we present the total cross sections obtained using `PBZp` with the NLO corrections switched off (solid blue), `Pythia`[28] (dashed green) and MG5 (dashed orange). The factorization scale was identified with the partonic CM energy, $\mu_f^2 = \hat{s}$, and the blue band

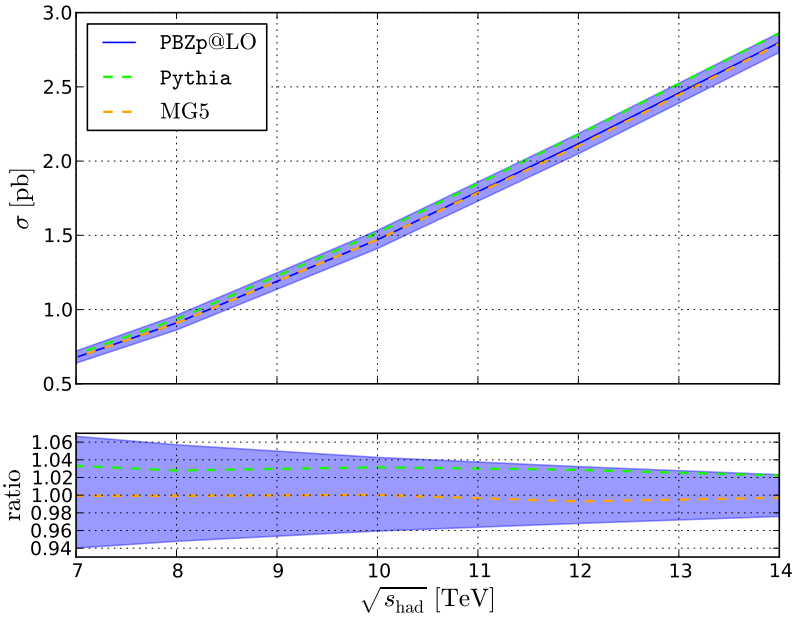

Figure 2.13: The comparison of the total cross section dependence on $\sqrt{s_{\text{had}}}$ for $M_{\text{Z}'} = 0.8$ TeV in `PBZp` (solid blue), `Pythia` (dashed green) and MG5 (dashed orange). The blue band represents the factorization scale variation uncertainty calculated using `PBzp`.

represents the variation of the factorization scale in the interval $\mu_f/\sqrt{\hat{s}} \in (0.5, 2)$ in `PBZp`. The lower part of Figure 2.13 shows the ratios with respect to the central prediction of `PBZp`.

We also compare the dependence of the total cross section on the mass of the Z′-boson in the range $M_{\text{Z}'} \in (0.8, 4)$ TeV at a fixed CM energy, $\sqrt{s_{\text{had}}} = 14$ TeV. This comparison is shown in Figure 2.14, in which we plot the predictions of `Pythia` and `PBZp` at LO accuracy.

As one can see in Figures 2.13 and 2.14, we obtain an excellent agreement with the predictions of MG5 and we also agree with the predictions of `Pythia` within the scale variation uncertainty.

Next-to-leading order

The `POWHEG BOX` implements a consistency check between the Born and the real contributions. As explained in Section 2.4.3, for each singular region the `POWHEG BOX` automatically calculates the ratios of soft and collinear QCD approximations of the real part and their limiting behaviours constructed from the colour correlated and spin correlated Born amplitudes, which are then written

[28] For the purpose of this comparison, we switch off the initial and final state radiation in `Pythia`.

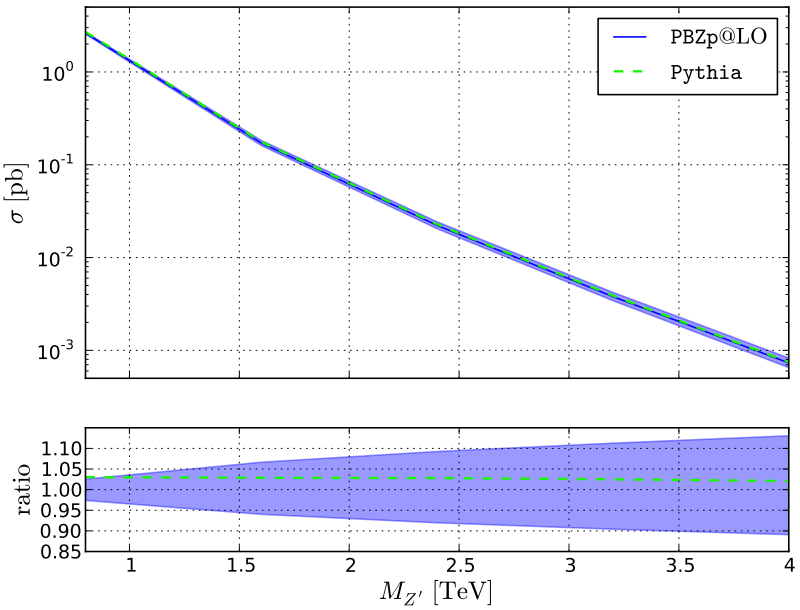

Figure 2.14: The comparison of the total cross section dependence on $M_{Z'}$ in `PBZp` (solid blue), `Pythia` (dashed green). The blue band represents the uncertainty due to factorization scale variation obtained using `PBZp`.

into the file `pwhg_checklimits`. We have verified that all the corresponding ratios in the $q\overline{q}$ channel are within the precision of the numerical evaluation equal to 1.

The real contribution originating from the gq and g$\overline{q}$ channels are IR finite with respect to QCD splittings. It is, thus, impossible to verify its consistency as we did in the case of the $q\overline{q}$ channel. Therefore, we have validated the gq and g$\overline{q}$ channels by comparing the predictions of `PBZp` against the ones of MG5, which is capable of calculating cross sections of $2 \to n$ processes, not including the contribution due to virtual corrections, in an automated fashion. In the left plot of Figure 2.15 we show the sum of the Born, $q\overline{q} \to \gamma \to \mathrm{t\bar{t}}$, and the real $\mathrm{g}q(\overline{q}) \to \gamma \to \mathrm{t\bar{t}}q(\overline{q})$ cross section contributions calculated in `PBZp` and MG5 as a function of CM energy $\sqrt{s_{\mathrm{had}}}$. On the central and the right part of Figure 2.15 we show similar cross sections for the subprocesses mediated by the Z- and Z′-boson respectively. Since in the MG5 framework, the treatment of IR singularities is possible only via the cuts on kinematic variables we have attempted to mimic the behaviour of MG5 by implementing a cut on the transverse momentum of the light final state quark, p_T^{min}. The cross sections shown in Figure 2.15 were obtained using a $p_T^{\mathrm{min}} > 10$ GeV cut in both `PBZp` and MG5. The predictions of `PBZp` and MG5 agree up to roughly 10% and the relative disagreement is most likely due to the difference in the implementation of the p_T^{min} cut. This, however, warrants a further investigation.

It is important to note that the real subprocesses in the channels g$q(\overline{q})$ at high energies constitute more than 50% of the total cross sections shown in Figure 2.15. Despite the fact that these subprocesses are suppressed by an additional power of α_S, the parton luminosity in the g$q(\overline{q})$ channel is at the LHC considerably larger than the luminosity in the $q\overline{q}$ channel.

Within the `POWHEG BOX` framework, the QED IR singularities are not taken care of automatically

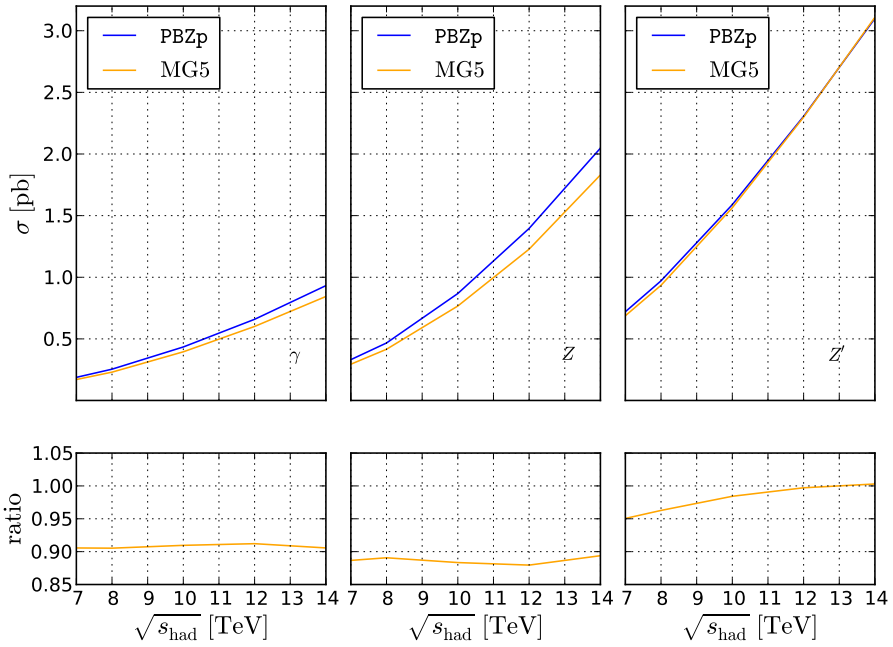

Figure 2.15: The contributions $q\bar{q} \to \gamma \to t\bar{t}$ and $gq(\bar{q}) \to \gamma \to t\bar{t}q(\bar{q})$ of the EW top-pair production with a $p_T^{\min} > 10$ GeV.

in contrast to the QCD ones. Therefore, we have treated the singularities originating from the real diagrams in the $gq(\bar{q})$ channels by giving the photon a non-zero mass[29]. Preferably, however, one would integrate the photon into the definition of the PDFs and perform the mass factorization to treat the initial state collinear QED singularities. For a better understanding, we have calculated the sensitivity of the sum of $q\bar{q} \to \gamma \to t\bar{t}$ and $gq(\bar{q}) \to \gamma \to t\bar{t}q(\bar{q})$ cross sections on the value of the photon mass and the results are shown in Figure 2.16. We see that the sensitivity of the cross section to the value of the photon mass is negligible as compared to the uncertainty due to the factorization scale variation.

2.6.2 The impact of next-to-leading order QCD corrections on the electroweak top-pair production at the Large Hadron Collider

Finally, we study the electroweak top-pair production and its NLO QCD corrections at the LHC beyond the SM. We show how the total cross section and the top-pair invariant mass distribution can be strongly affected by the NLO QCD corrections. Here we consider only the SSM Z′-boson with a mass $M_{Z'} = 4$ TeV and width $\Gamma_{Z'} = 0.1138$ TeV[30] at the LHC running at $\sqrt{s_{\text{had}}} = 14$ TeV. Similarly as in the previous section, the values of all the input parameters are set to their respective values extracted from experiment and the value of α_{em} to its value at the scale of the Z pole-mass.

For the fixed LO predictions as well as for the fixed NLO and the generation of the hardest emission we now use exclusively `PBZp`. The output of `PBZp` is then subsequently showered using the p_T ordered shower algorithm implemented in `Pythia`. The contribution at the LO accuracy

[29] A non-zero photon mass was introduced only in formulae for the real contribution in the $gq(\bar{q})$ channels.
[30] This width corresponds to the value calculated using `Pythia`.

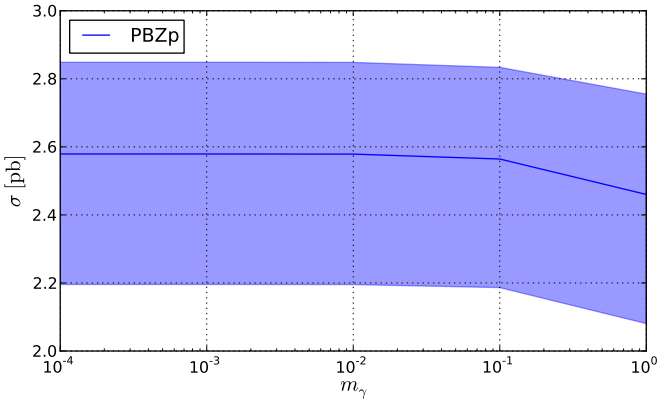

Figure 2.16: The sum of Born $q\overline{q} \to \gamma \to t\bar{t}$ and real $gq(\overline{q}) \to \gamma \to t\bar{t}q(\overline{q})$ contributions to the EW top-pair production as a function of the photon mass, which is used to regulate the initial state collinear singularities involving QED splittings.

consists of a single resonant γ, Z-boson and Z′-boson production including all the corresponding interferences. The NLO corrections include the virtual and real contribution at order $\mathcal{O}(\alpha_S \alpha_W^2)$ in the channels qq and $gq(\overline{q})$. The virtual contributions were calculated in dimensional regularization and renormalized in the $\overline{\text{MS}}$ and OS scheme for initial state quarks and final state top quarks, respectively. The QCD IR singularities were treated automatically within the framework of `POWHEG BOX` and the QED IR singularities by introducing a non-zero photon mass. For the PDFs we use the NLO MSTW distributions [62] both in the NLO and LO runs. The factorization and the renormalization scales are identified with the partonic CM energy $\mu_f = \mu_r = \sqrt{\hat{s}}$ and varied in the interval $\mu_f = \mu_r, \mu_{r(f)}/\sqrt{\hat{s}} \in (0.5, 2)$.

It Table 2.1, we list the LO and NLO cross sections in the high invariant mass region $M_{t\bar{t}} > 2.5$ TeV and in the mass slice around the resonance $M_{t\bar{t}} \in (3.9, 4.1)$ TeV. We find that while the NLO corrections yield a large contribution in the high mass region, they do not contribute significantly in the region close to the resonance mass.

Table 2.1: The total cross sections of the EW top-pair production at LO and NLO accuracy in the high mass region $M_{t\bar{t}} > 2.5$ TeV and in the mass slice around the resonance $M_{t\bar{t}} \in (3.9, 4.1)$ TeV.

	$\sigma(M_{t\bar{t}} > 2.5 \text{ TeV})$ [fb]	$\sigma(M_{t\bar{t}} \in (3.9, 4.1) \text{ TeV})$ [fb]
LO	$0.70^{+0.09}_{-0.07}$	$0.47^{+0.06}_{-0.05}$
NLO	$1.31^{+0.30}_{-0.20}$	$0.47^{+0.11}_{-0.06}$

The invariant mass distribution of the top-pair at the LO and NLO accuracy including the effects of the parton shower is shown in Figure 2.17. The uncertainty due to the variation of factorization and renormalization scales is represented by the corresponding error bars. As the cross sections in Table 2.1 suggest, we find that the NLO corrections lead to very large K-factors in the region below the mass of the resonance, while the invariant mass in the resonance regions is

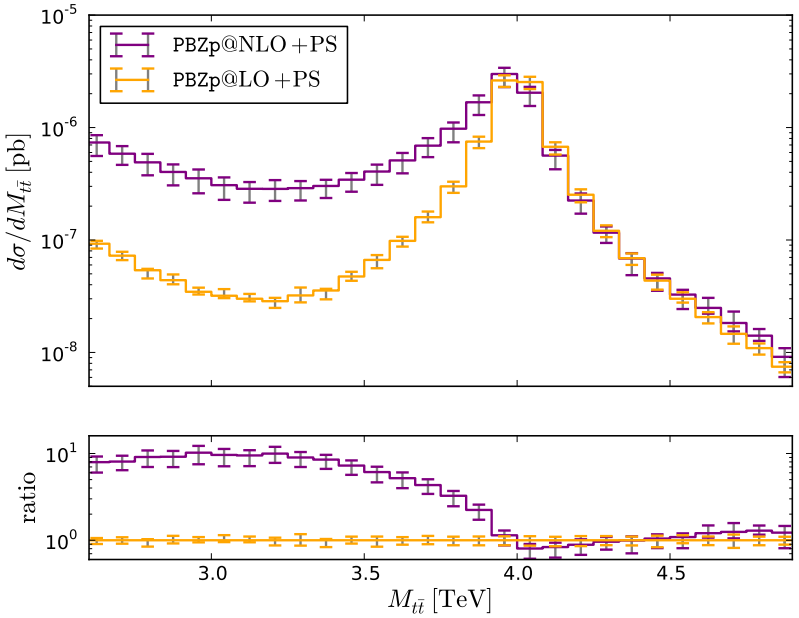

Figure 2.17: Top: The top-pair invariant mass of its electroweak production at LO (orange) and NLO (purple) accuracy including the effect of the parton shower. The error bars constitute the factorization scale and renormalization scale variation uncertainty. Bottom: The ratios of NLO predictions with respect to the LO prediction.

not affected.

Note that, although one would expect the uncertainty due to the variation of the factorization and renormalization scales to be reduced after the inclusion of higher-order corrections, this is not the case. This is caused by the fact that the dependence on the strong coupling constant α_S enters the partonic cross section of the EW top-pair production for the first time at order $O(\alpha_S\alpha_W^2)$. Inclusion of the corrections at order $O(\alpha_W^3)$ are expected to reduce the scale uncertainty.

2.7 Conclusions

Due to its large mass and short lifetime, the top quark may well provide an effective probe for the physics beyond the SM. Should the new physics be observed, predictions beyond the LO accuracy will likely play a vital role in the identification of the underlying theory since an accurate determination of the model parameters requires precise predictions. At the LHC running at its design energy and luminosity the top quark is expected to be produced abundantly and any deviations from the precise SM predictions for its properties will hint at physics BSM.

In this chapter we have presented the calculation of NLO QCD corrections to the EW top-pair production. We have calculated the Born contribution and its NLO virtual and real corrections in Sections 2.2, 2.3.1 and 2.3.2, respectively. As we have explained in detail, the virtual corrections containing integrals over the loop momentum, in general, suffer from UV and IR divergences. Moreover, the real contributions are also IR divergent. We have treated the UV divergences by the procedure of renormalization. The soft and final state divergences cancel in the sum over the

virtual and real contributions, while the initial state divergences are absorbed into the definition of the PDFs via the procedure of mass factorization. The cancellation of IR divergences is not trivial, but can be realized within the framework of dipole subtraction formalisms. Since the structure of initial state collinear singularities is universal, their treatment is often also included in the dipole subtraction framework.

The NLO QCD calculations have become standard tools for phenomenological studies at hadron collider. They are, however, not trivially compatible with the parton shower algorithm which could simulate hadronic collisions down to the detector level. Recently, methods allowing for consistent matching of the parton shower algorithm with fixed NLO QCD calculations have been developed. We have implemented our calculation of the EW top-pair production at order $\mathcal{O}(\alpha_S \alpha_W^2)$ within a framework employing one these methods, namely the `POWHEG BOX`. The POWHEG method and the `POWHEG BOX` framework were reviewed in Sections 2.4.

Within `POWHEG BOX`, the QCD IR divergences are treated in an automated fashion using the FKS dipole subtraction. We have provided the matrix element of the Born contribution, the real corrections and the virtual corrections calculated in dimensional regularization, renormalized and stripped off the remaining IR singularities. The remaining QED IR divergences, present in some of the channels of the real contribution, which are not accounted for within `POWHEG BOX` were treated by introducing a non-zero photon mass. The loop integrals originating from the virtual corrections have been reduced to a small set of master integrals, and the master integrals have been evaluated analytically. The details of this implementation, denoted as `PBZp`, were discussed in Section 2.4.3.

Finally, in Section 2.6, we have performed numerical studies of top-pair production including NLO QCD corrections in the SSM. The consistency of our implementation `PBZp` has been thoroughly verified. The LO predictions of `PZBp` were compared against the predictions of general purpose Monte Carlo generators. The consistency of the NLO corrections were verified either analytically in the case of the virtual corrections, or numerically using the tools provided by the `POWHEG BOX` framework, or by comparison against the predictions of general purpose Monte Carlo generators.

We have found that the NLO QCD corrections can be very large but the K-factors in the invariant mass region around the resonance mass are mild. We also observed that the real corrections in the quark-gluon channels yield at high-energies a very large contribution to the total cross section due to the high quark-gluon luminosity.

Summary and outlook

New vector bosons are a common occurrence in theories beyond the SM. They appear whenever the gauge group of the SM is extended. Often denoted as Z′- and W′-bosons, they are massive, neutral and charged spin-1 particles, respectively, and mediate neutral and charged current interactions of the SM fermions. If their couplings to the SM quarks and leptons are large enough and if they are not too heavy, they could be observed at colliders. For example, the Z′ and W′ bosons predicted in the SSM should be accessible at the LHC up to masses of 5 TeV, while the present ATLAS and CMS data exclude the SSM Z′ and W′ bosons with masses below roughly 3 TeV.

In this manuscript we have investigated the impact of the existence of hypothetical Z′ and W′ bosons on standard observables at the LHC. In Chapter 1, we studied the phenomenology of a class of SM extensions with an enlarged gauge group containing an additional SU(2). Scanning over the parameter space, restricted by the exclusion limits derived from low-energy and precision data, we have obtained predictions for the lepton and third-generation quark production cross sections. We have explored the reach of G(221) models at the LHC and studied how suitable correlations between cross sections can be used to distinguish between the underlying models. Chapter 2 was dedicated to precise calculations of the top-pair production beyond the SM. We have calculated the electroweak top-pair production cross section including the NLO corrections at order $\mathcal{O}(\alpha_S \alpha_W^2)$. This calculation was then implemented in a Monte Carlo event generator framework `POWHEG BOX`, which allows for consistent matching of NLO QCD calculations with the parton shower.

In Chapter 1, we showed how the Z′- and W′-boson couplings can be parametrized by a small set of common parameters and discussed their exclusion limits derived in a recent global analysis of low-energy and LEP constraints. The total cross sections of the predicted charged and neutral gauge bosons decaying into leptons and third-generation quarks were confirmed to be accessible at the LHC up to masses of 5 TeV within the allowed range of parameters. We proposed a novel and powerful method to distinguish general SU(2)× SU(2)×U(1) models. Individually, the total cross sections do not allow for the identification of the underlying G(221) model, however, correlations of these cross sections may well lead to a unique identification.

In Chapter 2, we presented the calculation of 1-loop corrections to the electroweak top-pair production at hadron colliders in the SM extensions featuring an additional Z′ boson. At the LHC the top quark is expected to be produced abundantly and any deviations from the SM predictions may hint at physics BSM. Precise predictions for the top quark related observables are thus highly desirable. We have calculated the Born contribution and its NLO virtual and real corrections of the electroweak top-pair production and implemented them in the `POWHEG BOX` Monte Carlo generator. The UV divergences have been treated by the procedure of renormalization, while the QCD soft and collinear IR divergences have been handled automatically within the dipole subtraction formalism implemented in `POWHEG BOX`. The QED IR divergences have been for the time being treated by introducing a non-zero mass of the photon.

Due to the lack of time, we have restricted our numerical study of the EW top-pair production

at NLO only to the SSM Z′ boson and showed a limited set of predictions. We plan to extend this by including the predictions for other observables, such as the top-pair p_T spectrum, and study the top-pair production in all the G(221) models investigated in Chapter 1. Although, most of our calculation has been thoroughly validated, the virtual corrections may require further validation. In particular, we plan to compare our predictions to those of Melnikov et al. as far as possible.

As a result of our calculation, `POWHEG BOX` now allows for studies of weakly coupled Z′-boson mediated top-pair production at orders $\mathcal{O}(\alpha_S^3)$ and $\mathcal{O}(\alpha_S\alpha_W^2)$. To close the gap, we have also undertaken steps to calculate the 1-loop corrections at order $\mathcal{O}(\alpha_S^2\alpha_W)$. The Born contribution, the bare virtual and the real corrections are available. The renormalization of the virtual corrections, however, requires more work due to the rich structure of SM extensions with an enlarged gauge group. Moreover, the `POWHEG BOX` framework needs to be extended to handle non-QCD singularities. The techniques acquired and the tool developed during this calculation are now being applied to the calculation of the single-top production in theories BSM [149].

Appendix A

G(221) models

In this appendix, we list the Lagrangian extracted from [48] which we have used for the derivation of couplings and masses of Z′- and W′-bosons predicted in the models from the G(221) class in Sections 1.3.2 and 1.3.3.

The fundamental Lagrangian in terms of the mass eigenstates for both neutral and charged gauge bosons can be written as:

$$\begin{aligned}
\mathcal{L}^{\text{mass}}_{\text{fund}} = & \frac{1}{2}\left(\widetilde{M}^2_{\text{Z}} - \frac{\delta\widetilde{M}^4_{\text{Z}}}{\widetilde{M}^2_{\text{Z}'}}\right) \text{Z}_\mu \text{Z}^\mu + \left(\widetilde{M}^2_{\text{W}} - \frac{\delta\widetilde{M}^4_{\text{W}}}{\widetilde{M}^2_{\text{W}'}}\right) \text{W}^+_\mu \text{W}^{-\mu} \\
& + \frac{1}{2}\left(\widetilde{M}^2_{\text{Z}'} + \Delta\widetilde{M}^2_{\text{Z}'} + \frac{\delta\widetilde{M}^4_{\text{Z}}}{\widetilde{M}^2_{\text{Z}'}}\right) \text{Z}'_\mu \text{Z}'^\mu + \left(\widetilde{M}^2_{\text{W}'} + \Delta\widetilde{M}^2_{\text{W}'} + \frac{\delta\widetilde{M}^4_{\text{W}}}{M^2_{\text{W}'}}\right) \text{W}'^+_\mu \text{W}'^{-\mu} \\
& + \text{Z}_\mu \left(J^{0\mu} - \frac{\delta\widetilde{M}^2_{\text{Z}}}{\widetilde{M}^2_{\text{Z}'}} K^{0\mu}\right) + \text{Z}'_\mu \left(K^{0\mu} + \frac{\delta\widetilde{M}^2_{\text{Z}}}{\widetilde{M}^2_{\text{Z}'}} J^{0\mu}\right) + A_\mu J^\mu \\
& + \left[\text{W}^+_\mu \left(J^{+\mu} - \frac{\delta\widetilde{M}^2_{\text{W}}}{\widetilde{M}^2_{\text{W}'}} K^{+\mu}\right) + \text{W}'^+_\mu \left(K^{+\mu} + \frac{\delta\widetilde{M}^2_{\text{W}}}{\widetilde{M}^2_{\text{W}'}} J^{+\mu}\right) + (+ \leftrightarrow -)\right], \qquad \text{(A.1)}
\end{aligned}$$

where the neutral currents (K^0_μ) and charged currents ($K^\pm_\mu$), for the various models are summarized in Tables A.1 and A.2. The masses of Z′- and W′-bosons can be written as:

$$M_{\text{Z}'} = \sqrt{\widetilde{M}^2_{\text{Z}'} + \Delta\widetilde{M}^2_{\text{Z}'} + \frac{\delta\widetilde{M}^4_{\text{Z}}}{\widetilde{M}^2_{\text{Z}'}}}, \qquad \text{(A.2)}$$

$$M_{\text{W}'} = \sqrt{\widetilde{M}^2_{\text{W}'} + \Delta\widetilde{M}^2_{\text{W}'} + \frac{\delta\widetilde{M}^4_{\text{W}}}{\widetilde{M}^2_{\text{W}'}}}, \qquad \text{(A.3)}$$

where $\widetilde{M}$, $\delta\widetilde{M}$ and $\Delta\widetilde{M}$ depend on the symmetry breaking pattern and are given in Table A.3.

	$\overline{\mathrm{u}}\gamma^\mu\mathrm{u}$	$\overline{\mathrm{d}}\gamma^\mu\mathrm{d}$	$\overline{\nu}\gamma^\mu\nu$	$\overline{\ell}\gamma^\mu\ell$
LR	$(\frac{1}{2}c_\phi g_2 - \frac{1}{6}s_\phi g_X)P_\mathrm{R}$ $-\frac{1}{6}s_\phi g_X P_\mathrm{L}$	$(-\frac{1}{2}c_\phi g_2 - \frac{1}{6}s_\phi g_X)P_\mathrm{R}$ $-\frac{1}{6}s_\phi g_X P_\mathrm{L}$	$(\frac{1}{2}c_\phi g_2 + \frac{1}{2}s_\phi g_X)P_\mathrm{R}$ $+\frac{1}{2}s_\phi g_X P_\mathrm{L}$	$(-\frac{1}{2}c_\phi g_2 + \frac{1}{2}s_\phi g_X)P_\mathrm{R}$ $+\frac{1}{2}s_\phi g_X P_\mathrm{L}$
LP	$(\frac{1}{2}c_\phi g_2 - \frac{1}{6}s_\phi g_X)P_\mathrm{R}$ $-\frac{1}{6}s_\phi g_X P_\mathrm{L}$	$(-\frac{1}{2}c_\phi g_2 - \frac{1}{6}s_\phi g_X)P_\mathrm{R}$ $-\frac{1}{6}s_\phi g_X P_\mathrm{L}$	$\frac{1}{2}s_\phi g_X P_\mathrm{L}$	$s_\phi g_X(\frac{1}{2}P_\mathrm{L} + P_\mathrm{R})$
HP	$-s_\phi g_X(\frac{1}{6}P_\mathrm{L} + \frac{2}{3}P_\mathrm{R})$	$-s_\phi g_X(\frac{1}{6}P_\mathrm{L} - \frac{1}{3}P_\mathrm{R})$	$(\frac{1}{2}c_\phi g_2 + \frac{1}{2}s_\phi g_X)P_\mathrm{R}$ $+\frac{1}{2}s_\phi g_X P_\mathrm{L}$	$(-\frac{1}{2}c_\phi g_2 + \frac{1}{2}s_\phi g_X)P_\mathrm{R}$ $+\frac{1}{2}s_\phi g_X P_\mathrm{L}$
FP	$-s_\phi g_X(\frac{1}{6}P_\mathrm{L} + \frac{2}{3}P_\mathrm{R})$	$-s_\phi g_X(\frac{1}{6}P_\mathrm{L} - \frac{1}{3}P_\mathrm{R})$	$\frac{1}{2}s_\phi g_X P_\mathrm{L}$	$s_\phi g_X(\frac{1}{2}P_\mathrm{L} + P_\mathrm{R})$
UU	$\frac{1}{2}c_\phi g_1 P_\mathrm{L}$	$-\frac{1}{2}c_\phi g_1 P_\mathrm{L}$	$-\frac{1}{2}s_\phi g_2 P_\mathrm{L}$	$\frac{1}{2}s_\phi g_2 P_\mathrm{L}$
NU	$\frac{1}{2}\begin{pmatrix} c_\phi g_1 \\ -s_\phi g_2 \end{pmatrix} P_\mathrm{L}$	$-\frac{1}{2}\begin{pmatrix} c_\phi g_1 \\ -s_\phi g_2 \end{pmatrix} P_\mathrm{L}$	$\frac{1}{2}\begin{pmatrix} c_\phi g_1 \\ -s_\phi g_2 \end{pmatrix} P_\mathrm{L}$	$-\frac{1}{2}\begin{pmatrix} c_\phi g_1 \\ -s_\phi g_2 \end{pmatrix} P_\mathrm{L}$

Table A.1: The couplings $g(\overline{f}, f, \mathrm{Z}')$ of the current $K^{0\mu} = \overline{f}\gamma^\mu g(\overline{f}, f, \mathrm{Z}')f$. For the top four models (LR, LP, HP, and FP), $\tan\phi \equiv g_X/g_2$. For the lower two models (UU and NU), $\tan\phi \equiv g_2/g_1$. For the NU model (last row), the top values denote the couplings to the first two generations of fermions, and the bottom values denote the couplings to the third generation.

	$\overline{d}\gamma^\mu u$	$\overline{e}\gamma^\mu\nu$
LR	$\frac{1}{\sqrt{2}}g_2 P_\mathrm{R}$	$\frac{1}{\sqrt{2}}g_2 P_\mathrm{R}$
LP	$\frac{1}{\sqrt{2}}g_2 P_\mathrm{R}$	0
HP	0	$\frac{1}{\sqrt{2}}g_2 P_\mathrm{R}$
FP	0	0
UU	$\frac{1}{\sqrt{2}}c_\phi g_1 P_\mathrm{L}$	$-\frac{1}{\sqrt{2}}s_\phi g_2 P_\mathrm{L}$
NU	$\frac{1}{\sqrt{2}}\begin{pmatrix} c_\phi g_1 \\ -s_\phi g_2 \end{pmatrix} P_\mathrm{L}$	$\frac{1}{\sqrt{2}}\begin{pmatrix} c_\phi g_1 \\ -s_\phi g_2 \end{pmatrix} P_\mathrm{L}$

Table A.2: The couplings $g(\overline{\psi}, \xi, \mathrm{W}')$ of the current $K^{+\mu} = \overline{\psi}\gamma^\mu g(\overline{\psi}, \xi, \mathrm{W}'^{+})\xi$. For the top four models (LR, LP, HP, and FP), $\tan\phi \equiv g_X/g_2$. For the lower two models (UU and NU), $\tan\phi \equiv g_2/g_1$. For the NU model (last row), the top values denote the couplings to the first two generations of fermions, and the bottom values denote the couplings to the third generation.

	$\widetilde{M}^2_{\mathrm{Z}'}$	$\widetilde{M}^2_{\mathrm{W}'}$	$\Delta\widetilde{M}^2_{\mathrm{Z}'}$	$\Delta\widetilde{M}^2_{\mathrm{W}'}$	$\delta\widetilde{M}^2_{\mathrm{Z}}$	$\delta\widetilde{M}^2_{\mathrm{W}}$
LR-D, LP-D HP-D, FP-D	$\frac{1}{4}(g_2^2+g_X^2)u_{\mathrm{D}}^2$	$\frac{1}{4}g_2^2u_{\mathrm{D}}^2$	$\frac{c_\phi^2}{4}g_2^2v^2$	$\frac{1}{4}g_2^2v^2$	$-\frac{c_\phi^2}{4e}g_1g_2g_Xv^2$	$-\frac{1}{4}g_1g_2v^2s_{2\tilde{\beta}}$
LR-T, LP-T HP-T, FP-T	$(g_2^2+g_X^2)u_{\mathrm{T}}^2$	$\frac{1}{2}g_2^2u_{\mathrm{T}}^2$	$\frac{c_\phi^2}{4}g_2^2v^2$	$\frac{1}{4}g_2^2v^2$	$-\frac{c_\phi^2}{4e}g_1g_2g_Xv^2$	$-\frac{1}{4}g_1g_2v^2s_{2\tilde{\beta}}$
UU, NU	$\frac{1}{4}(g_1^2+g_2^2)u^2$	$\frac{1}{4}(g_1^2+g_2^2)u^2$	$\frac{s_\phi^2}{4}g_2^2v^2$	$\frac{s_\phi^2}{4}g_2^2v^2$	$-\frac{s_\phi^2}{4e}g_1g_2g_Xv^2$	$-\frac{1}{4}g_1g_2v^2s_\phi^2$

Table A.3: The model-dependent parameters $\widetilde{M}^2_{\mathrm{Z}',\mathrm{W}'}$, $\Delta\widetilde{M}^2_{\mathrm{Z}',\mathrm{W}'}$ and $\delta\widetilde{M}^2_{\mathrm{Z},\mathrm{W}}$.

Appendix B

Feynman rules

Throughout the calculations in Chapter 2 we use the Pauli metric, the Feynman gauge and notations similar to the ones employed in [93]. In this appendix we summarize the Feynman rules and the spin and polarization used in Sections 2.2 and 2.3.

External lines

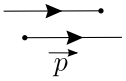

$u(p), \bar{u}(p),$

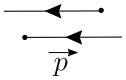

$\bar{v}(p), v(p),$

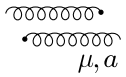

$\epsilon^a_\mu, \epsilon^{a*}_\mu,$

where

$$\begin{aligned} \sum u(p)\bar{u}(p) &= -i\not{p} + m, \\ \sum v(p)\bar{v}(p) &= -i\not{p} - m, \\ \sum \epsilon^a_\mu \epsilon^{a*}_\nu &= \delta_{\mu\nu}\delta^{ab}. \end{aligned} \tag{B.1}$$

Propagators

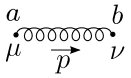

$$\frac{1}{i(2\pi)^4}\frac{\delta_{\mu\nu}\delta_{ab}}{p^2 - i\epsilon},$$

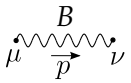

$$\frac{1}{i(2\pi)^4}\frac{\delta_{\mu\nu}}{p^2 + m_B^2 - i\epsilon},$$

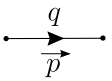

$$\frac{1}{i(2\pi)^4}\frac{-i\not{p} + m_q}{p^2 + m_q^2 - i\epsilon},$$

where $B \in \{\gamma, \mathrm{Z}, \mathrm{Z}'\}$.

Vertices

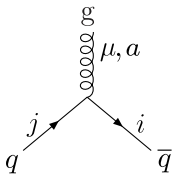

$$i(2\pi)^4 g_S \frac{1}{2}\gamma^\mu t^a_{ij},$$

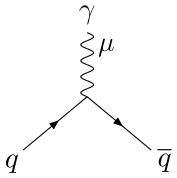

$$i(2\pi)^4 g_W \mathrm{s}_{\theta_W} Q_q \gamma^\mu,$$

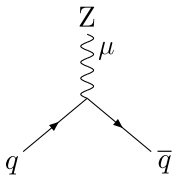

$$i(2\pi)^4 \frac{g_W}{4\mathrm{c}_{\theta_W}}\gamma^\mu \left(a^q_{\mathrm{Z}} + b^q_{\mathrm{Z}}\gamma_5\right),$$

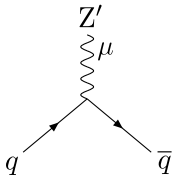

$$i(2\pi)^4 \frac{g_W}{4\mathrm{c}_{\theta_W}}\gamma^\mu \left(a^q_{\mathrm{Z}'} + b^q_{\mathrm{Z}'}\gamma_5\right),$$

where $g_W = \sqrt{4\pi\alpha_W}$ is the electroweak coupling constant, g_S is the strong coupling constant and θ_W the Weinberg angle. Furthermore Q_q is the electric charge of quark q, $a^u_{\mathrm{Z}} = 1 - 8/3 s^2_{\theta_W}$, $a^d_{\mathrm{Z}} = 4/3 s^2_{\theta_W} - 1$, $b^u_{\mathrm{Z}} = 1$, $b^d_{\mathrm{Z}} = -1$.

Appendix C

Real contribution to EW top-pair production

The total real contribution can be written as

$$\sigma^{\mathcal{R}} = \int d\mathbf{\Phi}_3 \mathcal{L}\mathcal{R} = \int d\mathbf{\Phi}_3 \mathcal{L} \sum_q \sum_{\text{ch}} \Bigg[\mathcal{R}_{q,\text{ch}}(\gamma,\gamma) + \mathcal{R}_{q,\text{ch}}(\text{Z},\text{Z}) + \mathcal{R}_{q,\text{ch}}(\text{Z}',\text{Z}') + \sum_{B \neq B'} \mathcal{R}_{q,\text{ch}}(B,B') \Bigg], \quad \text{(C.1)}$$

where we integrate over the three particle phase space $d\mathbf{\Phi}_3$, $B, B' \in \{\gamma, \text{Z}, \text{Z}'\}$ and we sum over all the possible light quarks in the initial state $q \in \{\text{d}, \text{u}, \text{s}, \text{c}, \text{b}\}$ and over the channels $\text{ch} \in \{q\overline{q}, \text{g}q, \text{g}\overline{q}\}$.

In this appendix, we list the full formulae for the terms $\mathcal{R}_{q,q\overline{q}}(B,B')$ including the coefficients $c^{\text{i(f)}}$ which were to lengthy to be shown in Section 2.3.2.

It is convenient to decompose $\mathcal{R}_{q,q\overline{q}}(B,B')$ into interference terms with gluon exchange only in the initial state, only in the final state or the mixed terms:

$$\mathcal{R}_{q,q\overline{q}}(B,B') = \mathcal{R}^{\text{i}}_{q,q\overline{q}}(B,B') + \mathcal{R}^{\text{if}}_{q,q\overline{q}}(B,B') + \mathcal{R}^{\text{fi}}_{q,q\overline{q}}(B,B') + \mathcal{R}^{\text{f}}_{q,q\overline{q}}(B,B'), \quad \text{(C.2)}$$

where

$$\mathcal{R}^{\text{i}}_{q,q\overline{q}}(B,B') = \sum_{p,p' \in \{k_1,k_2\}} \mathcal{R}^{p,p'}_{q,q\overline{q}}(B,B'), \quad \text{(C.3)}$$

$$\mathcal{R}^{\text{if}}_{q,q\overline{q}}(B,B') = \sum_{p \in \{k_1,k_2\}, p' \in \{p_1,p_2\}} \mathcal{R}^{p,p'}_{q,q\overline{q}}(B,B'), \quad \text{(C.4)}$$

$$\mathcal{R}^{\text{fi}}_{q,q\overline{q}}(B,B') = \sum_{p \in \{p_1,p_2\}, p' \in \{k_1,k_2\}} \mathcal{R}^{p,p'}_{q,q\overline{q}}(B,B'), \quad \text{(C.5)}$$

$$\mathcal{R}^{\text{i}}_{q,q\overline{q}}(B,B') = \sum_{p,p' \in \{p_1,p_2\}} \mathcal{R}^{p,p'}_{q,q\overline{q}}(B,B'). \quad \text{(C.6)}$$

Because there is no colour flow in the s-channel, the mixed terms $\mathcal{R}^{\text{if}}_{q,q\overline{q}}(B,B')$ and $\mathcal{R}^{\text{fi}}_{q,q\overline{q}}(B,B')$

are zero and the expression for $\mathcal{R}^{\mathrm{i(f)}}_{q,q\overline{q}}(B,B')$ read:

$$\begin{aligned}\mathcal{R}^{\mathrm{i(f)}}_{q,q\overline{q}}(B,B') = \frac{1}{64c_0^{\mathrm{i(f)}}}&\left((\Gamma_B-2iM_B)^2+4c_1^{\mathrm{i(f)}}\right)\left((\Gamma_{B'}+2iM_{B'})^2+4c_1^{\mathrm{i(f)}}\right)\\
&\Big\{A^q_{B'}\left[A^{\mathrm{t}}_{B'}\left(A^q_BA^{\mathrm{t}}_Bc_3^{\mathrm{i(f)}}+B^q_BB^{\mathrm{t}}_Bc_1^{\mathrm{i(f)}}c_2^{\mathrm{i(f)}}\right)+B^{\mathrm{t}}_{B'}\left(A^q_BB^{\mathrm{t}}_Bc_1^{\mathrm{i(f)}}c_2^{\mathrm{i(f)}}+B^q_BA^{\mathrm{t}}_Bc_4^{\mathrm{i(f)}}\right)\right]\\
&+B^q_{B'}\left[B^{\mathrm{t}}_{B'}\left(A^q_BA^{\mathrm{t}}_Bc_1^{\mathrm{i(f)}}c_2^{\mathrm{i(f)}}+B^q_BB^{\mathrm{t}}_Bc_4^{\mathrm{i(f)}}\right)+A^{\mathrm{t}}_{B'}\left(A^q_BB^{\mathrm{t}}_Bc_3^{\mathrm{i(f)}}+B^q_BA^{\mathrm{t}}_Bc_1^{\mathrm{i(f)}}c_2^{\mathrm{i(f)}}\right)\right]\Big\}. \quad \text{(C.7)}\end{aligned}$$

The expressions for coefficients $c_l^{\mathrm{i(f)}}$ read:

$$c_0^{\mathrm{i}} = \hat{t}'\hat{u}', \quad \text{(C.8)}$$

$$c_1^{\mathrm{i}} = \hat{s}+\hat{t}'+\hat{u}', \quad \text{(C.9)}$$

$$c_2^{\mathrm{i}} = 2\hat{s}(\hat{t}_1+\hat{t}'-\hat{u}_1-\hat{u}')+2\hat{t}_1\hat{t}'+(\hat{t}')^2-2\hat{u}_1\hat{u}'-(\hat{u}')^2, \quad \text{(C.10)}$$

$$\begin{aligned}c_3^{\mathrm{i}} = {}&2m_{\mathrm{t}}^2\left[2\hat{s}^2+2\hat{s}(\hat{t}'+\hat{u}')+(\hat{t}')^2+(\hat{u}')^2\right]+(\hat{s}+\hat{t}'+\hat{u}')\Big[2\hat{s}^2+2\hat{s}(\hat{t}_1+\hat{t}'+\hat{u}_1+\hat{u}')\\
&+2\hat{t}_1^2+2\hat{t}_1\hat{t}'+(\hat{t}')^2+2\hat{u}_1^2+2\hat{u}_1\hat{u}'+(\hat{u}')^2\Big], \quad \text{(C.11)}\end{aligned}$$

$$\begin{aligned}c_4^{\mathrm{i}} = {}&-2m_{\mathrm{t}}^2\left[2\hat{s}^2+2\hat{s}(\hat{t}'+\hat{u}')+(\hat{t}')^2+(\hat{u}')^2\right]+(\hat{s}+\hat{t}'+\hat{u}')\Big[2\hat{s}^2+2\hat{s}(\hat{t}_1+\hat{t}'+\hat{u}_1+\hat{u}')\\
&+2\hat{t}_1^2+2\hat{t}_1\hat{t}'+(\hat{t}')^2+2\hat{u}_1^2+2\hat{u}_1\hat{u}'+(\hat{u}')^2\Big], \quad \text{(C.12)}\end{aligned}$$

$$c_0^{\mathrm{f}} = (\hat{s}+\hat{t}_1+\hat{u}_1)^2(\hat{s}+\hat{t}_1+\hat{t}'+\hat{u}_1+\hat{u}')^2, \quad \text{(C.13)}$$

$$c_1^{\mathrm{f}} = \hat{s}, \quad \text{(C.14)}$$

$$\begin{aligned}c_2^{\mathrm{f}} = {}&\hat{s}\Big[-(\hat{u}')^2\left(-2m_{\mathrm{t}}^2+4\hat{t}_1+\hat{t}'+6\hat{u}_1\right)-2m_{\mathrm{t}}^2(\hat{t}')^2+2\hat{t}_1^3+8\hat{t}_1^2\hat{t}'+2\hat{t}_1^2\hat{u}_1+6\hat{t}_1(\hat{t}')^2\\
&+\hat{u}'(\hat{t}'-4\hat{u}_1)(2\hat{t}_1+\hat{t}'+2\hat{u}_1)+8\hat{t}_1\hat{t}'\hat{u}_1-2\hat{t}_1\hat{u}_1^2+(\hat{t}')^3+4(\hat{t}')^2\hat{u}_1-2\hat{u}_1^3-(\hat{u}')^3\Big]\\
&+\hat{u}'\Big[4m_{\mathrm{t}}^2\hat{t}'(\hat{t}_1-\hat{u}_1)+(\hat{t}_1+\hat{u}_1)\left(-2\hat{u}_1(\hat{t}_1+\hat{t}')+\hat{t}'(2\hat{t}_1+\hat{t}')-2\hat{u}_1^2\right)\Big]\\
&+\hat{t}'\Big[\hat{u}_1\left((2\hat{t}_1+\hat{t}')^2-4m_{\mathrm{t}}^2\hat{t}'\right)+\hat{u}_1^2(2\hat{t}_1+\hat{t}')+\hat{t}_1(\hat{t}_1+\hat{t}')(2\hat{t}_1+\hat{t}')\Big]\\
&-(\hat{u}')^2\Big[\hat{t}_1+\hat{u}_1)(\hat{t}_1+\hat{t}'+3\hat{u}_1)-4m_{\mathrm{t}}^2\hat{t}_1\Big]+2\hat{s}^3(\hat{t}_1+\hat{t}'-\hat{u}_1-\hat{u}')-(\hat{u}')^3(\hat{t}_1+\hat{u}_1)\\
&+\hat{s}^2\Big[4\hat{t}_1^2+8\hat{t}_1\hat{t}'-2\hat{u}'(\hat{t}_1+4\hat{u}_1)+3(\hat{t}')^2+2\hat{t}'\hat{u}_1-4\hat{u}_1^2-3(\hat{u}')^2\Big], \quad \text{(C.15)}\end{aligned}$$

$$\begin{aligned}c_3^{\mathrm{f}} = {}&4m_{\mathrm{t}}^4\hat{s}(\hat{t}'+\hat{u}')^2+2m_{\mathrm{t}}^2\Big\{2\hat{s}^4+4\hat{s}^3(\hat{t}_1+\hat{t}'+\hat{u}_1+\hat{u}')+\hat{s}^2\Big[2\hat{t}_1^2+6\hat{t}_1\hat{t}'+4\hat{t}_1\hat{u}_1+6\hat{t}_1\hat{u}'\\
&+3(\hat{t}')^2+6\hat{t}'\hat{u}_1+4\hat{t}'\hat{u}'+2\hat{u}_1^2+6\hat{u}_1\hat{u}'+3(\hat{u}')^2\Big]+2\hat{s}\Big[\hat{t}'\left(2\hat{u}_1(\hat{t}_1+\hat{t}')+\hat{t}_1(\hat{t}_1+\hat{t}')+\hat{u}_1^2\right)\\
&+\hat{u}'(\hat{t}_1+\hat{u}_1)(\hat{t}_1+\hat{t}'+\hat{u}_1)+(\hat{u}')^2(2\hat{t}_1+\hat{u}_1)\Big]+2(\hat{t}'\hat{u}_1-\hat{t}_1\hat{u}')^2\Big\}\\
&+\hat{s}(\hat{s}+\hat{t}_1+\hat{u}_1)(\hat{s}+\hat{t}_1+\hat{t}'+\hat{u}_1+\hat{u}')\Big[2\hat{s}^2+2\hat{s}(\hat{t}_1+\hat{t}'+\hat{u}_1+\hat{u}')+2\hat{t}_1^2+2\hat{t}_1\hat{t}'+(\hat{t}')^2\\
&+2\hat{u}_1^2+2\hat{u}_1\hat{u}'+(\hat{u}')^2\Big], \quad \text{(C.16)}\end{aligned}$$

$$
\begin{aligned}
c_4^{\mathrm{f}} = &-4m_{\mathrm{t}}^4\hat{s}(\hat{t}'+\hat{u}')^2 - 2m_{\mathrm{t}}^2\Big\{2\hat{s}^4 + 4\hat{s}^3(\hat{t}_1+\hat{t}'+\hat{u}_1+\hat{u}') + \hat{s}^2\Big[2\hat{t}_1^2 + 6\hat{t}_1\hat{t}' + 6\hat{u}'(\hat{t}_1+\hat{u}_1)\\
&+ 4\hat{t}_1\hat{u}_1 + (\hat{t}')^2 + 6\hat{t}'\hat{u}_1 + 2\hat{u}_1^2 + (\hat{u}')^2\Big] + 2\hat{s}\Big[\hat{t}'\left(\hat{t}_1(\hat{t}_1+\hat{t}') + 2\hat{t}_1\hat{u}_1 + \hat{u}_1^2\right)\\
&+ \hat{u}'(\hat{t}_1 - 2\hat{t}' + \hat{u}_1)(\hat{t}_1+\hat{t}'+\hat{u}_1) + (\hat{u}')^2(\hat{u}_1 - 2\hat{t}')\Big] - 2\Big[2\hat{t}'\hat{u}'\left(\hat{t}_1^2 + \hat{t}_1(\hat{u}_1+\hat{u}') + \hat{u}_1(\hat{u}_1+\hat{u}')\right)\\
&+ \hat{t}_1^2(\hat{u}')^2 + (\hat{t}')^2\left(2\hat{u}'(\hat{t}_1+\hat{u}_1) + \hat{u}_1^2\right)\Big]\Big\} + \hat{s}(\hat{s}+\hat{t}_1+\hat{u}_1)(\hat{s}+\hat{t}_1+\hat{t}'+\hat{u}_1+\hat{u}')\Big[2\hat{s}^2\\
&+ 2\hat{s}(\hat{t}_1+\hat{t}'+\hat{u}_1+\hat{u}') + 2\hat{t}_1^2 + 2\hat{t}_1\hat{t}' + (\hat{t}')^2 + 2\hat{u}_1^2 + 2\hat{u}_1\hat{u}' + (\hat{u}')^2\Big]. \qquad \text{(C.17)}
\end{aligned}
$$

Bibliography

[1] S. Glashow, "Partial Symmetries of Weak Interactions," *Nucl.Phys.* **22** (1961) 579–588.

[2] A. Salam and J. C. Ward, "Electromagnetic and weak interactions," *Phys.Lett.* **13** (1964) 168–171.

[3] S. Weinberg, "A Model of Leptons," *Phys.Rev.Lett.* **19** (1967) 1264–1266.

[4] S. Glashow, J. Iliopoulos, and L. Maiani, "Weak Interactions with Lepton-Hadron Symmetry," *Phys.Rev.* **D2** (1970) 1285–1292.

[5] S. Weinberg, "Mixing angle in renormalizable theories of weak and electromagnetic interactions," *Phys.Rev.* **D5** (1972) 1962–1967.

[6] D. Gross and F. Wilczek, "Asymptotically Free Gauge Theories. 1," *Phys.Rev.* **D8** (1973) 3633–3652.

[7] M. Kobayashi and T. Maskawa, "CP Violation in the Renormalizable Theory of Weak Interaction," *Prog.Theor.Phys.* **49** (1973) 652–657.

[8] D. Gross and F. Wilczek, "ASYMPTOTICALLY FREE GAUGE THEORIES. 2.," *Phys.Rev.* **D9** (1974) 980–993.

[9] H. D. Politzer, "Asymptotic Freedom: An Approach to Strong Interactions," *Phys.Rept.* **14** (1974) 129–180.

[10] G. Altarelli, B. Mele, and M. Ruiz-Altaba, "Searching for new heavy vector bosons in $p\bar{p}$ colliders," *Z. Phys.* **C45** (1989) 109. Erratum-ibid. C**47**, 676 (1990).

[11] E. Salvioni, G. Villadoro, and F. Zwirner, "Minimal Z′ models: Present bounds and early LHC reach," *JHEP* **0911** (2009) 068, arXiv:0909.1320 [hep-ph].

[12] E. Salvioni, A. Strumia, G. Villadoro, and F. Zwirner, "Non-universal minimal Z′ models: present bounds and early LHC reach," *JHEP* **1003** (2010) 010, arXiv:0911.1450 [hep-ph].

[13] C. Grojean, E. Salvioni, and R. Torre, "A weakly constrained W′ at the early LHC," *JHEP* **1107** (2011) 002, arXiv:1103.2761 [hep-ph].

[14] J. de Blas, J. Lizana, and M. Perez-Victoria, "Combining searches of Z′ and W′ bosons," *JHEP* **1301** (2013) 166, arXiv:1211.2229 [hep-ph].

[15] R. M. Harris and S. Jain, "Cross Sections for Leptophobic Topcolor Z′ Decaying to Top-Antitop," *Eur.Phys.J.* **C72** (2012) 2072, arXiv:1112.4928 [hep-ph].

[16] T. Ježo, M. Klasen, and I. Schienbein, "LHC phenomenology of general SU(2)xSU(2)xU(1) models," *Phys.Rev.* **D86** (2012) 035005, arXiv:1203.5314 [hep-ph].

[17] Q.-H. Cao, Z. Li, J.-H. Yu, and C. Yuan, "Discovery and Identification of W′ and Z′ in SU(2)xSU(2)xU(1) Models at the LHC," *Phys.Rev.* **D86** (2012) 095010, arXiv:1205.3769 [hep-ph].

[18] **ATLAS Collaboration** Collaboration, G. Aad *et al.*, "Observation of a new particle in the search for the Standard Model Higgs boson with the ATLAS detector at the LHC," *Phys.Lett.* **B716** (2012) 1–29, arXiv:1207.7214 [hep-ex].

[19] **CMS Collaboration** Collaboration, S. Chatrchyan *et al.*, "Observation of a new boson at a mass of 125 GeV with the CMS experiment at the LHC," *Phys.Lett.* **B716** (2012) 30–61, arXiv:1207.7235 [hep-ex].

[20] **CMS** Collaboration, G. Bayatian *et al.*, "CMS technical design report, volume II: Physics performance," *J.Phys.* **G34** (2007) 995–1579.

[21] **CMS** Collaboration, "Search for Resonances in the Dilepton Mass Distribution in pp Collisions at $\sqrt{s} = 8$ TeV," *CMS-PAS-EXO-12-061* .

[22] **ATLAS** Collaboration, "Search for high-mass dilepton resonances in 20 fb^{-1} of pp collisions at $\sqrt{s} = 8$ TeV with the ATLAS experiment," *ATLAS-CONF-2013-017* .

[23] **CMS** Collaboration, "Search for Resonances in the Dilepton Mass Distribution in pp Collisions at $\sqrt{s} = 8$ TeV," *CMS-PAS-EXO-12-060* .

[24] **ATLAS** Collaboration, G. Aad *et al.*, "ATLAS search for a heavy gauge boson decaying to a charged lepton and a neutrino in pp collisions at $\sqrt{s} = 7$ TeV," *Eur.Phys.J.* **C72** (2012) 2241, arXiv:1209.4446 [hep-ex].

[25] **ATLAS** Collaboration, G. Aad *et al.*, "Search for $t\bar{t}$ resonances in the lepton plus jets final state with atlas using 4.7 fb^{-1} of pp collisions at $\sqrt{s}$=7 TeV," *Phys. Rev. D* **88** (Jul, 2013) 012004. http://link.aps.org/doi/10.1103/PhysRevD.88.012004.

[26] **CMS** Collaboration, "Search for $t\bar{t}$ resonances in semileptonic final state," *CMS-PAS-B2G-12-006* .

[27] **ATLAS** Collaboration, "Search for W′ in single top using pp collisions at $\sqrt{s} = 8$ TeV," *ATLAS-CONF-2013-050* .

[28] **CMS** Collaboration, "Search for narrow $t + b$ resonances in the leptonic final state at $\sqrt{s} = 8$ TeV," *CMS-PAS-B2G-12-010* .

[29] **ATLAS** Collaboration, "Search for Z′ to tau tau in proton-proton collisions at 8 TeV with the ATLAS detector," *ATLAS-CONF-2013-066* .

[30] **CMS** Collaboration, S. Chatrchyan *et al.*, "Search for high mass resonances decaying into τ^- lepton pairs in pp collisions at $\sqrt{s} = 7$ TeV," *Phys.Lett.* **B716** (2012) 82–102, arXiv:1206.1725 [hep-ex].

[31] **CMS** Collaboration, "Search for Narrow Resonances using the Dijet Mass Spectrum with 19.6 fb^{-1} of pp Collisions at $\sqrt{s} = 8$ TeV," *CMS-PAS-EXO-12-059* .

[32] **ATLAS** Collaboration, "Dijet resonance search with 8 TeV data for HCP," *ATLAS-CONF-2012-148* .

[33] **ATLAS** Collaboration, "Search for heavy resonance decaying to WZ to $lvll$," *ATLAS-CONF-2013-015* .

[34] **ATLAS** Collaboration, "Search for heavy resonance decaying to ZZ/WZ to $lljj$ or llJ," *ATLAS-CONF-2012-150* .

[35] **CMS** Collaboration, "Search for W/*technirho* in WZ using leptonic final states," *CMS-PAS-EXO-12-025* .

[36] **CMS** Collaboration, "Search for heavy resonances in the W/Z-tagged dijet mass spectrum in pp collisions at 8 TeV," *CMS-PAS-EXO-12-024* .

[37] C.-W. Chiang, N. D. Christensen, G.-J. Ding, and T. Han, "Discovery in Drell-Yan Processes at the LHC," *Phys.Rev.* **D85** (2012) 015023, arXiv:1107.5830 [hep-ph].

[38] Y. Coutinho, V. S. Guimaraes, and A. Nepomuceno, "Bounds on Z′ from 3-3-1 model at the LHC energies," arXiv:1304.7907 [hep-ph].

[39] E. L. Berger, Q.-H. Cao, J.-H. Yu, and C.-P. Yuan, "Calculation of Associated Production of a Top Quark and a W′ at the LHC," *Phys.Rev.* **D84** (2011) 095026, arXiv:1108.3613 [hep-ph].

[40] J. Adelman, J. Ferrando, and C. White, "NLO QCD Corrections to tW′ and tZ′ Production in Forward-Backward Asymmetry Models," *JHEP* **1302** (2013) 091, arXiv:1206.5731 [hep-ph].

[41] S. Gopalakrishna, T. Han, I. Lewis, Z.-g. Si, and Y.-F. Zhou, "Chiral Couplings of W′ and Top Quark Polarization at the LHC," *Phys.Rev.* **D82** (2010) 115020, arXiv:1008.3508 [hep-ph].

[42] E. L. Berger, Q.-H. Cao, C.-R. Chen, and H. Zhang, "Top Quark Polarization As A Probe of Models with Extra Gauge Bosons," *Phys.Rev.* **D83** (2011) 114026, arXiv:1103.3274 [hep-ph].

[43] L. Basso, K. Mimasu, and S. Moretti, "Z′ signals in polarised top-antitop final states," *JHEP* **1209** (2012) 024, arXiv:1203.2542 [hep-ph].

[44] **Particle Data Group** Collaboration, K. Nakamura *et al.*, "Review of particle physics," *J.Phys.* **G37** (2010) 075021.

[45] R. Tenchini and C. Verzegnassi, "The physics of the Z and W bosons,".

[46] **Super-Kamiokande Collaboration** Collaboration, Y. Fukuda *et al.*, "Evidence for oscillation of atmospheric neutrinos," *Phys.Rev.Lett.* **81** (1998) 1562–1567, arXiv:hep-ex/9807003 [hep-ex].

[47] **SNO Collaboration** Collaboration, Q. Ahmad *et al.*, "Direct evidence for neutrino flavor transformation from neutral current interactions in the Sudbury Neutrino Observatory," *Phys.Rev.Lett.* **89** (2002) 011301, arXiv:nucl-ex/0204008 [nucl-ex].

[48] K. Hsieh, K. Schmitz, J.-H. Yu, and C.-P. Yuan, "Global Analysis of General SU(2)xSU(2)xU(1) Models with Precision Data," *Phys.Rev.* **D82** (2010) 035011, arXiv:1003.3482 [hep-ph].

[49] R. N. Mohapatra and J. C. Pati, "Left-Right Gauge Symmetry and an Isoconjugate Model of CP Violation," *Phys.Rev.* **D11** (1975) 566–571.

[50] V. D. Barger, W.-Y. Keung, and E. Ma, "Doubling of weak gauge bosons in an extension of the Standard Model," *Phys.Rev.Lett.* **44** (1980) 1169.

[51] H. Georgi, E. E. Jenkins, and E. H. Simmons, "Ununifying the Standard Model," *Phys.Rev.Lett.* **62** (1989) 2789.

[52] X. Li and E. Ma, "Gauge model of generation nonuniversality," *Phys.Rev.Lett.* **47** (1981) 1788.

[53] T. Appelquist and J. Carazzone, "Infrared Singularities and Massive Fields," *Phys.Rev.* **D11** (1975) 2856.

[54] K. Hsieh, "Private communication,".

[55] P. Langacker and S. Uma Sankar, "Bounds on the Mass of W(R) and the W(L)-W(R) Mixing Angle ξ in General $SU(2)_L \times SU(2)_R \times U(1)$ Models," *Phys. Rev.* **D40** (1989) 1569–1585.

[56] J. Chakrabortty, J. Gluza, R. Sevillano, and R. Szafron, "Left-Right Symmetry at LHC and Precise 1-Loop Low Energy Data," *JHEP* **1207** (2012) 038, arXiv:1204.0736 [hep-ph].

[57] A. Maiezza, M. Nemevsek, F. Nesti, and G. Senjanovic, "Left-Right Symmetry at LHC," *Phys.Rev.* **D82** (2010) 055022, arXiv:1005.5160 [hep-ph].

[58] **CMS** Collaboration, "Search for a heavy neutrino and right-handed W of the left-right symmetric model in pp collisions at 8 TeV," *CMS-PAS-EXO-12-017* .

[59] **ATLAS Collaboration** Collaboration, G. Aad *et al.*, "Search for heavy neutrinos and right-handed W bosons in events with two leptons and jets in pp collisions at $\sqrt{s} = 7$ TeV with the ATLAS detector," *Eur.Phys.J.* **C72** (2012) 2056, arXiv:1203.5420 [hep-ex].

[60] T. Sjostrand, S. Mrenna, and P. Skands, "PYTHIA 6.4 Physics and Manual," *JHEP* **05** (2006) 026, arXiv:hep-ph/0603175.

[61] J. Pumplin, D. Stump, J. Huston, H. Lai, P. M. Nadolsky, *et al.*, "New generation of parton distributions with uncertainties from global QCD analysis," *JHEP* **0207** (2002) 012, arXiv:hep-ph/0201195 [hep-ph].

[62] A. Martin, W. Stirling, R. Thorne, and G. Watt, "Parton distributions for the LHC," *Eur.Phys.J.* **C63** (2009) 189–285, arXiv:0901.0002 [hep-ph].

[63] M. Cacciari, G. P. Salam, and G. Soyez, "The Anti-k(t) jet clustering algorithm," *JHEP* **0804** (2008) 063, arXiv:0802.1189 [hep-ph].

[64] **ATLAS** Collaboration, "A Search for $t\bar{t}$ Resonances in the Lepton Plus Jets Channel using 2.05 fb^{-1} of pp Collisions at $\sqrt{s} = 7$ TeV," *ATLAS-CONF-2012-029* .

[65] R. K. Ellis, W. J. Stirling, and B. Webber, "QCD and collider physics," *Camb.Monogr.Part.Phys.Nucl.Phys.Cosmol.* **8** (1996) 1–435.

[66] B. Fuks, M. Klasen, F. Ledroit, Q. Li, and J. Morel, "Precision predictions for Z′-production at the CERN LHC: QCD matrix elements, parton showers, and joint resummation," *Nucl.Phys.* **B797** (2008) 322–339, arXiv:0711.0749 [hep-ph].

[67] A. Papaefstathiou and O. Latunde-Dada, "NLO production of W′ bosons at hadron colliders using the MC@NLO and POWHEG methods," *JHEP* **0907** (2009) 044, arXiv:0901.3685 [hep-ph].

[68] R. Bonciani, T. Ježo, F. Lyonnet, M. Klasen, and I. Schienbein, "QCD corrections to electroweak top-pair production in POWHEG BOX," *in preparation* .

[69] **Tevatron Electroweak Working Group, CDF, D0** Collaboration, "Combination of CDF and D0 results on the mass of the top quark using up to 5.8 fb^{-1} of data," arXiv:1107.5255 [hep-ex].

[70] G. Corcella, I. Knowles, G. Marchesini, S. Moretti, K. Odagiri, *et al.*, "HERWIG 6.5 release note," arXiv:hep-ph/0210213 [hep-ph].

[71] S. Frixione, P. Nason, and C. Oleari, "Matching NLO QCD computations with Parton Shower simulations: the to leading order POWHEG method," *JHEP* **0711** (2007) 070, arXiv:0709.2092 [hep-ph].

[72] S. Alioli, P. Nason, C. Oleari, and E. Re, "A general framework for implementing NLO calculations in shower Monte Carlo programs: the POWHEG BOX," *JHEP* **1006** (2010) 043, arXiv:1002.2581 [hep-ph].

[73] J. Gao, C. S. Li, B. H. Li, C.-P. Yuan, and H. X. Zhu, "Next-to-leading order QCD corrections to the heavy resonance production and decay into top quark pair at the LHC," *Phys.Rev.* **D82** (2010) 014020, arXiv:1004.0876 [hep-ph].

[74] H. X. Zhu, C. S. Li, D. Y. Shao, J. Wang, and C. Yuan, "Precise QCD predictions on top quark pair production mediated by massive color octet vector boson at hadron colliders," *Eur.Phys.J.* **C72** (2012) 2232, arXiv:1201.0672 [hep-ph].

[75] F. Caola, K. Melnikov, and M. Schulze, "A complete next-to-leading order QCD description of resonant Z′ production and decay into $t\bar{t}$ final states," *Phys.Rev.* **D87** no. 3, (2013) 034015, arXiv:1211.6387 [hep-ph].

[76] M. L. Mangano, P. Nason, and G. Ridolfi, "Heavy quark correlations in hadron collisions at next-to-leading order," *Nucl.Phys.* **B373** (1992) 295–345.

[77] H.-L. Lai, M. Guzzi, J. Huston, Z. Li, P. M. Nadolsky, *et al.*, "New parton distributions for collider physics," *Phys.Rev.* **D82** (2010) 074024, arXiv:1007.2241 [hep-ph].

[78] R. D. Ball, L. Del Debbio, S. Forte, A. Guffanti, J. I. Latorre, *et al.*, "A first unbiased global NLO determination of parton distributions and their uncertainties," *Nucl.Phys.* **B838** (2010) 136–206, arXiv:1002.4407 [hep-ph].

[79] J. Owens, A. Accardi, and W. Melnitchouk, "Global parton distributions with nuclear and finite-Q^2 corrections," *Phys.Rev.* **D87** (2013) 094012, arXiv:1212.1702 [hep-ph].

[80] A. Papanastasiou, R. Frederix, S. Frixione, V. Hirschi, and F. Maltoni, "Single-top t-channel production with off-shell and non-resonant effects," arXiv:1305.7088 [hep-ph].

[81] P. Nason, S. Dawson, and R. K. Ellis, "The Total Cross-Section for the Production of Heavy Quarks in Hadronic Collisions," *Nucl.Phys.* **B303** (1988) 607.

[82] P. Nason, S. Dawson, and R. K. Ellis, "The One Particle Inclusive Differential Cross-Section for Heavy Quark Production in Hadronic Collisions," *Nucl.Phys.* **B327** (1989) 49–92.

[83] W. Beenakker, H. Kuijf, W. van Neerven, and J. Smith, "QCD Corrections to Heavy Quark Production in p anti-p Collisions," *Phys.Rev.* **D40** (1989) 54–82.

[84] W. Beenakker, W. van Neerven, R. Meng, G. Schuler, and J. Smith, "QCD corrections to heavy quark production in hadron hadron collisions," *Nucl.Phys.* **B351** (1991) 507–560.

[85] W. Beenakker, A. Denner, W. Hollik, R. Mertig, T. Sack, *et al.*, "Electroweak one loop contributions to top pair production in hadron colliders," *Nucl.Phys.* **B411** (1994) 343–380.

[86] J. H. Kuhn, A. Scharf, and P. Uwer, "Electroweak corrections to top-quark pair production in quark-antiquark annihilation," *Eur.Phys.J.* **C45** (2006) 139–150, arXiv:hep-ph/0508092 [hep-ph].

[87] S. Moretti, M. Nolten, and D. Ross, "Weak corrections to gluon-induced top-antitop hadro-production," *Phys.Lett.* **B639** (2006) 513–519, arXiv:hep-ph/0603083 [hep-ph].

[88] W. Bernreuther, M. Fuecker, and Z.-G. Si, "Weak interaction corrections to hadronic top quark pair production," *Phys.Rev.* **D74** (2006) 113005, arXiv:hep-ph/0610334 [hep-ph].

[89] J. H. Kuhn, A. Scharf, and P. Uwer, "Electroweak effects in top-quark pair production at hadron colliders," *Eur.Phys.J.* **C51** (2007) 37–53, arXiv:hep-ph/0610335 [hep-ph].

[90] W. Hollik and M. Kollar, "NLO QED contributions to top-pair production at hadron collider," *Phys.Rev.* **D77** (2008) 014008, arXiv:0708.1697 [hep-ph].

[91] P. Duka, J. Gluza, and M. Zralek, "Quantization and renormalization of the manifest left-right symmetric model of electroweak interactions," *Annals Phys.* **280** (2000) 336–408, arXiv:hep-ph/9910279 [hep-ph].

[92] T. Abe, N. Chen, and H.-J. He, "LHC Higgs Signatures from Extended Electroweak Gauge Symmetry," *JHEP* **1301** (2013) 082, arXiv:1207.4103 [hep-ph].

[93] M. Veltman, "Diagrammatica: The Path to Feynman rules," *Cambridge Lect.Notes Phys.* **4** (1994) 1–284.

[94] P. Nogueira, "Automatic Feynman graph generation," *J.Comput.Phys.* **105** (1993) 279–289.

[95] M. Tentyukov and J. Fleischer, "A Feynman diagram analyzer DIANA," *Comput.Phys.Commun.* **132** (2000) 124–141, arXiv:hep-ph/9904258 [hep-ph].

[96] J. Vermaseren, "New features of FORM," arXiv:math-ph/0010025 [math-ph].

[97] G. van Rossum, "Python tutorial, Technical Report CS-R9526," *Centrum voor Wiskunde en Informatica (CWI)* (May 1995) .

[98] A. Kotikov, "Differential equations method: New technique for massive Feynman diagrams calculation," *Phys.Lett.* **B254** (1991) 158–164.

[99] T. Muta, "Foundations of quantum chromodynamics. Second edition," *World Sci.Lect.Notes Phys.* **57** (1998) 1–409.

[100] J. Vermaseren, "FORM reference manual," http://www.nikhef.nl/~form/maindir/documentation/.

[101] C. Studerus, "Reduze-Feynman Integral Reduction in C++," *Comput.Phys.Commun.* **181** (2010) 1293–1300, arXiv:0912.2546 [physics.comp-ph].

[102] A. Grozin, "Integration by parts: An Introduction," *Int.J.Mod.Phys.* **A26** (2011) 2807–2854, arXiv:1104.3993 [hep-ph].

[103] K. Chetyrkin and F. Tkachov, "Integration by Parts: The Algorithm to Calculate beta Functions in 4 Loops," *Nucl.Phys.* **B192** (1981) 159–204.

[104] T. van Ritbergen and R. G. Stuart, "On the precise determination of the Fermi coupling constant from the muon lifetime," *Nucl.Phys.* **B564** (2000) 343–390, arXiv:hep-ph/9904240 [hep-ph].

[105] A. Vogt, S. Moch, and J. Vermaseren, "The Three-loop splitting functions in QCD: The Singlet case," *Nucl.Phys.* **B691** (2004) 129–181, arXiv:hep-ph/0404111 [hep-ph].

[106] A. Smirnov and A. Petukhov, "The Number of Master Integrals is Finite," *Lett.Math.Phys.* **97** (2011) 37–44, arXiv:1004.4199 [hep-th].

[107] S. Laporta, "High precision calculation of multiloop Feynman integrals by difference equations," *Int.J.Mod.Phys.* **A15** (2000) 5087–5159, arXiv:hep-ph/0102033 [hep-ph].

[108] C. Anastasiou and A. Lazopoulos, "Automatic integral reduction for higher order perturbative calculations," *JHEP* **0407** (2004) 046, arXiv:hep-ph/0404258 [hep-ph].

[109] A. von Manteuffel and C. Studerus, "Reduze 2 - Distributed Feynman Integral Reduction," arXiv:1201.4330 [hep-ph].

[110] E. Remiddi, "Differential equations for Feynman graph amplitudes," *Nuovo Cim.* **A110** (1997) 1435–1452, arXiv:hep-th/9711188 [hep-th].

[111] M. Caffo, H. Czyz, S. Laporta, and E. Remiddi, "The Master differential equations for the two loop sunrise selfmass amplitudes," *Nuovo Cim.* **A111** (1998) 365–389, arXiv:hep-th/9805118 [hep-th].

[112] G. 't Hooft and M. Veltman, "Scalar One Loop Integrals," *Nucl.Phys.* **B153** (1979) 365–401.

[113] E. Remiddi and J. Vermaseren, "Harmonic polylogarithms," *Int.J.Mod.Phys.* **A15** (2000) 725–754, arXiv:hep-ph/9905237 [hep-ph].

[114] A. B. Goncharov, "Multiple polylogarithms, cyclotomy and modular complexes," *Math.Res.Lett.* **5** (1998) 497–516, arXiv:1105.2076 [math.AG].

[115] R. Bonciani, G. Degrassi, and A. Vicini, "On the Generalized Harmonic Polylogarithms of One Complex Variable," *Comput.Phys.Commun.* **182** (2011) 1253–1264, arXiv:1007.1891 [hep-ph].

[116] I. Aitchison and A. Hey, "Gauge theories in particle physics: A practical introduction. Vol. 1: From relativistic quantum mechanics to QED,".

[117] M. E. Peskin and D. V. Schroeder, "An Introduction to quantum field theory,".

[118] K. Melnikov and T. van Ritbergen, "The Three loop on-shell renormalization of QCD and QED," *Nucl.Phys.* **B591** (2000) 515–546, arXiv:hep-ph/0005131 [hep-ph].

[119] T. Kinoshita, "Mass singularities of Feynman amplitudes," *J.Math.Phys.* **3** (1962) 650–677.

[120] T. Lee and M. Nauenberg, "Degenerate Systems and Mass Singularities," *Phys.Rev.* **133** (1964) B1549–B1562.

[121] S. Frixione, Z. Kunszt, and A. Signer, "Three jet cross-sections to next-to-leading order," *Nucl.Phys.* **B467** (1996) 399–442, arXiv:hep-ph/9512328 [hep-ph].

[122] S. Catani, S. Dittmaier, M. H. Seymour, and Z. Trocsanyi, "The Dipole formalism for next-to-leading order QCD calculations with massive partons," *Nucl.Phys.* **B627** (2002) 189–265, arXiv:hep-ph/0201036 [hep-ph].

[123] S. Catani and M. Seymour, "NLO QCD calculations in DIS at HERA based on the dipole formalism," arXiv:hep-ph/9609521 [hep-ph].

[124] J. C. Collins, D. E. Soper, and G. F. Sterman, "Factorization of Hard Processes in QCD," *Adv.Ser.Direct.High Energy Phys.* **5** (1988) 1–91, arXiv:hep-ph/0409313 [hep-ph].

[125] S. Ovyn, X. Rouby, and V. Lemaitre, "DELPHES, a framework for fast simulation of a generic collider experiment," arXiv:0903.2225 [hep-ph].

[126] S. Alioli, "Matching Next-to-Leadin-Order QCD Calculations with Shower Monte Carlo Simulations: Single Vector Boson and higgs Boson Production in POWHEG," *PHD thesis* .

[127] S. Frixione and B. R. Webber, "The MC@NLO event generator," arXiv:hep-ph/0207182 [hep-ph].

[128] S. Alioli, P. Nason, C. Oleari, and E. Re, "NLO vector-boson production matched with shower in POWHEG," *JHEP* **0807** (2008) 060, arXiv:0805.4802 [hep-ph].

[129] S. Alioli, P. Nason, C. Oleari, and E. Re, "NLO Higgs boson production via gluon fusion matched with shower in POWHEG," *JHEP* **0904** (2009) 002, arXiv:0812.0578 [hep-ph].

[130] P. Nason and C. Oleari, "NLO Higgs boson production via vector-boson fusion matched with shower in POWHEG," *JHEP* **1002** (2010) 037, arXiv:0911.5299 [hep-ph].

[131] S. Alioli, P. Nason, C. Oleari, and E. Re, "NLO single-top production matched with shower in POWHEG: s- and t-channel contributions," *JHEP* **0909** (2009) 111, arXiv:0907.4076 [hep-ph].

[132] S. Frixione, P. Nason, and G. Ridolfi, "A Positive-weight next-to-leading-order Monte Carlo for heavy flavour hadroproduction," *JHEP* **0709** (2007) 126, arXiv:0707.3088 [hep-ph].

[133] M. Klasen, K. Kovarik, P. Nason, and C. Weydert, "Associated production of charged Higgs bosons and top quarks with POWHEG," *Eur.Phys.J.* **C72** (2012) 2088, arXiv:1203.1341 [hep-ph].

[134] B. Jager, A. von Manteuffel, and S. Thier, "Slepton pair production in the POWHEG BOX," *JHEP* **1210** (2012) 130, arXiv:1208.2953 [hep-ph].

[135] T. Gehrmann and E. Remiddi, "Numerical evaluation of harmonic polylogarithms," *Comput.Phys.Commun.* **141** (2001) 296–312, arXiv:hep-ph/0107173 [hep-ph].

[136] M. Whalley, D. Bourilkov, and R. Group, "The Les Houches accord PDFs (LHAPDF) and LHAGLUE," arXiv:hep-ph/0508110 [hep-ph].

[137] J. Alwall, A. Ballestrero, P. Bartalini, S. Belov, E. Boos, *et al.*, "A Standard format for Les Houches event files," *Comput.Phys.Commun.* **176** (2007) 300–304, arXiv:hep-ph/0609017 [hep-ph].

[138] T. Hahn, "Feynman Diagram Calculations with FeynArts, FormCalc, and LoopTools," *PoS* **ACAT2010** (2010) 078, arXiv:1006.2231 [hep-ph].

[139] V. Hirschi, R. Frederix, S. Frixione, M. V. Garzelli, F. Maltoni, *et al.*, "Automation of one-loop QCD corrections," *JHEP* **1105** (2011) 044, arXiv:1103.0621 [hep-ph].

[140] G. Cullen, N. Greiner, G. Heinrich, G. Luisoni, P. Mastrolia, *et al.*, "Automated One-Loop Calculations with GoSam," *Eur.Phys.J.* **C72** (2012) 1889, arXiv:1111.2034 [hep-ph].

[141] I. Wigmore, "The Automated Calculation of One-Loop Processes within MadGolem," *PhD thesis* (2013) .

[142] N. D. Christensen and C. Duhr, "FeynRules - Feynman rules made easy," *Comput.Phys.Commun.* **180** (2009) 1614–1641, arXiv:0806.4194 [hep-ph].

[143] C. Degrande, C. Duhr, B. Fuks, D. Grellscheid, O. Mattelaer, *et al.*, "UFO - The Universal FeynRules Output," *Comput.Phys.Commun.* **183** (2012) 1201–1214, arXiv:1108.2040 [hep-ph].

[144] A. Semenov, "LanHEP - a package for automatic generation of Feynman rules from the Lagrangian. Updated version 3.1," arXiv:1005.1909 [hep-ph].

[145] T. Binoth, A. Guffanti, J.-P. Guillet, G. Heinrich, S. Karg, *et al.*, "Precise predictions for LHC using a GOLEM," *Nucl.Phys.Proc.Suppl.* **183** (2008) 91–96, arXiv:0807.0605 [hep-ph].

[146] A. Lorca and T. Riemann, "An Integrated tool for loop calculations: aITALC," *Comput.Phys.Commun.* **174** (2006) 71–82, arXiv:hep-ph/0412047 [hep-ph].

[147] G. Passarino and M. Veltman, "One Loop Corrections for e+ e- Annihilation Into mu+ mu- in the Weinberg Model," *Nucl.Phys.* **B160** (1979) 151.

[148] G. Luisoni, P. Nason, C. Oleari, and F. Tramontano, "Merging HW/HZ + 0 and 1 jet at NLO with no merging scale using the POWHEG BOX interfaced to GoSam," arXiv:1306.2542 [hep-ph].

[149] R. Bonciani, T. Ježo, F. Lyonnet, M. Klasen, and I. Schienbein, "QCD corrections to electroweak single-top production in POWHEG BOX," *in preparation* .

[150] A. Mitov and S.-O. Moch, "QCD Corrections to Semi-Inclusive Hadron Production in Electron-Positron Annihilation at Two Loops," *Nucl.Phys.* **B751** (2006) 18–52, arXiv:hep-ph/0604160 [hep-ph].

[151] J. Alwall, M. Herquet, F. Maltoni, O. Mattelaer, and T. Stelzer, "MadGraph 5 : Going Beyond," *JHEP* **1106** (2011) 128, arXiv:1106.0522 [hep-ph].

Abstract

General SU(2)×SU(2)×U(1) models represent a well-motivated intermediate step towards the unification of the Standard Model (SM) gauge groups. Extended gauge group sector, as compared to that of the SM, leads to additional neutral and charged gauge bosons. These so-called Z' and W' bosons are actively searched for at the Large Hadron Collider (LHC). Based on a recent global analysis of low-energy and LEP constraints of these models, we perform numerical scans of their various signals at the LHC at Leading Order accuracy. We show that total cross sections for lepton and third-generation quark pairs, while experimentally easily accessible, provide individually only partial information about the model realized in Nature. In contrast, correlations of these cross sections in the neutral and charged current channels may well lead to a unique identification. Subsequently we study the electroweak top-pair production at Next-to-leading Order (NLO) accuracy in the SM extensions with an additional Z' boson assuming general flavour-diagonal couplings. We calculate the virtual and real corrections at order $\mathcal{O}(\alpha_S \alpha_W^2)$ and implement them in the `POWHEG BOX` framework which allows for consistent matching of NLO QCD calculations with parton showers. We find that the NLO corrections can be very important but the K-factors in the invariant mass region around the resonance mass are modest.

Résumé

Les modèles SU(2)×SU(2)×U(1) représentent une étape intermédiaire motivée par l'unification des groupes de jauge du Modèle Standard (MS). Un groupe de jauge étendu, par rapport à celui du MS, implique l'existence de nouveaux bosons de jauge, neutres et chargés. Ces bosons dénotés Z' et W' sont recherchés activement au Large Hadron Collider (LHC). Sur la base d'une analyse globale récente des contraintes sur ces modèles, provenant des expériences à basse énergie et du LEP, nous effectuons une analyse numérique au Leading Order (LO) des différentes signatures au LHC. Nous montrons que les sections efficaces totales pour les leptons et les paires de quarks de troisième génération, expérimentalement facilement accessibles, fournissent individuellement qu'une information partielles sur le modèle réalisé dans la nature. En revanche, les corrélations de ces mêmes sections efficaces pourraient bien conduire à une identification unique. Par la suite, nous étudions la production électrofaible d'une paire de quarks top au Next-to-Leading Order dans les extensions du MS prédisant un boson Z' supplémentaire et en supposant des couplages génériques et diagonaux dans la base des saveurs. Nous calculons les corrections virtuelles et réelles à l'ordre de $\mathcal{O}(\alpha_S \alpha_W^2)$ et les implémentons dans le générateur d'événements Monte Carlo `POWHEG BOX` qui permet de réaliser de manière cohérente la fusion du calcul QCD NLO avec les parton showers. Nous constatons que les corrections QCD NLO peuvent être très importantes, mais que les K-facteurs restent modestes dans la région de masse invariante centrée autour de la masse de la résonance.